



8-2015

An Application of Path-Percolation Theory and Lattice-Boltzmann Model on Mass Transfer in Inhomogeneous Porous Media

Ozgur Cekmer

University of Tennessee - Knoxville, ocekmer@vols.utk.edu

Recommended Citation

Cekmer, Ozgur, "An Application of Path-Percolation Theory and Lattice-Boltzmann Model on Mass Transfer in Inhomogeneous Porous Media." PhD diss., University of Tennessee, 2015.

https://trace.tennessee.edu/utk_graddiss/3403

This Dissertation is brought to you for free and open access by the Graduate School at Trace: Tennessee Research and Creative Exchange. It has been accepted for inclusion in Doctoral Dissertations by an authorized administrator of Trace: Tennessee Research and Creative Exchange. For more information, please contact trace@utk.edu.

To the Graduate Council:

I am submitting herewith a dissertation written by Ozgur Cekmer entitled "An Application of Path-Percolation Theory and Lattice-Boltzmann Model on Mass Transfer in Inhomogeneous Porous Media." I have examined the final electronic copy of this dissertation for form and content and recommend that it be accepted in partial fulfillment of the requirements for the degree of Doctor of Philosophy, with a major in Mechanical Engineering.

Matthew M. Mench, Major Professor

We have read this dissertation and recommend its acceptance:

Kivanc Ekici, Feng-Yuan Zhang, L. Montgomery Smith

Accepted for the Council:

Dixie L. Thompson

Vice Provost and Dean of the Graduate School

(Original signatures are on file with official student records.)

An Application of Path-Percolation Theory and Lattice-Boltzmann Model on Mass Transfer in Inhomogeneous Porous Media

**A Dissertation Presented for the
Doctor of Philosophy
Degree
The University of Tennessee, Knoxville**

**Ozgur Cekmer
August 2015**

Copyright © 2015 by Ozgur Cekmer
All rights reserved.

DEDICATION

To my dear wife, Hayriye Bozkurt Cekmer.

ACKNOWLEDGEMENTS

I am grateful to many people who contributed to this work. First of all, I would like to thank my advisor Dr. Matthew M. Mench for his invaluable impact on my academic career. His approach on his students in both personal and professional situations will be my guidance in the future. I feel that I have become a better researcher because of his mentorship. Dr. Sukkee Um taught me the path-percolation method, and how to obtain statistical results using probabilistic theory. I strongly appreciate his contributions to my dissertation. I also would like to thank my committee members; Dr. Feng-Yuan Zhang, Dr. L. Montgomery Smith, and Dr. Kivanc Ekici for their directions throughout my PhD program.

I would like to thank all my team members. It was a great privilege to be a member of such an elegant group of engineers. I also thank Kathy Williams and Vicki Smallman for their endless help and support.

Special thanks go to my family in Turkey. For their limitless support, I would like to thank my mother Gulsum Kupeli, my grandparents Hasan Cekmer and Sebahat Cekmer, my aunt Guler Cekmer, and my sister Ozge Cekmer.

Finally, I would like to thank my dear wife, Hayriye Bozkurt Cekmer for her patience and support during this program. She is the most important reason of what I achieved so far. Thank you very much for walking with me in this challenging path of the life. I hope we will read our names together in our children's dissertations in the future.

ABSTRACT

In this dissertation, random inhomogeneous porous channels were generated statistically, and single- and multi-phase flow models were developed to investigate diffusion behavior of gases in porous media. Three different methods were used to simulate inhomogeneous porous flow channels. First, the path-percolation theory was adapted in diffusion studies to generate random high-tortuosity (above 1.07) porous channels with a desired porosity within a specified confidence level. Cluster labeling process was applied to simulate paths for the gas molecules, and the resulting effective porosity was investigated statistically. Second, the double-path-percolation theory was introduced to simulate low-tortuosity (between 1.0005 and 1.0700) flow channels. Using a combined void- and solid-cluster labeling process, this new model also simulates paths in both solid and void regions in the channel, hence transport analysis can be performed in both regions. Third, two dimensional slices of the micro-computed tomographies of Mitsubishi Rayon Corp. MRC-105 and Sigracet SGL-25BA gas diffusion layer samples, which are used in polymer electrolyte fuel cells, were digitized, and the effective porosities were determined statistically by cluster labeling process. A single-phase Lattice-Boltzmann model (LBM) was developed to simulate gas flow in the channels generated. Velocity distributions were obtained to evaluate the effective tortuosity in gas diffusion layer samples and different channels generated by single- and double-path-percolation theories. Furthermore, multi-phase LBMs were developed to investigate the impact of liquid formation on mass transfer in porous channels. Statistical results of porosity, effective porosity, and tortuosity of the system with different liquid volumes were investigated. Velocity distributions in porous channels with different solid-liquid-vapor combinations were analyzed. Moreover, a portion of the solid surface

inside the channel was set hydrophobic, and multi-phase effects on mass transport were examined. A software was developed for a combined path-percolation – Lattice-Boltzmann model, and the performance was improved by different high-performance computing system implementations. The techniques introduced in this dissertation can be utilized in inhomogeneous porous media application involved with single- and multi-phase mass transport with surface-fluid interactions. This work is unique through its statistical approach and cluster labeling process.

TABLE OF CONTENTS

INTRODUCTION	1
CHAPTER I Application of Path-Percolation Theory and Lattice-Boltzmann Method to Investigate Structure-Property Relationship in Porous Media.....	6
Abstract	7
Introduction.....	7
Path-Percolation Theory	10
Confidence Level Studies	10
Random Porous Media Generation with Cluster Labeling	11
Lattice-Boltzmann Method	12
RAE Selection.....	13
LBM Utilization.....	15
Results.....	19
Path-Percolation Theory	19
The Lattice Boltzmann Model	20
A New D_{eff}/D_{bulk} Model	22
Conclusion	24
Appendix.....	25
CHAPTER II A Combined Path-Percolation - Lattice-Boltzmann Model applied to multi-phase Mass Transfer in Porous Media	42
Abstract	43
Introduction.....	43
Methodology.....	46
Inhomogeneous Porous Media Construction.....	46
The Lattice-Boltzmann Model.....	48
OpenMP Implementation.....	54
Results and Discussion	57
Conclusion	63
Appendix.....	65
CHAPTER III Single- and multi-phase flow analysis in inhomogeneous random porous channels: I. Single-phase, low-tortuosity flow with double path-percolation theory	86
Abstract	87
Introduction.....	88
Methodology.....	89
Double-path-percolation theory	90
Lattice-Boltzmann method	93
Parallel Implementation.....	96
Results and Discussion	99
Conclusions.....	104
Appendix.....	106
CHAPTER IV Single- and multi-phase flow analysis in inhomogeneous random porous channels: II. Effects of hydrophobic solid structures on mass transfer with single- and double-path-percolation theories.....	122

Abstract	123
Nomenclature	124
Introduction	126
Methodology	128
Confidence-Level Calculations	128
Hydrophobic Solid Addition	130
SRAE Selection Process	132
A Multi-Phase Lattice-Boltzmann Model	132
Pthreads Implementation	136
Effective Diffusion in Porous Channels	137
Results and Discussion	137
Conclusions	142
Appendix	144
CHAPTER V Single- and multi-phase flow analysis in inhomogeneous porous channels: III.	
Micro-computed PEFC gas diffusion layer geometries	158
Abstract	159
Nomenclature	159
Introduction	161
Methodology	165
Results and Discussion	174
Conclusions	177
Appendix	179
CONCLUSION	193
LIST OF REFERENCES	196
APPENDIX	201
VITA	204

LIST OF TABLES

Table 1.1. History calculations for path-percolation model.....	26
Table 1.2. History calculations for Lattice-Boltzmann model.....	27
Table 2.1. History calculations for multi-phase Lattice-Boltzmann model.....	66
Table 2.2. History calculations for RAEs in multi-phase Lattice-Boltzmann model.....	67
Table 2.3. Effective porosity, tortuosity, and diffusion ratio calculation example for SRAE with 0% condensation.....	68
Table 3.1. History calculations for double-path-percolation model.....	107
Table 3.2. History calculations for single-phase Lattice-Boltzmann model in double-path percolation theory.....	108
Table 5.1. History calculations for MRC-105 and SGL-25BA.....	180

LIST OF FIGURES

Figure 1.1 Random porous medium generation for three cases: (a) the worst case; porosity: 0.6002, effective porosity: 0.1634 (b) the medium case; porosity: 0.5975, effective porosity: 0.3119 (c) the best case; porosity: 0.6051, effective porosity: 0.5144.	28
Figure 1.2. SRAE size determination.....	29
Figure 1.3. SRAE size determination results.	30
Figure 1.4. SRAE element number determination; tortuosity against the element number.	31
Figure 1.5. A D_2Q_9 lattice (a) a lattice and its velocity components (b) red arrows are the lattice velocities at boundaries; the dashed ones are unknown.....	32
Figure 1.6. Probability distributions of porosities of three cases for three confidence levels, (a) $\Phi=90\%$, (b) $\Phi=75\%$, (c) $\Phi=60\%$	33
Figure 1.7. Probability distributions of porosities and effective porosities for three cases. Confidence level is 99%. (a) All three porosities (b) $\Phi=90\%$, (c) $\Phi=75\%$, (d) $\Phi=60\%$	34
Figure 1.8. Initial and final forms of three porous samples (a) Best Case ($\Phi=0.605050$, $\Phi_{\text{eff}}=0.499025$), (b) Medium Case ($\Phi=0.598900$, $\Phi_{\text{eff}}=0.321900$), (c) Worst Case ($\Phi=0.597200$, $\Phi_{\text{eff}}=0.139800$	35
Figure 1.9. Path-Percolation results – (a) Effective porosity vs. porosity. The horizontal axis is the target porosities of the domains generated by path-percolation method. For higher porosities, the effective porosities are quite predictable. When the target porosity decreases, effective porosities can take many different values, hence become difficult to predict, (b) tortuosity vs. porosity, (c) tortuosity vs. effective porosity.	36
Figure 1.10. An example procedure for a 60% porosity medium; (a) inhomogeneous porous domain with $\Phi=0.59705$, (b) effective domain with $\Phi_{\text{eff}}=0.59705$, (c) $\tau=1.30127$, (d) $\tau=1.39888$, (e) $\tau=1.31409$	37
Figure 1.11. Probability distributions of tortuosities for three cases with a confidence level of 99%, (a) $\Phi=60\%$, (b) $\Phi=75\%$, (c) $\Phi=90\%$	40
Figure 1.12. Bruggeman, Carman, and the new effective diffusivity model – $D_{\text{eff}}/D_{\text{bulk}}$ vs. effective porosity.	41
Figure 2.1. A D_2Q_9 lattice (a) a lattice and its velocity components (b) red arrows are the lattice velocities at boundaries; the dashed ones are unknown.....	69
Figure 2.2. Flowchart of the serial code for a single trial.	70
Figure 2.3. OpenMP implementation to the serial code. Flowchart of the parallel code for a single trial and demonstration of the fork-join model with 4 threads.owchart of the serial code for a single trial.....	71
Figure 2.4. Path-percolation model for initial porous medium generation (a) domain before cluster labelling (b) cluster labelling (c) effective domain (d) - (f) three random RAEs.	72
Figure 2.5. Effective porosity & tortuosity calculations for RAEs of an example trial with 80% porosity and 0% condensation (a) Φ_{eff} with 0% condensation (b) τ_{eff} with 0% condensation (a) Φ_{eff} with 10% condensation (b) τ_{eff} with 10% condensation (a) Φ_{eff} with 20% condensation (b) τ_{eff} with 20% condensation.....	73
Figure 2.6. Velocity vectors along RAE #2. Tortuosity is 1.153163.....	74
Figure 2.7. Evolution of phase separation of a 10% condensed two-phase fluid in REV #2.	75

Figure 2.8. Vapor phase mass transfer with a 10% condensation (a) liquid formation (b) the voids occupied by liquid are shown in gray (c) Mass transfer in vapor phase, the effective tortuosity is 1.310.....	76
Figure 2.9. Vapor phase mass transfer with a 20% condensation (a) liquid formation (b) liquid formations are shown in gray (c) Velocity field of the vapor phase, the effective tortuosity is 1.552.....	77
Figure 2.10. Effects of condensation on mass transfer for a single example trial (a) effective porosity and tortuosity vs. condensation (b) diffusion ratio vs. condensation.....	78
Figure 2.11. Confidence level results for initially generated 100x100 porous media with 70%, 80%, and 90% porosity.	79
Figure 2.12. Confidence level results for SRAEs with (a) 90%, (b) 80%, and (c) 70% porosity. Figures on the left and right are probability distributions of effective porosity and tortuosity, respectively.	80
Figure 2.13. Liquid formation in an example RAE for 70% target porosity (a) 10%, (b) 20%. .	81
Figure 2.14. Velocity fields in effective domains with (a) 0%, (b) 10%, (b) 20% condensation. Computed tortuosities are 1.403323, 1.447953, and 1.28602, respectively.	82
Figure 2.15. Diffusion ratio probability distributions with a medium with (a) 0%, (b) 10%, (c) 20% liquid formation.	83
Figure 2.16. Critical liquid formation probability distributions with a medium with 70%, 80%, and 90% target porosity.	84
Figure 2.17. Performance analysis for parallel application.	85
Figure 3.1. Random inhomogeneous porous medium generation.	109
Figure 3.2. Random porous medium with an aspect ratio and target porosity of 10 and 60%, respectively.	110
Figure 3.3. A D_2Q_9 lattice (a) a square lattice with nine velocity components (b) lattices at the boundaries with the unknown (dashed) components.	111
Figure 3.4. Flowchart of the single-phase serial code for a single trial.	112
Figure 3.5. SRAE extraction by (a) the serial code, and (b) the parallel code with 5 processors.	113
Figure 3.6. Results of the confidence level study for porosity. Target porosities and aspect ratios are (a) 55%, A=5, (b) 60%, A=15, and (c) 65%, A=10.	114
Figure 3.7. Results of the confidence level study for effective porosity with all three target porosities. The aspect ratios are (a) A=5, (b) A=10, and (c) A=15.	115
Figure 3.8. Two random porous channels generated by double-path-percolation theory. The aspect ratios are: (a) A=5, and (b) A=15.	116
Figure 3.9. A sample double-path-percolation and LBM procedure; (a) initially generated porous domain, target porosity = 0.6000, resulting porosity= 0.6002, (b) effective domain with an effective porosity of 0.6659, LBM results for (c) RAE #1 ($\Phi_{eff} = 0.6661, \tau_{eff} = 1.0010$) and (c) RAE #20 ($\Phi_{eff} = 0.6975, \tau_{eff} = 1.0028$).	117
Figure 3.10. Double-path-percolation results – (a) Tortuosity vs. effective porosity vs. porosity, (b) new diffusion model, (c) comparison with high-tortuosity (single-path-percolation) model.....	120
Figure 3.11. Speedup and performance achieved by three different high performance systems.	121

Figure 4.1. An inhomogeneous random domain with 52.5% hydrophobic content by single-path-percolation model. The active hydrophobic area is 54.0% of the total.....	145
Figure 4.2. A simple schematic of an active hydrophobic solid content in a representative inhomogeneous porous medium. The active hydrophobic area is 50%.....	146
Figure 4.3. An inhomogeneous random domain with 51.23% hydrophobic content by double-path-percolation model. The active hydrophobic area is 30.03% of the total.	147
Figure 4.4. 33% liquid formation in a channel with (a) 100% hydrophilic, (b) 100% hydrophobic surfaces.	148
Figure 4.5. Confidence level results for (a) porosity, (b) hydrophobic solid content ratio on the surface, (c) active hydrophobic area ratio.	149
Figure 4.6. Single-path-percolation model - Confidence level results for effective tortuosity for 0%, 50%, and 100% hydrophobic surface for the domains with porosities (a) higher than 75%, (b) between 60% and 75%, (c) lower than 60%.	150
Figure 4.7. Double-path-percolation model - Confidence level results for effective tortuosity for 0%, 50%, and 100% hydrophobic surface for the domains with porosities (a) higher than 75%, (b) between 60% and 75%, (c) lower than 60%.	151
Figure 4.8. Single-path-percolation model - Confidence level results of effective tortuosity for 10%, and 20% liquid formation for the domains with porosities (a) higher than 75%, (b) between 60% and 75%, (c) lower than 60%.	152
Figure 4.9. Double-path-percolation model - Confidence level results of effective tortuosity for 10%, and 20% liquid formation for the domains with porosities (a) higher than 75%, (b) between 60% and 75%, (c) lower than 60%.	153
Figure 4.10. Confidence level results for diffusion ratio for the domains with porosities above 75%. Hydrophobic surface content is (a) 0%, (b) 50%, (c) 100%.	154
Figure 4.11. Confidence level results for diffusion ratio for the domains with porosities between 60% and 75%. Hydrophobic surface content is (a) 0%, (b) 50%, (c) 100%.	155
Figure 4.12. Double-path-percolation model, diffusion ratio confidence level results with 0%, 50%, and 100% hydrophobic surface for the domains with porosities above 75%.	156
Figure 4.13. Speedup and performance achieved by pthreads implementation.....	157
Figure 5.1. Three-dimensional micro-tomography of (a) MRC-105, (b) SGL-25BA.....	181
Figure 5.2. A square D_2Q_9 lattice with nine velocity components for LBM.	182
Figure 5.3. A two-dimensional slice extracted from the three-dimensional digitized micro-tomography of MRC-105.....	183
Figure 5.4. A small portion of the selected 2-D slice with 5% PTFE loading.....	184
Figure 5.5. A subdomain extracted from the 2-D slice.....	185
Figure 5.6. RAE # 1 of the constructed SRAE set.....	186
Figure 5.7. Single-phase velocity distribution in RAE # 1.....	187
Figure 5.8. 10% liquid formation in RAE #1; (a) density distribution, (b) the effective domain after cluster labeling, (c) velocity distribution of a single-phase gas in the saturated medium.	188
Figure 5.9. 20% liquid formation in RAE #1; (a) density distribution, (b) the effective domain after cluster labeling, (c) velocity distribution of a single-phase gas in the saturated medium.	189

Figure 5.10. Effective porosity distributions of subdomains and RAEs extracted from MRC-105 and SGL-25BA data.....	190
Figure 5.11. PTFE loading (a) PTFE content in solid surface, (b) the ratio of active and total PTFE areas.....	191
Figure 5.12. Effects of liquid formation on effective porosity for (a) SGL-25BA, (b) MRC-105.	192

INTRODUCTION

In this dissertation, the effects of the internal structure of inhomogeneous porous media on single- and multi-phase mass transfer were investigated. A statistical approach called the path-percolation theory, and single- and multi-phase lattice-Boltzmann models were used with parallel programming implementations. Effects of liquid formation on two important functions of mass diffusion called the effective porosity and the effective tortuosity were analyzed. Furthermore, changes in effective diffusion coefficient of a gas with liquid formation in the channel were examined. The critical liquid formation in randomly generated channels was also presented statistically. The model was improved by including the surface-fluid effects, and the impact of hydrophobic material loading on the surface of the channel on two-phase mass flow was investigated. In addition to randomly generated porous channels, the micro-tomographies of two actual porous materials used in polymer electrolyte fuel cells (PEFC) as a gas diffusion layer (GDL) were digitized by an in-house program, and the diffusion analysis was performed with a statistical approach in two dimensions. Nano-scale computational simulations were performed to obtain macro-scale properties, and new effective diffusion models were developed for low- and high-tortuosity flow systems to be used in macro-scale diffusion models. The methodology introduced here provides an alternative aspect for mass diffusion analyses in porous medium applications.

Percolation theory is a probabilistic approach to simulate systems with multiple phases [1], hence can be used to simulate an inhomogeneous porous medium, constituted by solid particles and void. The percolation theory was adapted to statistically investigate the diffusion behavior of gasses in randomly generated porous channels in this project, and with an additional

process, called the cluster labeling process, a specific path-percolation model was developed, noting that the original path-percolation theory was developed by Jung et al. [2] to investigate the electrical property variations in inhomogeneous porous media.

The Lattice-Boltzmann Method (LBM) is a mesoscopic approach based on the kinetic theory of gases developed by Ludwig Boltzmann [3]. For transport simulations, a statistical treatment is performed for fluid molecules, and the interactions of these particles are described by streaming and collision mechanisms in kinetic theory [3-6]. The derivation of the cornerstone of the kinetic theory of gases, “the Lattice-Boltzmann equation” [4], is shown in the Appendix. In this model, behavior of a collection of particles as a unit [3, 6, 7] is investigated, and a distribution function represents any property of these units. LBM is used to simulate single and multiphase flows with a wide range of behaviors including condensation, cavitation, phase separation, and surface interaction.

These two models; the percolation theory and LBM, were combined in a limited number of studies, to investigate mass diffusion in inhomogeneous porous media. A few of them are explained briefly here. Ghanbarian et al. [8] introduced analytical models for gas and solute transfer in porous media using the percolation theory and the effective medium approximation. The results of this work were overlapped with the LBM simulations for all pore sizes. In their two-dimensional study, Nabovati and Sousa [9] simulated fluid flow in random porous media using LBM to determine the relation between permeability and porosity. Identical rectangles with free overlapping were located in the channels randomly. It was found that the permeability decreased when the regularity of the porous medium was disturbed in channels with the same porosity. Furthermore, permeability varied exponentially with porosity, regardless of the porous

media organization. Adrover and Giona [10] developed a model for permeability using a two-dimensional digitized porous structure image, starting from the Carman-Kozeny equation [11, 12]. Koponen et al. [13] used a lattice-gas cellular automation method to investigate the relationship between tortuosity and porosity. Overlapping of the rectangular solid particles, which were placed in the porous domain randomly, was allowed in the simulations. Tortuosity varied linearly with porosity, for a porosity range of 50% - 90%. Using the same methods, permeability and effective porosity of two-dimensional porous media were examined in another study of the same authors [14]. An incompressible Newtonian flow was studied, and curve fit equations for tortuosity, effective porosity, and permeability as functions of porosity were developed. Matyka et al. [15] performed a numerical investigation on tortuosity-porosity relation, using a microscopic porous medium model. The domain was arranged by freely overlapping squares, and streamlines of the flow were presented using LB theory. Moreover, a curve fit model was developed for tortuosity as a function of the system size and porosity. Grucelski and Pozorski [16] simulated fluid flow by LBM in a domain constructed by uniformly placing circular particles with different diameters within a certain range. Free overlapping and intersection of the particles with the system boundaries were allowed in domain construction method. The temperature profiles and pressure drop were obtained as the results of the study.

Many scientific articles [17-25] with multi-phase LBM in porous media were studied before constructing the current model. In multi-phase transport part of this project, a single-component multiphase (SCMP) LBM model was developed similar to the model developed by Chau et al. [26], in which a two-dimensional, SCMP LBM code was developed to investigate the effects of gravity on liquid formation, hence the gaseous diffusion in partially saturated porous

media. It was found that the effective diffusion coefficient shows a difference about 25% by different liquid configurations under zero gravity. Another consideration of this work is the effects of surface-fluid interactions on multi-phase mass transfer in inhomogeneous porous channels. A SCMP LBM was developed using the van der Waals equation of state to include the effects of the attractive forces between the molecules as introduced by Shan and Chen [27], and He and Doolen [28]. Moreover, the adhesive surface-fluid interaction force was also included in the model as introduced by Martys and Chen [29], and the impact of hydrophobic surface on multi-phase mass transfer was analyzed. Furthermore, effective diffusion coefficient of gases in two of PEFC GDL materials was also investigated computationally. Many previous works were performed with the same purpose [20, 30-40]. The uniqueness of this study is based on the statistical modeling it pursues, and the cluster labeling process. Preventing the overlap of the randomly distributed solid particles is also another novel outcome described in this work.

The outline of the dissertation is explained here. In Chapter I, a single-phase LBM was developed to investigate the diffusion behavior of gases in high-tortuosity inhomogeneous porous systems. Single-path-percolation theory was explained in detail, and effective porosity and tortuosity results with different confidence levels were examined. A multi-phase LBM was developed in Chapter II to observe a phase-separation in a multi-phase flow. Effects of liquid formation on effective diffusivity were investigated. The first high-performance system application on the code was introduced. Critical liquid formation was analyzed statistically. In Chapter III, a novel model called the double-path-percolation theory was introduced. Low-tortuosity flow systems were constructed, and a single-phase LBM was developed to investigate the gas diffusion in these systems. Three different high-performance computing systems were

implemented on the code, and computing performance was tested. In Chapter IV, the surface-fluid interactions were included in the model, and multi-phase and hydrophobicity effects on effective diffusion in both high- and low-tortuosity systems were investigated. The developed techniques in the previous chapters were applied on micro-computed tomographies of two GDL samples; MRC-105 and SGL-25BA with 5% polytetrafluoroethylene (PTFE) in Chapter V. A two-dimensional multi-phase model with surface effects was developed, and the statistical effective diffusion results were presented.

This work provides; a statistical approach to the transport modeling in porous media applications, a better understanding of the effects of internal structure of the porous layers on low- and high-tortuosity porous systems, more accurate effective diffusion models to be used in macroscopic models, and a path to a more accurate three-dimensional mesoscopic models with the introduced high-performance computing system implementations. The novel techniques introduced in this study can be utilized in any application area of heterogeneous porous media involved with single- and/or multi-phase mass and momentum transport with surface-fluid effects as multi-phase mass transport in a fuel cell, water supply management in hydrogeology, nuclear waste disposal, and underground water flow modeling. To the best of the researcher's knowledge, there has been no prior attempt to use such techniques.

CHAPTER I
APPLICATION OF PATH-PERCOLATION THEORY AND LATTICE-
BOLTZMANN METHOD TO INVESTIGATE STRUCTURE-PROPERTY
RELATIONSHIP IN POROUS MEDIA

A version of this chapter was originally published by Ozgur Cekmer, Sukkee Um, and Matthew M. Mench:

Ozgur Cekmer, Sukkee Um, Matthew M. Mench. “Application of path-percolation theory and Lattice-Boltzmann method to investigate structure-property relationship in porous media”, International Journal of Heat and Mass Transfer 86 (2015) 101-112.

Abstract

In this study, the path-percolation theory was applied to randomly generate porous media, and effective porosities of these domains were determined. A statistical approach was pursued to determine effective porosity with confidence levels of 95%, 97%, and 99%. Furthermore, the Lattice-Boltzmann method was applied to obtain the velocity distribution throughout the porous channels to evaluate effective tortuosity. Two dimensional lattices with nine velocity components were utilized for fluid flow simulations. A new effective diffusivity model for porous media was developed using effective porosity and tortuosity determined by path-percolation and Lattice-Boltzmann theories, respectively. Diffusion behavior of gasses in porous media as a function of porosity is typically unpredictable when the porosity is below 0.6, but the developed diffusion model as a function of effective porosity is shown to be useful in all effective porosity ranges.

Introduction

Percolation theory describes a probabilistic model that includes a phase transition [1]. This theory can be used to simulate an inhomogeneous medium, which must be constituted by at least two phases. As an example, a virtual, square porous media can be constructed randomly with void and solid constituents and it can be considered as a flow path. Let us assign the probability of generating a void (pore) as p , hence the solid generation probability becomes $1-p$. Percolation theory dictates that the fluid particles can only move in four directions; up, down,

left, and right, and they cannot move to cross nodes. The probability of an open path from the center of the porous domain to any of the sides is called the *percolation probability* and denoted by $\theta(p)$ [41]. Percolation probability becomes one if the whole domain is void, $\theta(1)=1$, and it starts decreasing as p decreases. After a critical point called the *percolation threshold*, p_c , it becomes zero.

The Lattice Boltzmann Method (LBM) is a mesoscopic scale technique, which lies between microscopic and macroscopic scale analyses, and is utilized by investigating the behavior of a collection of particles as a unit [3, 6, 7]. A distribution function represents any property of these units. LBM can be used to simulate single and multiphase flows with a wide range of behaviors including condensation, cavitation, phase separation, surface interaction, etc. In this study, LBM was utilized to simulate mass and momentum flow in randomly generated porous media.

There are a few studies which combine percolation theory and Lattice-Boltzmann applications to examine flow in porous media. Nabovati and Sousa [9] simulated fluid flow in two dimensional random porous media by using the Lattice-Boltzmann method to determine the relation between permeability and porosity. They randomly placed identical rectangles with free overlapping to construct the porous domains. It was found that the permeability decreased when the regularity of the porous medium was disturbed for the same porosity. Furthermore, permeability varied exponentially with porosity, independently from porous media organization. Koponen et al. [13] investigated the relationship between tortuosity and porosity by using a lattice-gas cellular automation method. In their simulations, they constructed their domain by randomly placing rectangles of the same size with free overlapping. A porosity range of 0.5 – 0.9

was used, while the tortuosity varied linearly with porosity. They also analyzed permeability and effective porosity of porous media by using the same methods as in [13] in another study [14]. A Newtonian, incompressible, two dimensional flow was used for the simulations and they obtained curve fit equations for tortuosity, effective porosity, and permeability as functions of porosity. Matyka et al. [15] performed a numerical study on the relation between tortuosity and porosity in a microscopic model of porous medium. The domain was arranged by freely overlapping squares and they obtained streamlines of the flow by using Lattice-Boltzmann theory. A new curve fit model was found for tortuosity depending on system size and porosity. Grucelski and Pozorski [16] applied the Lattice Boltzmann method to perform fluid flow and heat transfer computations. The domain was constructed by uniformly placing circular particles with different diameters within a certain range. They provided free overlapping and intersection of the particles with the system boundaries. The temperature profiles and pressure drop were obtained as the results of their study.

A new alternative method called *path-percolation modeling* was developed by Jung et al. [2] to simulate the electrical property variations in a spatially disordered porous medium. This method was adapted to the determination of micro-properties related to mass transfer through a porous medium in this study. After randomly constructing the porous domain, and performing the cluster labeling, the Lattice-Boltzmann method was utilized to solve the momentum balance equation and obtain the velocity distribution throughout the channel. The uniqueness of this study is based on the statistical modeling it pursues and the cluster labeling process, which is described in detail in the following section. Preventing the overlapping is also another novel outcome described in this study. Besides the stochastic based random diffusion media

generation, the other target of the study is to develop a new effective diffusivity model suitable for all values of porosity using effective porosity, tortuosity, and diffusion ratio determined by combined path-percolation and Lattice Boltzmann methods. The results of this study will be useful to predict the mass diffusion behavior in any porous medium application.

Path-Percolation Theory

There are three steps in this adaptation of statistical based path-percolation theory. The first step is determination of the system characteristics, specifically; total node numbers, trials and porosity. To do this; a confidence-level study must be performed. After determining the system characteristics, a random porous media generation is done as the second step. Pores or solids are assigned to each node in the porous medium depending on the specified porosity. A cluster labeling process is followed to eliminate the unconnected (orphan) pores, since they have no ability to transport through porous media. The physical counterpart of the percolation probability is the effective porosity, which is a micro-property of the porous domain. The effective porosity is distinct from the porosity, and obtained after the cluster labeling process.

Confidence Level Studies

The confidence level [42] expresses the reliability of any estimate and values of 95%, 97%, and 99% confidence levels were analyzed for our model.

$$Pr \left\{ \left| \frac{k}{n} - p \right| \leq \varepsilon \right\} = CL \tag{1.1}$$

In Equation (1.1), p stands for the probability of an event to occur, which is the probability of a pore to occur in a node in our analysis. Total trial number is represented by n whereas k stands for the number of cases of $Pr \{void\} = p$ in n trials. Error is represented by ε and shows the

difference between the true and estimated probabilities of an event. Finally, Pr and CL represent the probability of the event in the brackets and confidence level, respectively.

Equation (1.2) is obtained after applying the law of large numbers [42]:

$$Pr \left\{ \left| \frac{k}{n} - p \right| \leq \varepsilon \right\} = 2 \mathbb{G} \left(\varepsilon \sqrt{\frac{n}{pq}} \right) - 1 = CL \quad (1.2)$$

where $q=1-p$ is the probability of generating a solid, and \mathbb{G} is the Gaussian function which is related to error function as follows:

$$\mathbb{G}(z) - \frac{1}{2} = \text{erf}(z) \quad (1.3)$$

after combining Equations (1.2) and (1.3), the following relation is obtained:

$$\text{erf} \left(\varepsilon \sqrt{\frac{n}{pq}} \right) = \frac{CL}{2} \quad (1.4)$$

Error, ε , is accepted as 3×10^{-4} for this study. Although a wide porosity range was investigated in this study, confidence level studies of three cases with $\Phi=0.60$, $\Phi=0.75$, and $\Phi=0.90$ were analyzed in detail, and the related p values are 0.60, 0.75, and 0.90, respectively. Hence, the q values ($1-p$) become 0.40, 0.25, and 0.10. The total number of histories were calculated by using Equation (1.4) and an error function table [42]. Mathematically, the number of the history is the trial number multiplied by the total nodes. The calculations and the results are shown in Table 1.1.

Random Porous Media Generation with Cluster Labeling

After determining the trial numbers needed and the total node numbers, porous media generation with cluster labeling can be started. It should be emphasized that the porous media generated here are considered as gas diffusion channels, and the lower and upper boundaries are

accepted as inflow and outflow boundaries, respectively, while the side walls are impervious boundaries, and thus reflective.

An in-house program was developed to construct a porous medium by randomly assigning numbers between 1 and 100 to each node. After the random number assignment, the nodes with the values greater than 60 were accepted as solid and the remaining nodes became pores for a 60% porous medium simulation. Figures 1.1(a), (b), and (c) show a sample procedure for 60% porous media with low, medium, and high effective porosities, respectively. In this simple demonstration, 100 by 100 nodes were used. At this point, it must be emphasized that, since the transport of molecules is the basic consideration in this study; low, medium, and high effective porosities are therefore referred as worst, medium, and best cases, respectively. Hence, Figures 1.1(a), (b), and (c) show the worst, medium, and best cases for transport, respectively. The next step is the cluster labeling. The connected pores are grouped into clusters. Clusters that are connected to neither inflow nor outflow boundaries are eliminated and considered as orphaned and isolated, and are therefore equivalent to a solid. After cluster labeling, the effective diffusion domains are obtained as shown in Figure 1.1. The porosity of the effective domain is called the effective porosity. For the cases shown in Figures 1.1(a), (b), and (c) the effective porosities obtained are 0.1634 for the worst case, 0.3119 for the medium case, and 0.5144 for the best case, respectively. The entire path-percolation method procedure including the confidence level analyses was analyzed in the results section to explain and illustrate this model thoroughly.

Lattice-Boltzmann Method

Ludwig Boltzmann's works [3] are based on a statistical treatment performed for the particles that constitute a gas. Actions of the gas particles can be described by two mechanisms;

streaming in space and collisions. Detailed information about the kinetic theory of gases can be found in references [3, 6, 7]. The Lattice-Boltzmann Method (LBM) is a simplified form of Boltzmann's original view, by which the particle spatial positions are reduced and time is discretized into distinct steps. In this study, it was applied to obtain the velocity distribution and tortuosity for the porous channels, which were generated by statistical path-percolation theory.

RAE Selection

Although LBM is not as mathematically complicated as Navier-Stokes equations, since it is a first order partial differential equation (PDE), whereas the latter is second order, it is still computationally intensive. Therefore, before applying LBM to the current problem, a representative smaller domain should be chosen from the entire domain, which is called the representative area element (RAE). The RAE is a finite area in the domain, which represents the macroscopic properties of the entire domain with a specified accuracy.

In the current problem, the represented (post-cluster-labeling) macroscopic property is the effective porosity. However, the aim of using LBM is to solve the momentum balance equations and to determine the effective tortuosity. Hence, a single RAE may not represent the tortuosity of the entire porous domain with the desired accuracy, although it may represent the porosity of the entire area. Therefore, an alternative method is used in this study; instead of choosing a single RAE, a set of small areas called a statistical representative area element set (SRAE Set) is optimally chosen from the entire domain [43, 44]. There are two steps to determine SRAE. First, the size of the small areas must be considered. Then, the number of the

small areas in a set should be determined. For the first step, the domain was divided into sixteen regions, as shown in Figure 1.2.

Starting from a 1x1 matrix from the top-left corner of each section, matrix sizes are increased as 2x2, 3x3, etc. and the porosities are plotted against the matrix size. To do this, a random porous medium with 75% porosity is generated as described in Section 2. Then, the relative error between the porosities of the domain and the SRAEs were plotted against the SRAE size for each section shown in Figure 2. Four of these plots can be seen in Figure 3 and will be analyzed in the results section.

After the determination of the SRAE size, the number of elements in an SRAE set must be determined as the second step. To do this, confidence level studies are revisited. Total number of histories were already determined in Section 2.1, and as explained in Section 4.1, 99% confidence level is applied for tortuosity determination. Therefore, the node number and the total SRAE set number must be calculated for the momentum balance analysis regarding to the total history numbers shown in Table 1.1. The results are shown in Table 1.2.

The procedure is the same as before, except the node numbers. In this table, total history is defined as the multiplication of the SRAE set number (number of small RAEs), trial number, and node number of a single RAE.

To choose the constituents of the sets optimally, the entire domain is scanned and all possible SRAEs with the determined size are extracted and the errors are calculated. Starting from the SRAE with the smallest error (the best option), several SRAEs are added, respectively, and the ensemble average of the porosities with the relative errors are calculated (Figure 1.4).

It is expected that when the number of elements in an SRAE set increases, the relative error between the effective porosity of the entire domain and the ensemble averaged porosities will also increase, since the elements are optimally chosen. The ensemble averages for any property can be calculated as follows:

$$\hat{X} = \frac{1}{N} \sum_{m=1}^N X_m \quad (1.5)$$

In Equation (1.5), X_m is any property of the m^{th} element, N is the total element number, and \hat{X} is the ensemble average. The detailed analysis is explained in the results section.

LBM Utilization

In this section, application of LBM to the SRAEs are described. D₂Q₉ is a Cartesian lattice with 2 dimensions and 9 velocity components as seen in Figure 1.5(a) where f represents the velocity distribution function.

All nodes of the domain, which was obtained from path-percolation theory, are treated as D₂Q₉ lattices. The velocities of the lattices can be written as follows:

$$\begin{aligned} c_{0,x} = 0, c_{0,y} = 0, & \quad c_{1,x} = 1, c_{1,y} = 0, & \quad c_{2,x} = 0, c_{2,y} = 1 \\ c_{3,x} = -1, c_{3,y} = 0, & \quad c_{4,x} = 0, c_{4,y} = -1, & \quad c_{5,x} = 1, c_{5,y} = 1 \\ c_{6,x} = -1, c_{6,y} = 1, & \quad c_{7,x} = -1, c_{7,y} = -1, & \quad c_{8,x} = 1, c_{8,y} = -1 \end{aligned} \quad (1.6)$$

Collisions and streaming can be calculated by Equations (1.7) and (1.8), respectively, where f is defined as the distribution function.

$$f_k(x + c\Delta t, y + c\Delta t, t + \Delta t) - f_k(x, y, t) = -\mathbf{\Omega}[f_k(x, y, t) - f_k^{eq}(x, y, t)] \quad (1.7)$$

$$f_k(x + \Delta x, y + \Delta y, t + \Delta t) = f_k(x, y, t + \Delta t) \quad (1.8)$$

In Equations (1.7) and (1.8), c , x , y , and t represent speed of sound, horizontal coordinate, vertical coordinate, and time, respectively. $\mathbf{\Omega}$ is the collision matrix as shown in Equation (1.9):

$$\mathbf{\Omega} = M^{-1}SM \quad (1.9)$$

The constant matrix, M , and the relaxation matrix, S , are shown in Equations (1.10) and (1.11), respectively [6].

$$M = \begin{bmatrix} 1 & 1 & 1 & 1 & 1 & 1 & 1 & 1 & 1 \\ -4 & -1 & -1 & -1 & -1 & 2 & 2 & 2 & 2 \\ 4 & -2 & -2 & -2 & -2 & 1 & 1 & 1 & 1 \\ 0 & 1 & 0 & -1 & 0 & 1 & -1 & -1 & 1 \\ 0 & -2 & 0 & 2 & 0 & 1 & -1 & -1 & 1 \\ 0 & 0 & 1 & 0 & -1 & 1 & 1 & -1 & -1 \\ 0 & 0 & -2 & 0 & 2 & 1 & 1 & -1 & -1 \\ 0 & 1 & -1 & 1 & -1 & 0 & 0 & 0 & 0 \\ 0 & 0 & 0 & 0 & 0 & 1 & -1 & 1 & -1 \end{bmatrix} \quad (1.10)$$

$$S = \begin{bmatrix} s_0 & 0 & 0 & 0 & 0 & 0 & 0 & 0 & 0 \\ 0 & s_1 & 0 & 0 & 0 & 0 & 0 & 0 & 0 \\ 0 & 0 & s_2 & 0 & 0 & 0 & 0 & 0 & 0 \\ 0 & 0 & 0 & s_3 & 0 & 0 & 0 & 0 & 0 \\ 0 & 0 & 0 & 0 & s_4 & 0 & 0 & 0 & 0 \\ 0 & 0 & 0 & 0 & 0 & s_5 & 0 & 0 & 0 \\ 0 & 0 & 0 & 0 & 0 & 0 & s_6 & 0 & 0 \\ 0 & 0 & 0 & 0 & 0 & 0 & 0 & s_7 & 0 \\ 0 & 0 & 0 & 0 & 0 & 0 & 0 & 0 & s_8 \end{bmatrix} \quad (1.11)$$

$$s_0 = s_3 = s_5 = 1, \quad s_4 = s_6 = 1.2, \quad s_1 = s_4 - 0.1 \quad (1.12)$$

$$s_2 = s_1 - 0.1, \quad s_7 = s_8 = \frac{2}{1 + 6\nu}$$

where ν is the kinematic viscosity. f_k^{eq} is the equivalent distribution factor and can be formulated as follows:

$$f_k^{eq}(x, y, t) = w_k \rho(x, y, t) \left[1 + 3 \frac{\vec{c}_k \cdot \vec{V}}{c^2} + \frac{9 (\vec{c}_k \cdot \vec{V})^2}{2 c^4} - \frac{3 \vec{V}^2}{2 c^2} \right] \quad (1.13)$$

where, k , ρ , \vec{c}_k , and \vec{V} are lattice index, macroscopic density, unit lattice velocity, and velocity vector ($\vec{V} = u\vec{i} + v\vec{j}$), respectively. w_k is the weighting factor, which is defined for all lattice components in Equation (1.14) and c is equal to $1/\sqrt{3}$.

$$\begin{aligned} w_0 &= 4/9 \\ w_1 &= w_2 = w_3 = w_4 = 1/9 \\ w_5 &= w_6 = w_7 = w_8 = 1/36 \end{aligned} \quad (1.14)$$

The lattice density, and horizontal and vertical components of a lattice velocity can be determined by Equations (1.15), (1.16), and (1.17), respectively.

$$\rho = \sum_{k=0}^8 f_k \quad (1.15)$$

$$u = \frac{1}{\rho} \sum_{k=0}^8 c_{k,x} f_k \quad (1.16)$$

$$v = \frac{1}{\rho} \sum_{k=0}^8 c_{k,y} f_k \quad (1.17)$$

Bounce back boundary conditions were applied on side walls, whereas the lower boundary is input and the upper boundary is open. In Figure 5(b), three lattices at the boundaries are shown. The velocity vectors shown by dashed lines are not known, whereas the solid lines were calculated from streaming process. For the left and right side boundaries; fluid molecules bounce back from the walls. Hence, the dashed vectors become equal to solid ones. For inflow boundary, which is at the bottom of the channel; an equilibrium condition is used as shown in Equations (1.18) to (1.20).

$$f_2 - f_2^{eq} = f_4 - f_4^{eq} \quad (1.18)$$

$$f_6 - f_6^{eq} = f_8 - f_8^{eq} \quad (1.19)$$

$$f_5 - f_5^{eq} = f_7 - f_7^{eq} \quad (1.20)$$

Tortuosity (τ) is a measure of the actual path travelled by a particle, λ , divided by the shortest distance between the same points, H .

$$\tau = \frac{\lambda}{H} \quad (1.21)$$

An alternative way to determine the tortuosity by using the velocity profiles in the porous channel is shown in Equation (1.22).

$$\tau = \frac{\int_A V dA}{\int_A v dA} \quad (1.22)$$

Bruggeman's equation [45] is an approximation for the effective diffusion coefficient in porous media calculations and can be written as follows:

$$D_{eff} = D_{bulk} \Phi^m \quad (1.23)$$

D_{eff} and D_{bulk} represent the effective diffusion coefficient and bulk diffusion coefficient, respectively. In this equation, the power of the porosity is caused by the tortuosity which is assumed to be the denominator. Bruggeman's approximation estimates the tortuosity as follows [46]:

$$\tau = \Phi^{-0.5} \quad (1.24)$$

Hence, m becomes 1.5.

Carman [11], related the tortuosity to the effective diffusion coefficient:

$$D_{eff} = D_{bulk} \frac{\Phi}{\tau} \quad (1.25)$$

Both approximations are analyzed in this study.

Results

This study was initiated with random porous media generation by path-percolation method. The first step was the confidence level studies to obtain the needed total histories. Then, three effective porous domains were demonstrated for the worst, the medium, and the best transport cases. Path-percolation results are analyzed in Section 4.1. Before applying the LBM, SRAE sets were chosen and statistical representative area elements were determined. Hence, velocity fields were obtained in several domains and tortuosities were calculated using Equation (1.22). LBM results are discussed in Section 4.2. Effective porosities resulted by path-percolation theory and tortuosities calculated by LBM were used to derive a new model for effective diffusion coefficient. These results are summarized in Section 4.3.

Path-Percolation Theory

The path-percolation theory was applied for 60%, 75%, and 90% porous media with 95%, 97%, and 99% confidence levels. Probability distributions against porosity were plotted for all three porous media and confidence levels as seen in Figure 1.6.

To do this, porosities were divided into subgroups and after each simulation, the resulting porosity was added to its subgroup. The vertical axis is the occurrence frequency of the subgroups. As seen in the figures, the probability curves are Gaussian. In the case of 99% confidence level, the porosity ranges are smaller than the other cases. When confidence level decreases, the range of the probable porosity of the randomly generated porous media increases. Furthermore, the frequency of the desired porosity level increases with confidence level. Based on Figure 6, 99% confidence level was used in the remaining results described in this work.

In Figure 1.7(a), the probability distributions for porosities and effective porosities were plotted for all three porous cases with 99% confidence level. In Figure 1.7(b), the target porosity

is 90%, and it is observed that the probability distribution of effective porosity almost coincides with that for porosity. As seen in Figures 1.7(c) for 75% porosity, and (d) for 60% porosity, when the target porosity decreases, the effective porosity - probability distribution curve becomes wider in range, and shifts to the left. The Gaussian shape becomes more disturbed when the target porosity approaches to the percolation threshold. Figure 1.7(d) shows that the porosity probability curve is quite narrow in range and the frequency of the target porosity range almost reaches to 50%. As seen in Table 1.1, the node numbers and the trial number for this case are 200x200 and 443, respectively. However, the effective porosities are in a wide porosity range.

The same result is also explained in Figure 8. Here, three different simulations can be seen for the case of 60% porosity and 99% confidence level. Figures 1.8 (a), (b), and (c) demonstrates the best, medium, and worst transport cases, respectively. Porosities in all these cases are almost the same; 0.60505, 0.59890, and 0.59720. On the other hand, the *effective* porosities show significant differences. They are 0.499025, 0.321800, and 0.139800 for the best, medium, and worst cases, respectively.

The same conclusion can also be seen in Figure 9 (a). In this figure, porosities before and after the cluster labeling are plotted, and the effective porosities observed as more predictable for higher porosities. It is important to note that when porosity approaches the percolation threshold (Section 1) or the confidence level decreases, significant variances occur in the effective porosities.

The Lattice Boltzmann Model

Before utilizing LBM on the current problem, an SRAE set was constructed for each porous domain created by path-percolation theory as described in Section 3.1. A porous domain

was created and divided into 16 regions, as seen in Figure 1.2. Starting from the left upper part of each section by a 1x1 matrix (just a node), the node numbers were increased until the subdomain took the entire region. The relative errors between the porosities of the entire domain and the subdomains against the total node numbers of the subdomains, named statistically representative area elements, were plotted. Four of these sixteen regions were selected randomly for presentation as seen in Figure 1.3. For this study, it was decided that the relative errors of less than 1% was acceptable. Hence, 40x40 nodes were considered as sufficient after observing the results in all regions.

After deciding the total node number of an SRAE, element number in a SRAE was determined by confidence level studies. For each SREV set, 25 RAEs were determined as seen in Table 1.2. To optimally select these representative areas, the entire effective porous domain was scanned and all possible 40x40 area elements were extracted. Porosities and relative errors were calculated and the extracted areas were ranked according to their errors. Starting from one area element, tortuosities against the area element number were plotted, as seen in Figure 1.4. It should be noted that the ensemble averages were calculated by Equation (1.5), whereas the tortuosities were computed as explained in Section 3.2. To do this, Lattice-Boltzmann method in two dimensions was utilized to simulate the momentum transfer in the SRAE sets, which were extracted from porous media created by path-percolation theory. After obtaining the velocity distribution, tortuosity was calculated by using Equation (1.22). As a summary, an SRAE set, including twenty-five statistical area elements with 40x40 nodes, was considered as an RAE. Therefore, the ensemble averaged properties of these sets were considered as the property of the

RAE. Hence, tortuosities of the porous media generated by path-percolation theory were computed by using Lattice-Boltzmann method to obtain a new diffusion model.

One of the tests for 60% porosity is explained here in detail to clarify the entire procedure. An inhomogeneous porous medium was generated as seen in Figure 1.10(a) and the effective domain was obtained after cluster labelling process as shown in Figure 1.10(b). The porosity and effective porosity of this example are 0.597050 and 0.305625, respectively. Then, 25 representative area elements were extracted from the domain. The maximum relative error between the effective porosities of the selected RAEs and the entire domain is 1.287×10^{-12} . Then, momentum balance equation in all the RAEs was solved using LBM and the ensemble tortuosity of the SRAE was determined as 1.33467. Three of the RAEs with the velocity directions are shown in Figure 1.10(c) to (e).

The probability distributions for effective tortuosities for all porosity cases with 99% confidence level is shown in Figure 1.11.

As seen in the figure, the effective tortuosity has a great probability to have values between 1.0 and 1.2 for the case of 90% porosity. When porosity decreases, the range of the probable tortuosity values broadens. In addition, it can be seen that when the porosity increases, the occurrence frequency of a value of tortuosity also increases, hence the tortuosity can be said more predictable for higher porosities.

A New D_{eff}/D_{bulk} Model

A new approach was pursued in developing a new effective diffusion model using effective porosity instead of porosity. Further simulations were performed in addition to the results with the porosities of 60%, 75%, and 90% to include a wider range of porosity. Figure

1.12 shows a comparison between Bruggeman and Carman models with effective diffusion coefficient.

It must be stated that in both of these models, the porosity term was changed to the effective porosity. D_{eff}/D_{bulk} values were calculated using Φ_{eff} and τ obtained from path-percolation theory and Lattice-Boltzmann model and plotted against effective porosity for both models. As the effective porosity increases, two models predict closer effective diffusion coefficients. For the lower effective porosities, the Carman model has higher estimates. This is caused by the tortuosity factor. A new model is developed by using the path-percolation and LBM results and it can be seen in Figure 1.12 and Equation (1.26). The superscript counts for the tortuosity factor.

$$D_{eff} = D_{bulk} \Phi_{eff}^{1.6556} \quad (1.26)$$

This model is a starting point for this series of diffusion studies. There are several sources of potential error, which are the subject of ongoing study. First of all, this model is two-dimensional and there is a significant loss of accuracy because of this lack of geometry in the third dimension. Second, only the Carman model and simulation results were used for this model, and experimental validation is needed.

The advantage of including effective porosity instead of porosity in this model is the better accuracy in effective diffusion coefficient prediction especially when porosity is lower than 0.6. It is caused by the effects of tortuosity as shown in Figures 1.9(b) and (c). In these figures, it can be observed that when porosity is 0.6, the tortuosity range is much wider than that for the effective porosity. In other words, tortuosity is more predictable as a function of effective porosity than porosity. Therefore, the effective diffusion coefficient becomes much predictable

since it is strongly dependent on tortuosity. Note that, the effective porosity becomes zero when the porosity is below 0.6 and there is no mass flow observed in the domain at this porosity range. Thus, tortuosity becomes indeterminate. On the other hand, the physical porosity of any porous sample can be obtained experimentally very easily, but the effective porosity determination implies a path-percolation application, hence an additional effort. Hence, a digitized domain of the porous sample must be obtained to determine the effective porosity, before using this model.

Conclusion

Statistical based path-percolation theory was utilized to investigate the effective porosity of porous media in this study. Porous media were generated in a random manner and the orphan pores were eliminated by cluster labelling. Confidence levels of 95%, 97%, and 99% were examined and probability distributions for porosities and effective porosities were analyzed. When the porosity approaches the percolation threshold, or the confidence level decreases, the effective porosity becomes less predictable. A representative area element was determined to utilize the Lattice-Boltzmann simulations. A statistical approach was pursued and instead of using one RAE, an optimal set of statistical area elements were optimally extracted from the porous domain. After the size and the number of elements in a set were determined, LBM was performed to obtain the velocity distributions and tortuosity in porous channels. Using the effective porosities determined by path-percolation theory and the tortuosity values determined by LBM, an effective diffusion model was developed for dry porous media. In the new model, effective diffusion coefficient is a function of effective porosity instead of porosity and it is valid for all effective porosity ranges. The results of this work can be used in any porous media application related to heat and mass transfer.

Appendix

Table 1.1. History calculations for path-percolation model.

Confidence Level	$\text{erf}\left(\varepsilon \sqrt{\frac{n}{pq}}\right)$	$\varepsilon \sqrt{\frac{n}{pq}}$	ϕ	n	Trials	Nodes
95%	0.475	1.9604	0.90	3,843,168	384	100x100
			0.75	8,006,600	801	
			0.60	10,248,448	1025	
97%	0.485	2.1707	0.90	4,711,938	209	150x150
			0.75	9,816,539	436	
			0.60	12,565,169	558	
99%	0.495	2.5767	0.90	6,639,383	166	200x200
			0.75	13,832,048	346	
			0.60	17,705,021	443	

Table 1.2. History calculations for Lattice-Boltzmann model.

Confidence Level	$\text{erf}\left(\varepsilon \sqrt{\frac{n}{pq}}\right)$	$\varepsilon \sqrt{\frac{n}{pq}}$	ϕ	n	Trials	SREV Nodes	SREV Set Number
99%	0.495	2.5767	0.90	6,639,383	166	40x40	25
			0.75	13,832,048	346		
			0.60	17,705,021	443		

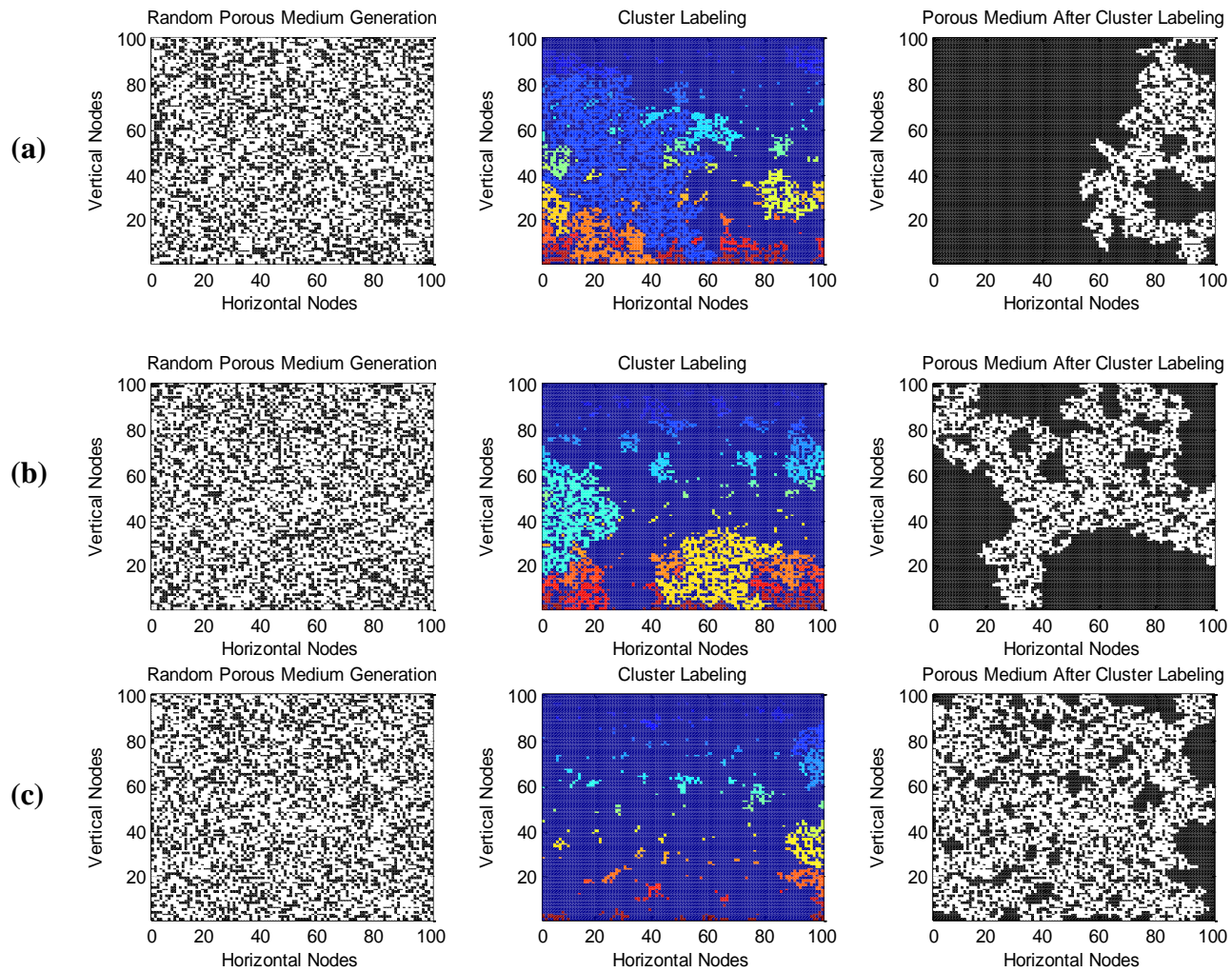
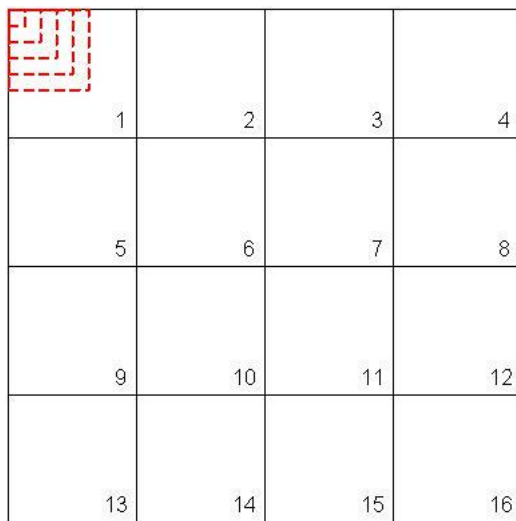


Figure 1.1 Random porous medium generation for three cases: (a) the worst case; porosity: 0.6002, effective porosity: 0.1634 (b) the medium case; porosity: 0.5975, effective porosity: 0.3119 (c) the best case; porosity: 0.6051, effective porosity: 0.5144.



1	2	3	4
5	6	7	8
9	10	11	12
13	14	15	16

Figure 1.2. SRAE size determination.

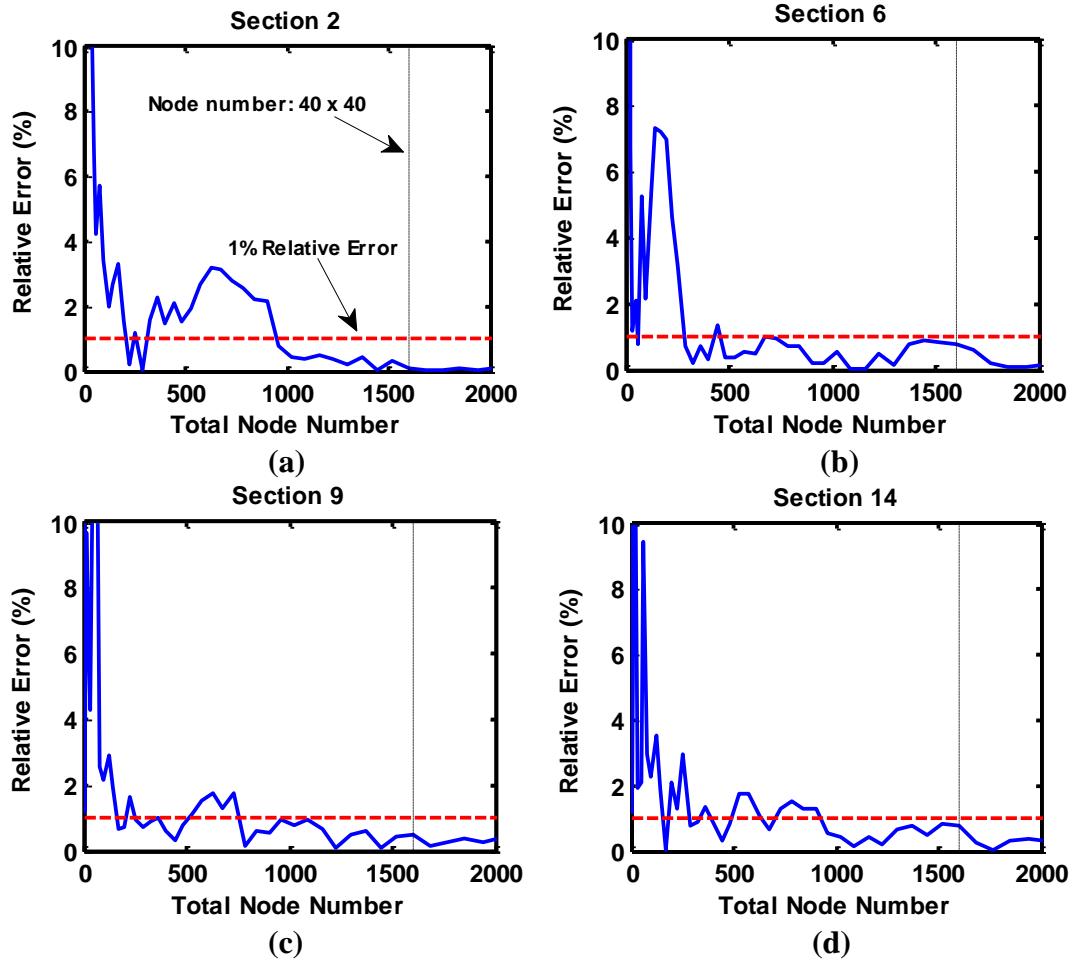


Figure 1.3. SRAE size determination results.

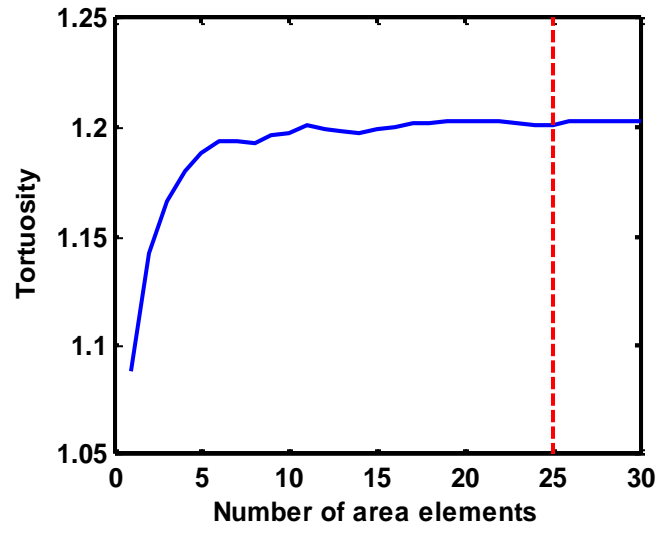


Figure 1.4. SRAE element number determination; tortuosity against the element number.

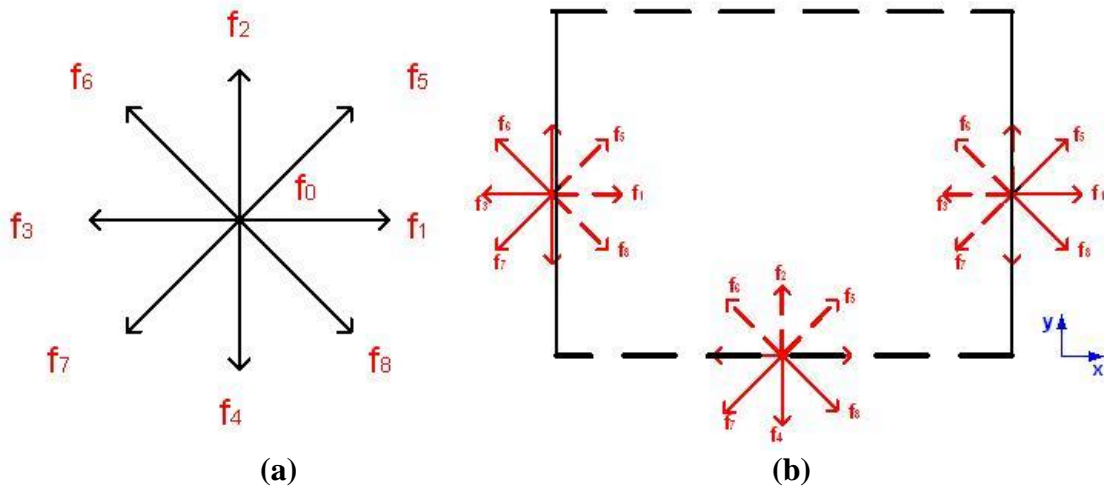


Figure 1.5. A D₂Q₉ lattice (a) a lattice and its velocity components (b) red arrows are the lattice velocities at boundaries; the dashed ones are unknown.

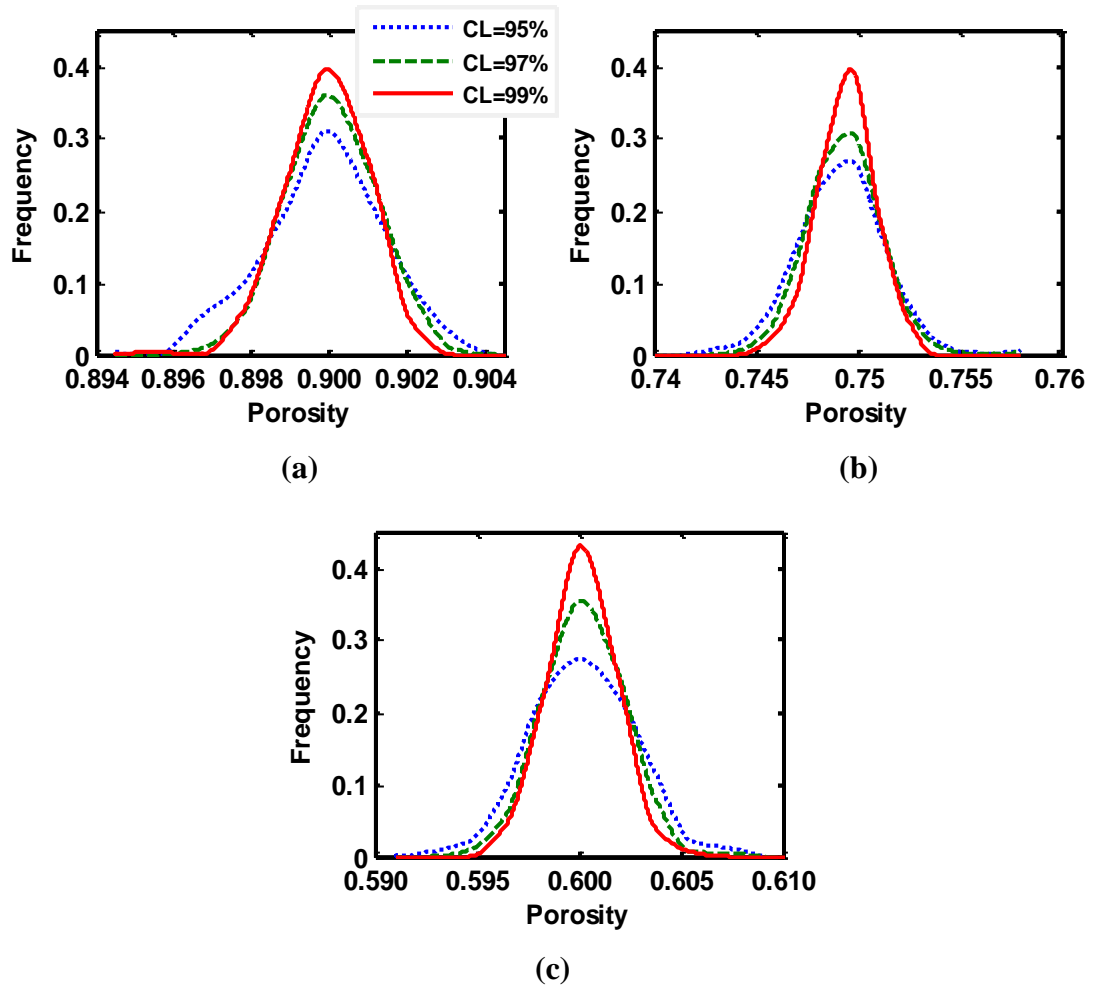
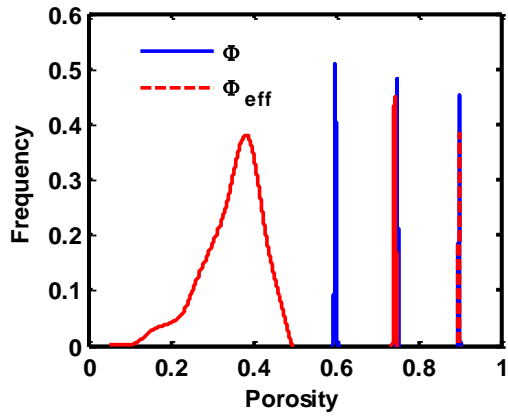
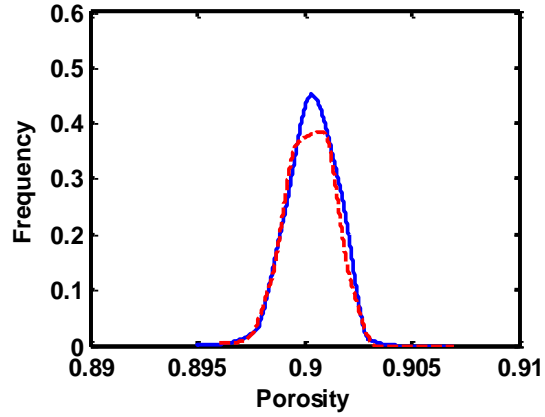


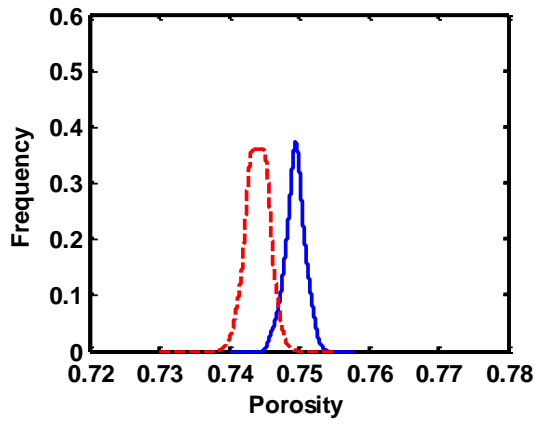
Figure 1.6. Probability distributions of porosities of three cases for three confidence levels, (a) $\Phi=90\%$, (b) $\Phi=75\%$, (c) $\Phi=60\%$.



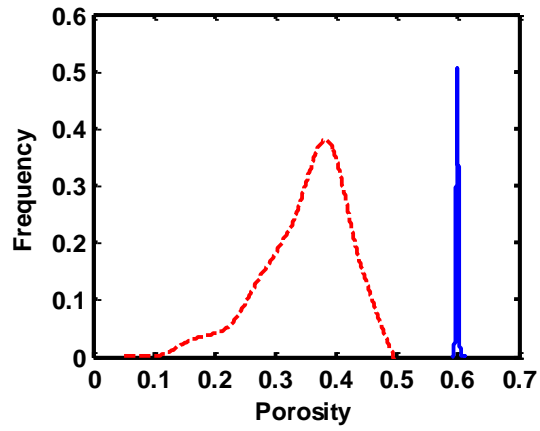
(a)



(b)



(c)



(d)

Figure 1.7. Probability distributions of porosities and effective porosities for three cases. Confidence level is 99%. (a) All three porosities (b) $\Phi=90\%$, (c) $\Phi=75\%$, (d) $\Phi=60\%$.

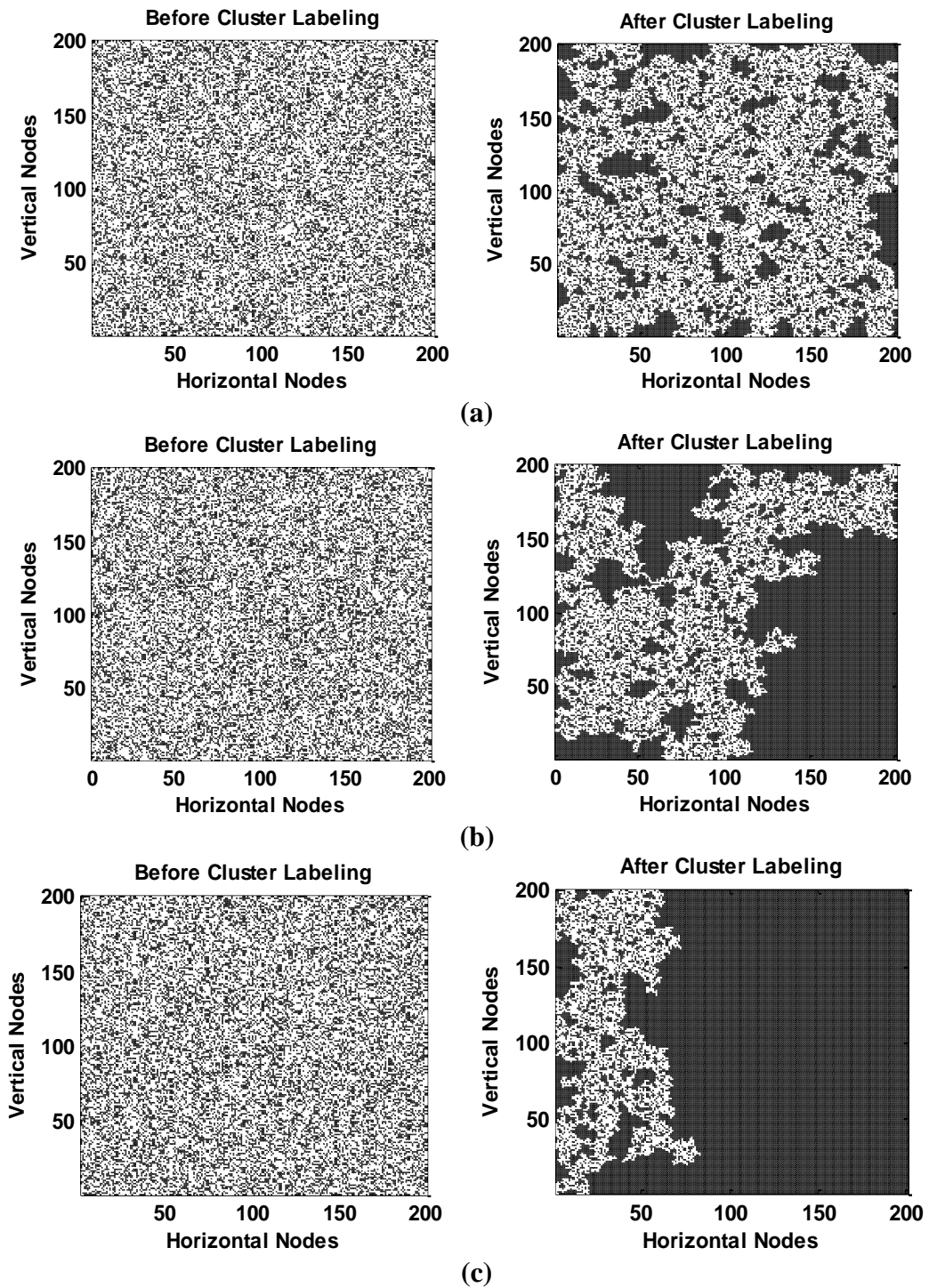


Figure 1.8. Initial and final forms of three porous samples (a) Best Case ($\Phi=0.605050$, $\Phi_{\text{eff}}=0.499025$), (b) Medium Case ($\Phi=0.598900$, $\Phi_{\text{eff}}=0.321900$), (c) Worst Case ($\Phi=0.597200$, $\Phi_{\text{eff}}=0.139800$).

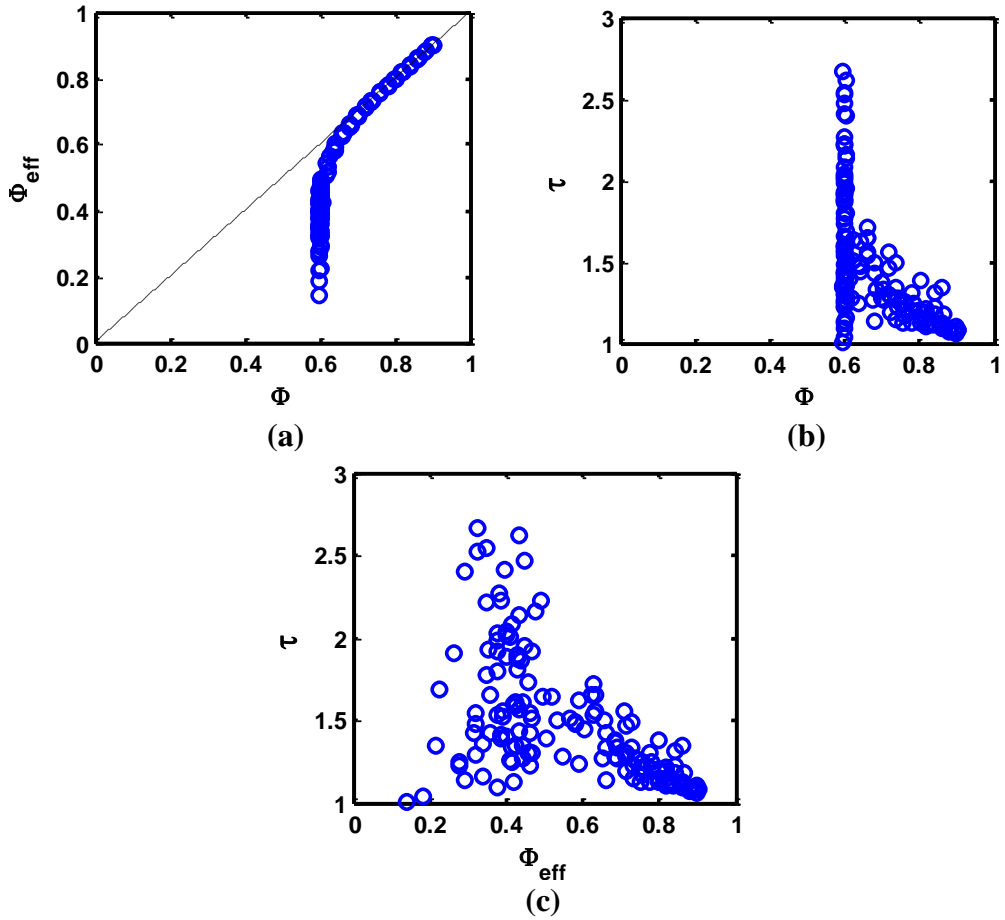


Figure 1.9. Path-Percolation results – (a) Effective porosity vs. porosity. The horizontal axis is the target porosities of the domains generated by path-percolation method. For higher porosities, the effective porosities are quite predictable. When the target porosity decreases, effective porosities can take many different values, hence become difficult to predict, (b) tortuosity vs. porosity, (c) tortuosity vs. effective porosity.

Figure 1.10. An example procedure for a 60% porosity medium; (a) inhomogeneous porous domain with $\Phi=0.59705$, (b) effective domain with $\Phi_{\text{eff}}=0.59705$, (c) $\tau=1.30127$, (d) $\tau=1.39888$, (e) $\tau=1.31409$.

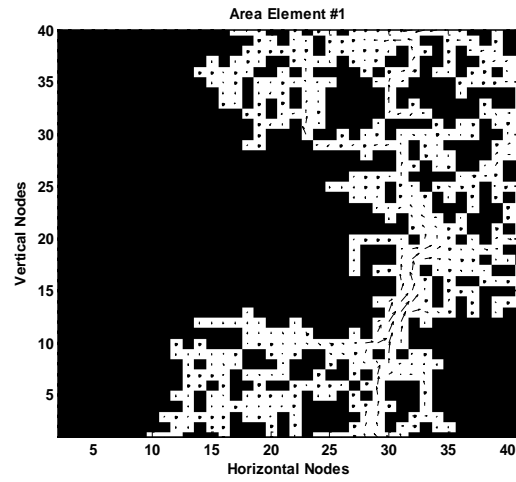
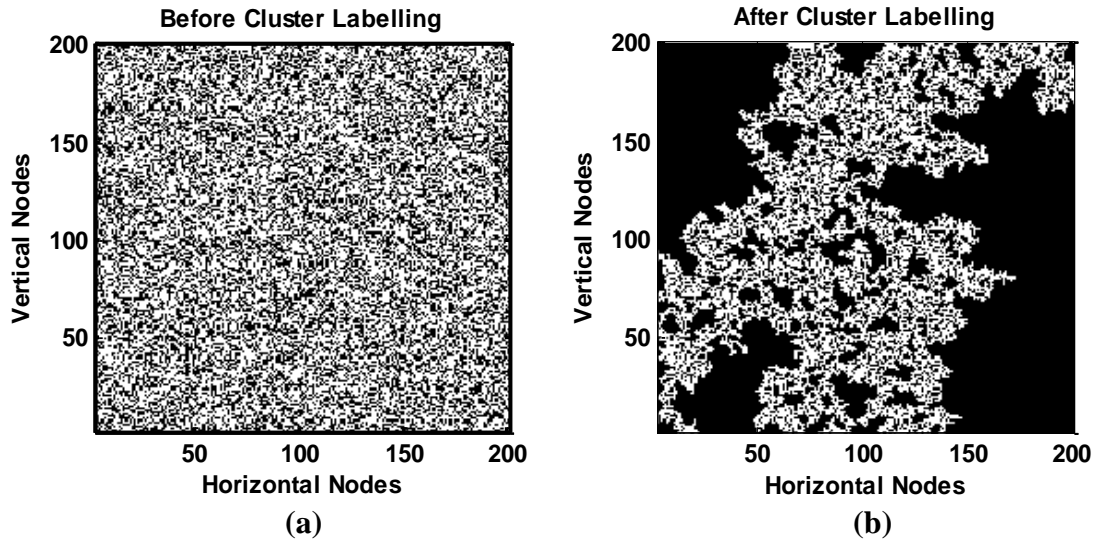
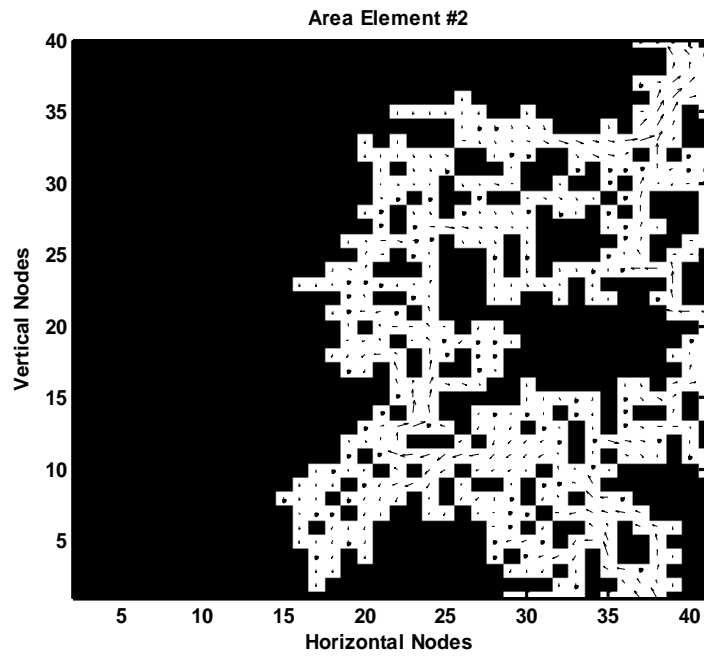
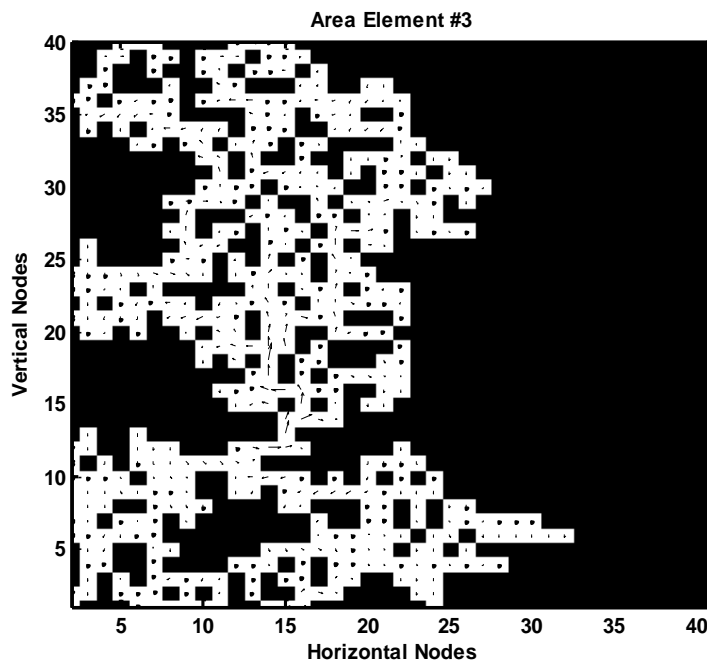


Figure 1.10. Continued



(d)



(e)

Figure 1.10. Continued

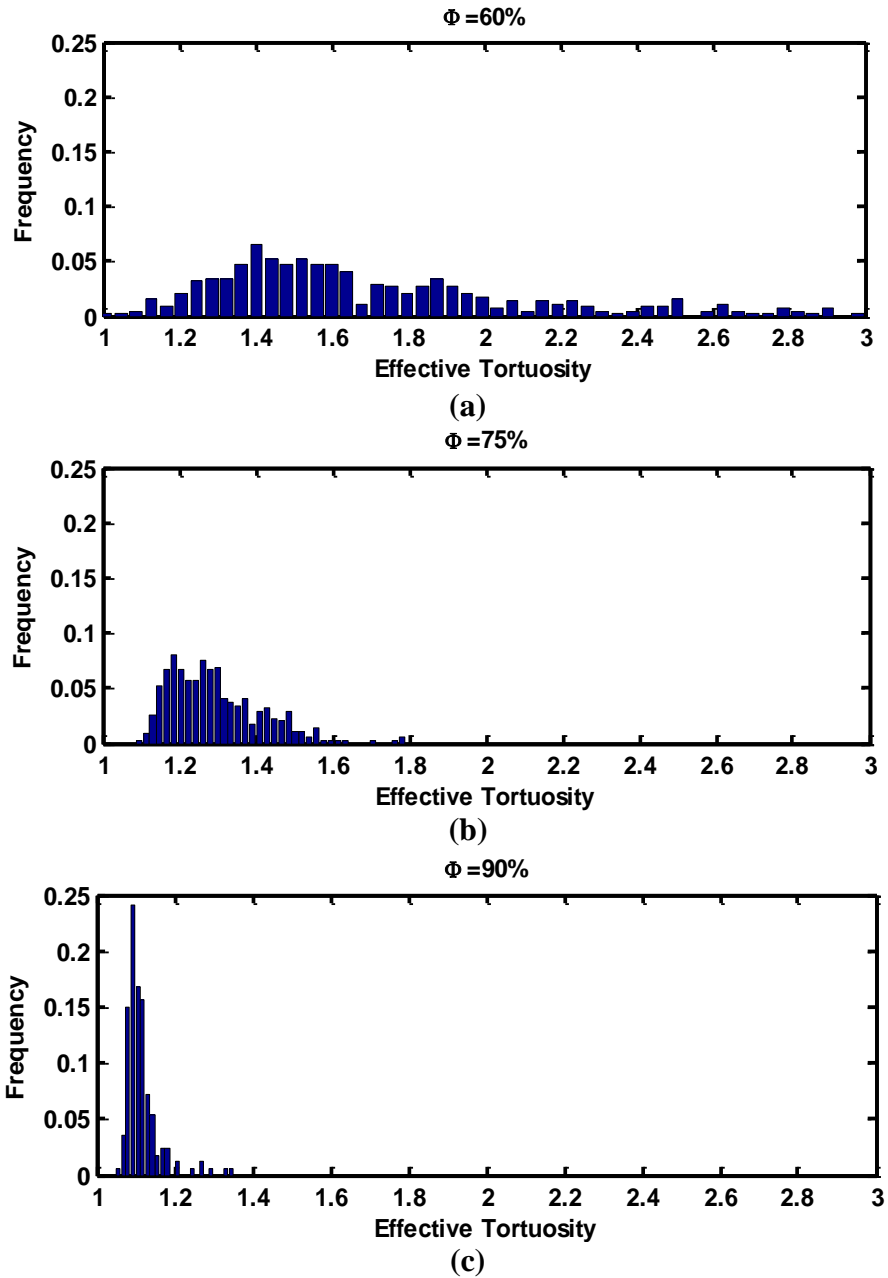


Figure 1.11. Probability distributions of tortuosities for three cases with a confidence level of 99%, (a) $\Phi=60\%$, (b) $\Phi=75\%$, (c) $\Phi=90\%$.

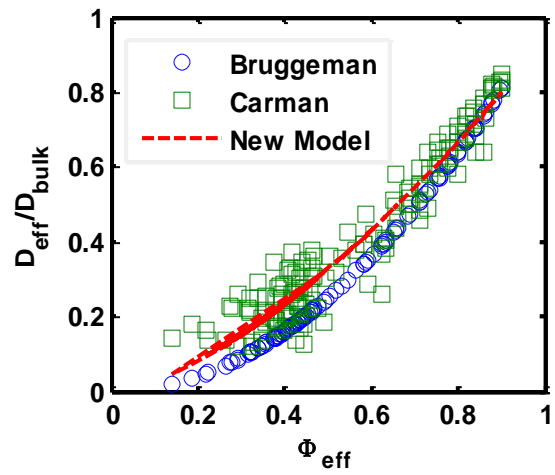


Figure 1. 12. Bruggeman, Carman, and the new effective diffusivity model – $D_{\text{eff}}/D_{\text{bulk}}$ vs. effective porosity.

CHAPTER II
A COMBINED PATH-PERCOLATION - LATTICE-BOLTZMANN
MODEL APPLIED TO MULTI-PHASE MASS TRANSFER IN POROUS
MEDIA

Abstract

In this chapter, single-component single-phase, and single-component multi-phase Lattice-Boltzmann models were developed to investigate the effects of liquid formation on mass transfer in porous channels via path-percolation theory. A two-dimensional lattice with nine velocity components was used in both lattice-Boltzmann models. A confidence level of 99% was utilized to obtain statistical results of porosity, effective porosity, and tortuosity of the system with 0%, 10%, and 20% liquid formation. Velocity distributions in randomly generated inhomogeneous porous channels with different solid-liquid-vapor combinations were analyzed. The statistical results show that the porosity range of the initially generated porous media lies between the specified error limit of 0.001 determined by the confidence level study for all three cases with 70%, 80%, and 90% target porosity. When target porosity decreases, the difference between porosity and effective porosity increases and the effective porosity range gets wider than the range of porosity. Effective diffusion coefficient decreases with increase in liquid formation, since the effective porosity decreases. An application programming interface called OpenMP was implemented on the developed serial in-house program and the effects of 1 to 4 threads on program performance and efficiency were investigated. The maximum speedup and performance gained are 3.3553 and 1.275 GFlops for 4 threads of a personal computer with a 38.4 GFlops peak performance.

Introduction

The Lattice-Boltzmann equation was derived by Ludwig Boltzmann in 1872, and is counted as the cornerstone of the kinetic theory of gases [4]. The Lattice-Boltzmann Method (LBM) is an explicit technique based on Ludwig Boltzmann's kinetic theory of gases [3] used to

simulate transport equations. In kinetic theory, a statistical treatment is performed for fluid particles, and the actions of these particles are described by streaming and collision mechanisms. Detailed information about the kinetic theory of gases can be found in references [3-6]. The LBM treats a group of particles as a lattice unit and investigates the behavior of the units in the system. In terms of computational fluid dynamics, LBM can be used to simulate single and multiphase flows, and in this study it was applied to simulate two-phase momentum transfer in porous media. Many studies with multi-phase LBM in porous media can be found in literature [17-25]. Among these, the authors decided to develop a single-component multiphase (SCMP) LBM model similar to that in the study of Chau et al. [26]. They used a two-dimensional, SCMP LBM code to investigate the effects of gravity on liquid formation, hence the gaseous diffusion in partially saturated porous media. They found that the relative (effective) diffusion coefficient shows about a 25% difference between different liquid configurations under zero gravity. The target of the current study is observing the effects of liquid formation on diffusivity by determining the effective porosity and tortuosity in randomly generated inhomogeneous porous channels with 0%, 10%, and 20% liquid formation based on a statistical point of view.

A statistical based “path-percolation theory” was developed by Jung et al. [2] to investigate the electrical property variations in inhomogeneous porous media. A process called “cluster labelling” was applied for a path determination scheme. Cekmer et al. [47] applied this theory with a combination of a single-phase lattice-Boltzmann model to investigate the mass transfer in randomly generated inhomogeneous porous media. A new effective diffusion model was developed in terms of effective porosity obtained by eliminating the orphan pores, which were not connected to the pathways between the inlet and outlet of a channel. This model was

also tested and compared with two well-known diffusion models [11, 45]. In this study, the path-percolation theory was utilized to generate random inhomogeneous porous channels and determine the effective porosity after liquid particles plugged some of the paths for the particles in vapor-phase.

In addition, an application programming interface called open multi-processing (OpenMP) was implemented to the code to gain higher performance and speedup, which is defined as the runtime ratio of the codes with single- and multi- threads. OpenMP was applied to solve SCMP LBM for many representative area elements of random porous channels by multi threads simultaneously instead of sharing a single LBM simulation to avoid the time lost by message passing between the nodes. However, the main novelty of this article is its statistical results of multi-phase effective diffusion process for a number of different solid-vapor-liquid configurations determined by the confidence level studies.

The motivation of this work is to develop a statistical based diffusion behavior estimation of two-phase systems in inhomogeneous porous media, following on previously developed work valid for single-phase flow only [47]. This work will provide a better understanding of the effects of internal structure of the porous channels on multi-phase mass flow than macroscopic approaches. The novel methods introduced and the outcome of the work can be utilized in any application area of heterogeneous porous media involving single- and multi-phase mass and momentum transport. Furthermore, the increased performance of the computational model with OpenMP implementation is another significant improvement, since it has a potential to provide a more accurate statistical results with a higher confidence level using high performance computing systems.

Methodology

Three different models were used in this study to investigate the effects of liquid formation on mass transfer in randomly generated porous media. The first one is called the path-percolation model and used for random porous media generation and cluster labelling process, which are explained in the following section. Then, a single-component single-phase (SCSP) LBM was utilized to solve the momentum balance equation and obtain the velocity distribution in representative area elements of the randomly generated channels. As the third model, a SCMP LBM was applied to observe the effects of liquid formation on mass transfer. Furthermore, parallel processing by OpenMP was implemented to the code and a performance analysis was performed.

Inhomogeneous Porous Media Construction

The statistical based path-percolation theory was used to generate random inhomogeneous porous media as the first step of the current study. To start with, a confidence level study was performed to obtain the necessary trial and node numbers of the simulations. A detailed analysis of confidence level studies can be found in [2, 47, 48]. In the current work, 99% confidence level was considered and procedure of the history number determination is as follows:

The confidence level [48] expresses the reliability of any estimate:

$$CL = Pr \left\{ \left| \frac{k}{n} - p \right| \leq \varepsilon \right\} \quad (2.1)$$

In Equation (2.1), p is the probability of a pore to occur in a node, which is called the porosity in this study. Total history number is represented by n whereas k stands for the number of void generation in n histories. Error is represented by ε and shows the difference between the

true and estimated probabilities of an event. As an example, if ε is 1% for a target porosity of 90%, then the resulting porosity of the statistically generated porous media would be between 89% and 91%, by a 99% of probability. Finally, Pr and CL represent the probability of the event in the brackets and confidence level, respectively. In this study, CL and ε are 0.99 and 0.001, respectively. Hence, Equation (2.1) says that the confidence level of 99% is the probability of the difference between the estimated and the true probabilities of the porosity to be lower than or equal to the assigned error, which is 0.001. After the application of the law of large numbers [48], Equation (2.2) is obtained:

$$Pr \left\{ \left| \frac{k}{n} - p \right| \leq \varepsilon \right\} = 2 \mathbb{G} \left(\varepsilon \sqrt{\frac{n}{pq}} \right) - 1 = CL \quad (2.2)$$

In Equation (2.2), q is the probability of generating a solid, hence it is $1-p$, and \mathbb{G} is the Gaussian function which is related to the error function as follows:

$$\mathbb{G}(z) - \frac{1}{2} = \text{erf}(z) \quad (2.3)$$

The following equation is obtained after inserting Equation (2.3) into Equation (2.2):

$$\frac{CL}{2} = \text{erf} \left(\varepsilon \sqrt{\frac{n}{pq}} \right) \quad (2.4)$$

Confidence level of 99% was applied to all three cases of $\Phi=0.70$, $\Phi=0.80$, and $\Phi=0.90$ reminding that the related p values are 0.70, 0.80, and 0.90, respectively. Hence, the q values ($1-p$) become 0.30, 0.20, and 0.10. The total number of history (n) is the trial number of the simulations multiplied by the total node number and is calculated by Equation (2.4) and an error function table [48]. The calculations and the results are shown in Table 2.1.

Hence, the trial number and node number for all three cases were determined and the next step is performing the simulations. An in-house program was developed to random inhomogeneous porous media generation by assigning random numbers to each 10,000 nodes. Then, depending on the porosity, the nodes are labeled as solid or void, reminding that the porous media generated here are considered as gas diffusion channels, and the lower and upper boundaries are accepted as inflow and outflow boundaries, respectively, while the side walls are impervious boundaries, and thus reflective.

For the next step, the cluster labeling process was performed [2, 47] by clustering the inter-connected pores. Orphaned (or isolated) clusters, which were not connected to either inflow and outflow boundaries, were eliminated and considered equivalent to a solid. The domain obtained after the cluster labeling process is called the effective domain, and the porosity of the effective domain is called the effective porosity. Thus, a single-component multiphase model can be developed now to investigate the momentum flow in the effective domains (channels) constructed by the path-percolation theory.

The Lattice-Boltzmann Model

The Lattice-Boltzmann Method (LBM) is a mesoscopic approach which lies between microscopic and macroscopic approaches. In LBM, individual particle tracking is not followed as in a true microscopic approach nor are the averaged properties of the entire system averaged as in a macroscopic approach. Instead, the average property of a selected cluster of molecules is used. The probability density function, f , must be introduced before analyzing the Lattice-Boltzmann model (LBM). The probability of a molecule to be at position \vec{x} at time t with momentum \vec{p} is called the probability density (or probability distribution) function, and

symbolized as $f(\vec{x}, \vec{p}, t)$. In this study, a two-dimensional lattice system called D₂Q₉ is applied to solve the momentum balance equation as shown in Figure 1(a). A D₂Q₉ has nine velocity components in two dimensions. The following coupled discretized equations are used for the collision and streaming steps [4].

$$f_k(x + c\Delta t, y + c\Delta t, t + \Delta t) - f_k(x, y, t) = -\frac{1}{\tau} [f_k(x, y, t) - f_k^{eq}(x, y, t)] \quad (2.5)$$

$$f_k(x + \Delta x, y + \Delta y, t + \Delta t) = f_k(x, y, t + \Delta t) \quad (2.6)$$

f_k^{eq} is the equivalent distribution function, and formulated for D₂Q₉ lattice as follows [5]:

$$f_k^{eq}(x, y, t) = w_k \rho(x, y, t) \left[1 + 3 \frac{\vec{c}_k \cdot \vec{u}}{c_s^2} + \frac{9}{2} \frac{(\vec{c}_k \cdot \vec{u})^2}{c_s^4} - \frac{3}{2} \frac{\vec{u}^2}{c_s^2} \right] \quad (2.7)$$

where, k , ρ , and \vec{c}_k are lattice index (0 to 8 as shown in Figure 1), macroscopic density, and unit lattice velocity vector, respectively. The lattice speed of sound is represented by c_s and equal to 1/3. The unit velocities of the lattice shown in Figure 1(a) can be written as:

$$\begin{aligned} c_{0,x} = 0, c_{0,y} = 0, & \quad c_{1,x} = 1, c_{1,y} = 0, & \quad c_{2,x} = 0, c_{2,y} = 1 \\ c_{3,x} = -1, c_{3,y} = 0, & \quad c_{4,x} = 0, c_{4,y} = -1, & \quad c_{5,x} = 1, c_{5,y} = 1 \\ c_{6,x} = -1, c_{6,y} = 1, & \quad c_{7,x} = -1, c_{7,y} = -1, & \quad c_{8,x} = 1, c_{8,y} = -1 \end{aligned} \quad (2.8)$$

Furthermore, w_k in Equation (2.7) is the weighting factor and defined for all lattice components as:

$$w_0 = 4/9 \quad (2.9)$$

$$w_1 = w_2 = w_3 = w_4 = 1/9$$

$$w_5 = w_6 = w_7 = w_8 = 1/36$$

The lattice density, and lattice velocity components are related to the probability distribution function as shown in Equations (2.10) to (2.12).

$$\rho = \sum_{k=0}^8 f_k \quad (2.10)$$

$$u_x = \frac{1}{\rho} \sum_{k=0}^8 c_{k,x} f_k \quad (2.11)$$

$$u_y = \frac{1}{\rho} \sum_{k=0}^8 c_{k,y} f_k \quad (2.12)$$

For the boundaries in Figure 1(b), bounce back boundary conditions were set on side walls, hence the dashed (unknown) vectors become equal to solid ones (computed by streaming process). The upper and lower boundaries are periodic. Thus, a single-component, single-phase D₂Q₉ model was constructed. To investigate the mass transfer in simulated porous media, a significant parameter called “effective tortuosity”, τ_{eff} , which is defined as the actual path travelled by a particle, divided by the shortest distance between the same points, should be computed. To do this, the velocity profile in the channel is used as follows [15]:

$$\tau_{eff} = \frac{\int_A u dA}{\int_A u_y dA} \quad (2.13)$$

To investigate the multiphase flow, a single-component multi-phase LBM must be constructed [5, 27]. No long-range attractive forces are considered between the molecules in a single-component single-phase model. In a single-component multi-phase model, intermolecular

interactions are considered and the attractive forces between the molecules cause a phase separation between liquid and vapor. Interaction between the solid surface and the fluid is not considered here and is left as a further study. In this paper, the main focus is on the effects of liquid volume on mass transfer in inhomogeneous porous media. The van der Waals equation of state (EOS), which is a non-ideal EOS, is used to account the intermolecular attractive forces in the model:

$$P = \frac{n_m RT}{V - n_m b} - a \left(\frac{n}{V} \right)^2 \quad (2.14)$$

where, T , V , n_m , and P are temperature, volume, number of moles, and pressure of the fluid, respectively, and R is gas constant. In Equation (2.14), the second term on RHS accounts for intermolecular attractive forces and $n_m b$ represents the non-negligible volume of molecules. The following equation, that was obtained by He and Doolen [28], is used as a simpler form of the van der Waals EOS and it is applied to compute the pressure distribution along the channel:

$$P = \frac{\rho}{3} + \frac{G}{6} \Psi^2 \quad (2.15)$$

where Ψ and G are interaction potential and interaction strength, respectively. The interaction potential is consistent in isothermal processes with the following formula [27]:

$$\Psi = \Psi_0 \exp\left(\frac{-\rho_0}{\rho}\right) \quad (2.16)$$

where, Ψ_0 and ρ_0 are arbitrary constants. Finally, the attractive force can be computed for a D_2Q_9 LBM by Equation (2.17).

$$F = -G\Psi(x, t) \sum_{k=1}^8 w_k \Psi(x + c_k dt, t) c_k \quad (2.17)$$

It must be noted that the non-negligible volume term of the van der Waals EOS is neglected in this approach. It is assumed that a two-phase fluid with a nonzero thermodynamic quality percolated an inhomogeneous channel, and then a phase separation occurred due to intermolecular attractive forces as time passes. Hence, there is no phase change in the channels. The initial density is the controlling parameter of the two-phase system. A typical simulation is demonstrated in the results section.

The developed single-component multi-phase LBM was not applied to the entire domain with the node number of 100x100 (Table 1). Instead, a set of representative area elements (SRAE) were used as domain. A representative area element (RAE) is defined as a smaller area that represents the entire domain. The represented parameters by RAE in this study are effective porosity and tortuosity since the mass transfer is investigated. However, only the effective porosity of the entire domain is known. Hence, a single RAE may not represent the entire domain, because there is no information about the tortuosity. To increase the accuracy of the representation, a certain number of RAEs were optimally extracted from the entire domain. The term "optimally extracted" means that the effective porosities of all possible RAEs were computed, then the relative errors between those and the effective porosity of the entire domain were determined, all RAEs were ranked, and the ones with the least errors were selected. To determine the node number of a single RAE and the number of RAEs in an SRAE, confidence level studies were repeated, as presented in Table 2. In this case, the total number of histories is the multiplication of trial number, node number of an RAE, and number of RAEs in an SRAE. The details of the SRAE selection procedure can be found in [43, 44, 47]. The ensemble average of any property of an SRAE can be calculated as follows:

$$\hat{X} = \frac{1}{N_{RAE}} \sum_{m=1}^{N_{RAE}} X_m \quad (2.18)$$

In Equation (2.18), X_m is any property of the m^{th} element, N_{RAE} is the total element number, and \hat{X} is the ensemble average. Hence, a single-component multi-phase model was completed.

To investigate the diffusion behavior, a dimensionless parameter called diffusion ratio, which is the ratio of the effective (D_{eff}) and bulk (D_{bulk}) diffusion coefficients, must be computed. Three diffusion models were discussed in this study. Bruggeman's model [45] approximates the effective diffusion coefficient as a function of porosity as follows:

$$D_{eff} = D_{bulk} \Phi^m \quad (2.19)$$

In this equation, the power of the porosity is caused by the tortuosity which is the denominator.

Tortuosity is estimated by the following equation, and m becomes 1.5 [46]:

$$\tau = \Phi^{-0.5} \quad (2.20)$$

Carman's model [11] includes tortuosity in addition to porosity to calculate the effective diffusion coefficient:

$$D_{eff} = D_{bulk} \frac{\Phi}{\tau} \quad (2.21)$$

The last model discussed in this study was developed by Cekmer et al.[47], and it will be tested in this study. In this new model, the tortuosity term was modeled as:

$$\tau = \Phi^{-0.6556} \quad (2.22)$$

Thus, the developed effective diffusion equation becomes:

$$D_{eff} = D_{bulk} \Phi_{eff}^{1.6556} \quad (2.23)$$

The resulting diffusion ratios will be computed by all these models, and discussed in the results section.

OpenMP Implementation

An in-house program was developed to utilize the path-percolation and Lattice-Boltzmann models to investigate the multi-phase mass transfer in randomly generated porous media. A simple flowchart of the serial code for a single trial is shown in Figure 2.2.

The program reads the input parameters and starts the path-percolation model. After applying the cluster labeling process, it prints the porosity and the effective porosity of the randomly generated inhomogeneous domain, then starts the SRAE selection process. It optimally extracts 16 RAEs for an SRAE and starts LBM to solve momentum balance equation for each RAE. Single-phase results are printed and the multi-phase loop starts by increasing the controlling parameter, which is the initial density. An automated scanning system is developed and applied to the code to obtain the exact liquid formations of 10% and 20% in the system and a critical liquid formation value where the effective porosity becomes zero and beyond that no fluid flow occurs. Multi-phase LBM followed by cluster labelling process is applied for all initial density values until the effective porosity of the RAE reaches zero (the critical liquid formation). When the liquid formation becomes 10% or 20%, the program sets up the new effective domain by treating the liquid volume that plugged the channels as solids, and then starts cluster labelling and single-phase LBM to obtain the effective porosity and tortuosity, respectively. Then, the computations for the new RAE starts until the set number is reached. Finally, the effective porosity and the tortuosity of an SRAE is calculated by Equation (2.18). Furthermore, the diffusion ratio of the SRAE is calculated by three models discussed in the previous section by Equations (2.19), (2.21), and (2.23).

As shown in Table 2.2, there are 4912 simulations to perform (total trials multiplied by the number of RAEs in a set). In a serial code, only one CPU with a single thread is used.

Parallelizing a code in CPU provides the execution of multiple sets of instructions (or threads) [49]. To use multi-threads in this study, OpenMP was implemented in the serial code. OpenMP is the abbreviation of Open Multi-Processing and it is a shared-memory application programming interface [50]. The parallel implementation is demonstrated in Figure 2.3.

After the SRAE set extraction and before the LBM application on the RAEs, an OpenMP FOR directive was implemented to allow multi-threads to work simultaneously. In Figure 2.3, in the upper red box, the term “chunk” stands for the number of tasks assigned per thread. Hence, each thread is assigned for one RAE (chunk=1). The command “dynamic” makes a thread be dynamically assigned to another RAE after completing one. If “static” assignment was selected, then the total number of the RAEs would be divided by the thread number and all the threads would be assigned to equal number of RAEs. A dynamic for loop was applied in this implementation. The fork-join model of OpenMP with four threads is also demonstrated in the figure. The program starts with a single thread, called master thread. When a parallel region starts, the master thread generates a specified number of threads. All the threads except the master thread are terminated at the end of the parallel region.

Speedup (S), which is defined as the ratio of the runtime with a single processor (T_1) to the runtime of the parallel configuration with n threads (T_n), is used in performance analysis of parallel implementation [49]:

$$S = \frac{T_1}{T_n} \quad (2.24)$$

Another parameter to demonstrate the performance of the parallel code is the parallel efficiency which is determined by dividing the speedup by the number of threads [50]:

$$\varepsilon_{parallel} = \frac{T_1}{n \cdot T_n} \quad (2.25)$$

To comment on the performance of the parallelized code, it will be useful to compare it with the peak performance of the used hardware. A personal computer with 4 processors with 2.40 GHz speed, each manages 4 instructions per cycle, in other words 4 floating-point operation (Flop) per cycle was used in this project. Hence, the peak performance becomes:

$$P_{peak} = \frac{2.40 \text{ GHz}}{1 \text{ core}} \times \frac{4 \text{ Flop}}{\text{cycle}} \times 4 \text{ cores} = 38.4 \frac{\text{GFlop}}{\text{sec}} \quad (2.26)$$

To calculate the performance of the code, total floating-point operations, which is a function of RAE effective porosity and number of multi-phase iterations per RAE, must be determined and divided by the runtime. The resulting number of the total floating-point operations in the code is calculated below:

$$N = 5.55 \times 10^9 \sum_{i=1}^{16} \Phi_{eff}(i)[ITER(i) + 3.4145] + 8.0128 \times 10^4 + 3 \sum_{i=1}^{16} ITER(i) \quad (2.27)$$

In Equation (2.27), ITER (i) is the iteration number for RAE number i where i=1,2,,...,16. In this equation, the second and the third terms do not contribute to the result, hence they are considered negligible. The resulting performance equation is shown in Equation (2.28).

$$P = 5.55 \times 10^3 \sum_{i=1}^{16} \Phi_{eff}(i)[ITER(i) + 3.4145] / \text{Execution Time} \quad (2.28)$$

A performance application programming interface (PAPI) timer [51] was used to measure the execution time. Three simulations per each porosity level were performed with different thread numbers and the results of the parallel program performance were analyzed in the following section.

Results and Discussion

The first step of this study is the confidence-level analysis, which is the beginning part of the statistical based path-percolation theory. As seen in Table 2.1, porous media with 70%, 80%, and 90% porosity and 100x100 nodes were generated, and the calculated trial numbers with 99% confidence level are 140, 107, and 60, respectively. Then, the cluster labelling process was performed for each trial to obtain the effective domains. Before, discussing the confidence level results, a typical trial with an 80% of target porosity is explained here.

In this example simulation, a random inhomogeneous porous medium was generated as seen in Figure 2.4(a) with a porosity of 0.809. Then, cluster labelling process was performed to group the interconnected pores, and eliminate the orphan pore clusters. In Figure 2.4(b), the orphan clusters can be seen with different colors. The effective domain was obtained after treating the orphan clusters as solid nodes as seen in Figure 2.4(c). The effective domain is now considered as a porous flow channel with an inlet at the bottom and an outlet at the top boundaries. The effective porosity was computed as 0.796. The next step is the SRAE extraction. The program optimally extracted 16 RAEs from the effective domain. Three samples are shown in Figure 2.4 (d)-(f).

The effective porosities of all of the RAEs can be seen in Figure 2.5(a). Then, a single-component single-phase LBM was applied to obtain the velocity distribution in these 16 domains and the effective tortuosities were computed as seen in Figure 2.5(b).

The same results were also demonstrated in Table 2.3 with an addition of effective porosity and tortuosity calculated for SRAE by Equation (2.31), and the diffusion ratios by three different models.

It can be concluded that the Carman model and the new model overlap within this effective porosity range (about 80%). The results for REV #2 were analyzed in detail in the remaining part of this example. The effective domain of this representative area can be seen in Figure 2.4(d). The path of the fluid particles was obtained after the application of single-phase LBM as shown in Figure 2.6.

The tortuosity was computed as 1.153 whereas the effective porosity was 0.8. The effects of liquid formation on effective porosity and tortuosity will be discussed in the next step. A multi-phase LBM was applied to the 16 RAEs of the domain of the example. At this time, a portion of the percolated fluid was assumed to be in two-phase and the liquid particles started to merge due to intermolecular attractive forces. The time evolution of this intermolecular attraction of a 10% condensed fluid in RAE #2 is shown in Figure 2.7.

It must be noted that all the units of the lattice parameters are called the lattice units and the relation to the SI units can be found in [4-6]. After 5 lattice seconds (ls) liquid and vapor phases started to separate from each other and the liquid particles clustered together as time passes. After 20,000 ls the system reached steady-state. To analyze the vapor flow in the channel, single-phase LBM must be applied. Before that, the system was set up by considering the liquid clusters as solid, since they plugged some of the void nodes. Then, the cluster labelling process was performed to obtain the new effective domain with 10% condensate as seen in Figure 8. Liquid formation is shown in gray in Figure 8(b) and they were considered solid as were orphan pore clusters. The effective domain with an effective porosity of 0.714 can be seen with the velocity field of the molecules in vapor phase in Figure 2.8(c). The effective tortuosity is observed to be increased to 1.310 when the condensate became 10%.

Figure 2.5(c) and (d) shows the effective porosities and tortuosities of all RAEs with a condensate of 10%, respectively. The effective porosity values decreased about 10% and a slight increase in tortuosity levels are observed. Similarly, 20% liquid formation effects is shown in Figure 2.9 and the effective porosity and tortuosity are 0.584 and 1.552, respectively.

In Figure 2.5(e) and (f), all the RAE parameters are demonstrated by a bar plot and the SRAE properties with diffusion ratio results are shown in Figure 10(a) and (b), respectively.

The statistical results guided by confidence level studies can be discussed at this point. The previous example was a single trial with 80% porosity. As seen in Table 2.1, 140, 107, and 60 trials must be completed for 70%, 80%, and 90% porosity, respectively, each with one SRAE constituted by 16 RAEs. The results for the porosities and the effective porosities of the initially generated random porous media are shown in Figure 2.11. In this figure, probability distributions for both porosities and effective porosities for the media with all three target porosities with a confidence level of 99% were plotted. The results for all trials were divided into subgroups and these subgroups were plotted versus their occurrence frequency. It is observed that all six curves have Gaussian shapes. For 90% target porosity, the effective porosity and porosity probability curves almost coincide. When the target porosity decreases, the effective porosity - probability distribution curve becomes wider in range, and shifts to the left.

Figure 2.12 shows the effects of liquid formation on effective porosity and tortuosity. In Figure 2.12(a), the results for 90% target porosity is shown. Effective porosity was decreased by increased liquid formation in the channel and the effective porosity probability distribution range was increased. Furthermore, the occurrence frequency was also decreased. Similar results were observed for the other target porosity cases, Figure 2.12(b) for 80%, and (c) for 70% target

porosity, respectively, only the distribution ranges got wider, and the occurrence frequency was decreased with target porosity. The effective tortuosity results do not show a certain trend as the effects of liquid formation on effective porosity as seen in the figures on the right, especially for the target porosity of 70% (Figure 2.12(c)). To start with, as the target porosity decreases the tortuosity in dry media and the probability distribution range of tortuosity increase. For a target porosity of 80% and 90%, the liquid formation increases the tortuosity (Figure 2.12(a) and (b)) as in the example for 80% target porosity discussed above (Figures 2.4 to 2.10). For 70% target porosity, the results do not follow this trend for 20% condensate as seen in Figure 2.24(c). For 10% liquid formation, tortuosity probability distribution curve slightly shifts to the right and the width of the curve slightly increases. For 20% liquid formation, the curve shifts to the left and gets wider in range. To understand this behavior, many trials were examined, one of which is discussed here. The trial had a target porosity of 70% and the resulting porosity and effective porosity values are 0.701 and 0.687, respectively. Multi-phase effects in RAE #1 was studied and shown in Figures 2.13 and 2.14.

In Figure 2.13 (a) and (b), 10% liquid formation is observed and the cluster labelling was applied to the figures on the right. The domains in Figure 2.14 are the effective domain obtained after cluster labelling process. In Figure 2.14(a), the velocity field in a dry domain is shown. The computed effective porosity and tortuosity are 0.686 and 1.403, respectively. With 10% liquid formation, a portion of the channel at bottom left was closed by liquid clusters and a little portion of that was constituted by orphan clusters, hence eliminated and considered as solid by cluster labelling process. Then, tortuosity increased to 1.448 whereas the effective porosity decreased to 0.576. The related velocity field can be seen in Figure 2.14(b). With 20% condensate, the liquid

clusters from the previous case with 10% condensate widened and a new liquid cluster occurred as seen in Figure 2.13(b). The velocity field in the effective domain for this case can be seen in Figure 2.14(c). After comparing the paths of the molecules between dry and 20% liquid cases, it is observed that two main paths (one on the left and one at the center) were eliminated as seen in Figure 2.14(c). Hence, the most of the molecules travel from the right part of the channel with a tortuosity of 1.286. The effective porosity in this case is 0.522. It can be concluded that the eliminated paths by liquid formation made the tortuosity decrease. Although a reduced tortuosity improves the mass transfer [11], the effective diffusion coefficient can still decrease, because of the changes in the effective porosity, which have a great impact on mass transfer. Figure 2.15 shows the effects of liquid formation on diffusion ratio in porous media with a target porosity of 70% for three diffusion models. As observed in the figure, diffusion ratios calculated by all three model equations decreased with increasing liquid formation in porous channels and the probability distribution curves of diffusion ratio got wider in range. Furthermore, it can be seen that the diffusion ratio calculated by the Carman model differed significantly from the other models in media with 20% liquid formation. The reason is clearly the tortuosity effect. From Figure 2.15, it can be concluded that the effects of tortuosity become more important in mass transfer when the liquid formation increases and the effective porosity decreases.

The critical liquid formation is another consideration of mass transfer. When the liquid formation reaches a critical value where the effective porosity becomes zero, no more mass transfer occurs in a channel. Figure 2.16 shows the critical liquid formation probability distributions for all target porosities. For 90% target porosity, critical liquid formation had values between 0.5 and 0.8, and the range was approximately 0.3, as seen in the Figure 2.16. The

maximum occurrence frequency is 22% and the related critical liquid formation is around 70%. Critical liquid formation probability range increases significantly by decreased target porosity. The maximum occurrence frequency for 80% porosity is about 20% and the most encountered critical liquid formation values are around 45%. The critical liquid formation has values between 0.32 and 0.69, hence the range is 0.37, which is 7% greater than that for 90% target porosity. For 70% target porosity, the critical liquid formation has values between 0.16 and 0.57, hence the probability distribution range is 0.41, which is 4% and 11% larger than the cases with 80% and 90% target porosity. On the other hand, the maximum occurrence frequency reduced to 16% for around 32% critical liquid formation.

OpenMP was implemented to the code and the plots for speedup, parallel efficiency, and performance of the simulations for three domains with 70%, 80%, and 90% target porosity can be seen in Figure 2.17. The maximum performance was obtained with 4 threads for the channel with 90% porosity as 1.275 GFlops, which is 2.6% of the peak performance. The related speedup and efficiency were computed 3.355 and 83.88%, respectively. The performance and speedup decreased with reduced target porosity. The reason of this result is that the total iteration number also decreases with the target porosity, since the program finds the critical liquid formation faster. It is concluded that the change in iteration number gets greater than the change in execution time (Equation 2.40), when target porosity increases. On the other hand, when more than 4 threads were used, no further speedup was achieved and the efficiency continued to decrease. Therefore, the most efficient way for this particular program with used hardware is assigning one thread to each physical core. The best option with the specified confidence level study is using 16 physical cores and assigning 16 threads.

This model is a two-dimensional approximation to a multi-phase problem in a porous medium and there are several sources of potential error. The surface-liquid interaction effects were neglected. Furthermore, the neglected third dimension would cause a significant loss of accuracy. Moreover, an experimental validation is needed for this computational study. On the other hand, an improvement on parallel application can be performed by utilizing an alternative hybrid parallel model to increase the speedup, efficiency, and performance. These missing physics are the subject of the ongoing study.

Conclusion

In this chapter, the path-percolation theory and Lattice-Boltzmann method were utilized to develop a model to investigate the effects of liquid formation on mass transfer in porous media. A statistical study with 99% confidence level was performed to analyze the behavior of effective porosity and tortuosity under different solid-liquid-vapor configurations of the media with 70%, 80%, and 90% porosity. The results show that the effective porosity decreases when the liquid formation in a channel increases. The impact of liquid formation on effective tortuosity changes with porosity. For porous media with 80% and 90% target porosity, effective tortuosity increases with liquid formation. For 70%-porosity media, it increases slightly when the liquid formation becomes 10%. When there is 20% liquid in the channel, the tortuosity decreases because of plugged long paths of the vapor molecules by liquid clusters. Effective diffusion coefficients of randomly generated inhomogeneous porous channels with liquid formations of 0%, 10%, and 20% were also studied, and it is concluded that the diffusion ratio decreases with liquid formation. Furthermore, critical liquid formation was investigated for all three media and its value increased with increased target porosity as expected. On the other hand, when the target

porosity decreases, it becomes hard to predict the critical liquid formation since the range of the possible results gets wider. Finally, OpenMP was implemented to the model code and a performance analysis was applied using multi threads. The observed maximum speedup was 3.355 with a performance of 1.275 GFlops using four threads.

The results of this study can be used for any porous media application related to two-phase mass transfer and it is expected to provide an alternative statistical source to estimate the effective porosity, tortuosity, and diffusion ratio in porous media with a range of porosity and liquid formation.

Appendix

Table 2.1. History calculations for multi-phase Lattice-Boltzmann model.

Confidence Level	$\text{erf}\left(\varepsilon \sqrt{\frac{n}{pq}}\right)$	$\varepsilon \sqrt{\frac{n}{pq}}$	Nodes	ϕ	n	Trials
99%	0.495	2.5767	100x100	0.70	1,394,270	140
				0.80	1,062,301	107
				0.90	597,544	60

Table 2.2. History calculations for RAEs in multi-phase Lattice-Boltzmann model.

Confidence Level	$\text{erf}\left(\varepsilon \sqrt{\frac{n}{pq}}\right)$	$\varepsilon \sqrt{\frac{n}{pq}}$	ϕ	n	Trials	RAE Nodes	SRAE Set Number
99%	0.495	2.5767	0.70	1,394,270	140	25x25	16
			0.80	1,062,301	107		
			0.90	597,544	60		

Table 2.3. Effective porosity, tortuosity, and diffusion ratio calculation example for SRAE with 0% condensation.

RAE							
#	ϕ_{eff}	τ_{eff}	$\phi_{\text{eff,SRAE}}$	$\tau_{\text{eff,SRAE}}$	$Q_{\text{Bruggeman}}$	Q_{Carman}	Q_{NewModel}
1	0.795200	1.150737					
2	0.800000	1.153163					
3	0.801600	1.154434					
4	0.798400	1.157320					
5	0.793600	1.155720					
6	0.798400	1.162446					
7	0.796800	1.173685					
8	0.792000	1.161168	0.795200	1.164617	0.709112	0.682800	0.684272
9	0.795200	1.130812					
10	0.798400	1.161545					
11	0.792000	1.169265					
12	0.788800	1.170493					
13	0.788800	1.175958					
14	0.790400	1.177900					
15	0.792000	1.196414					
16	0.801600	1.182811					

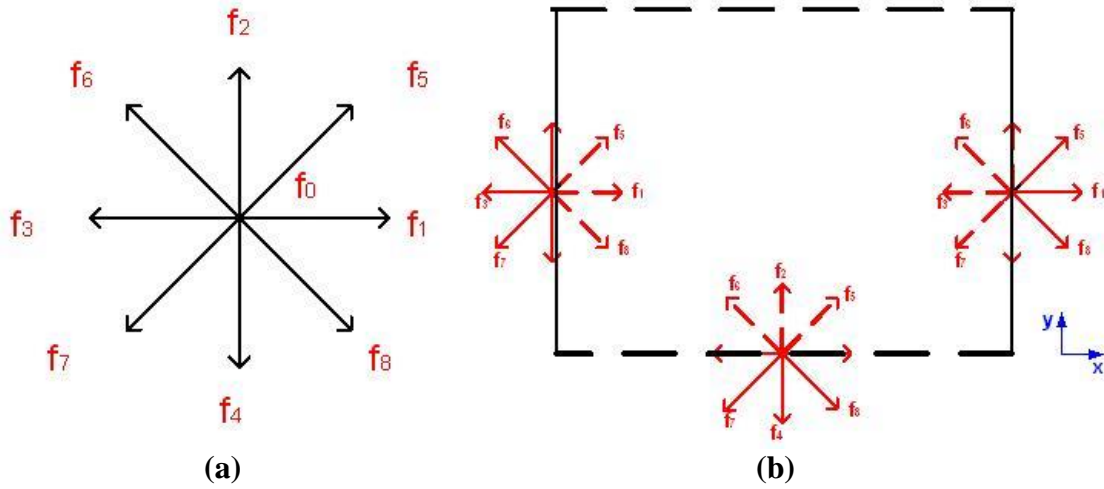


Figure 2.1. A D_2Q_9 lattice (a) a lattice and its velocity components (b) red arrows are the lattice velocities at boundaries; the dashed ones are unknown.

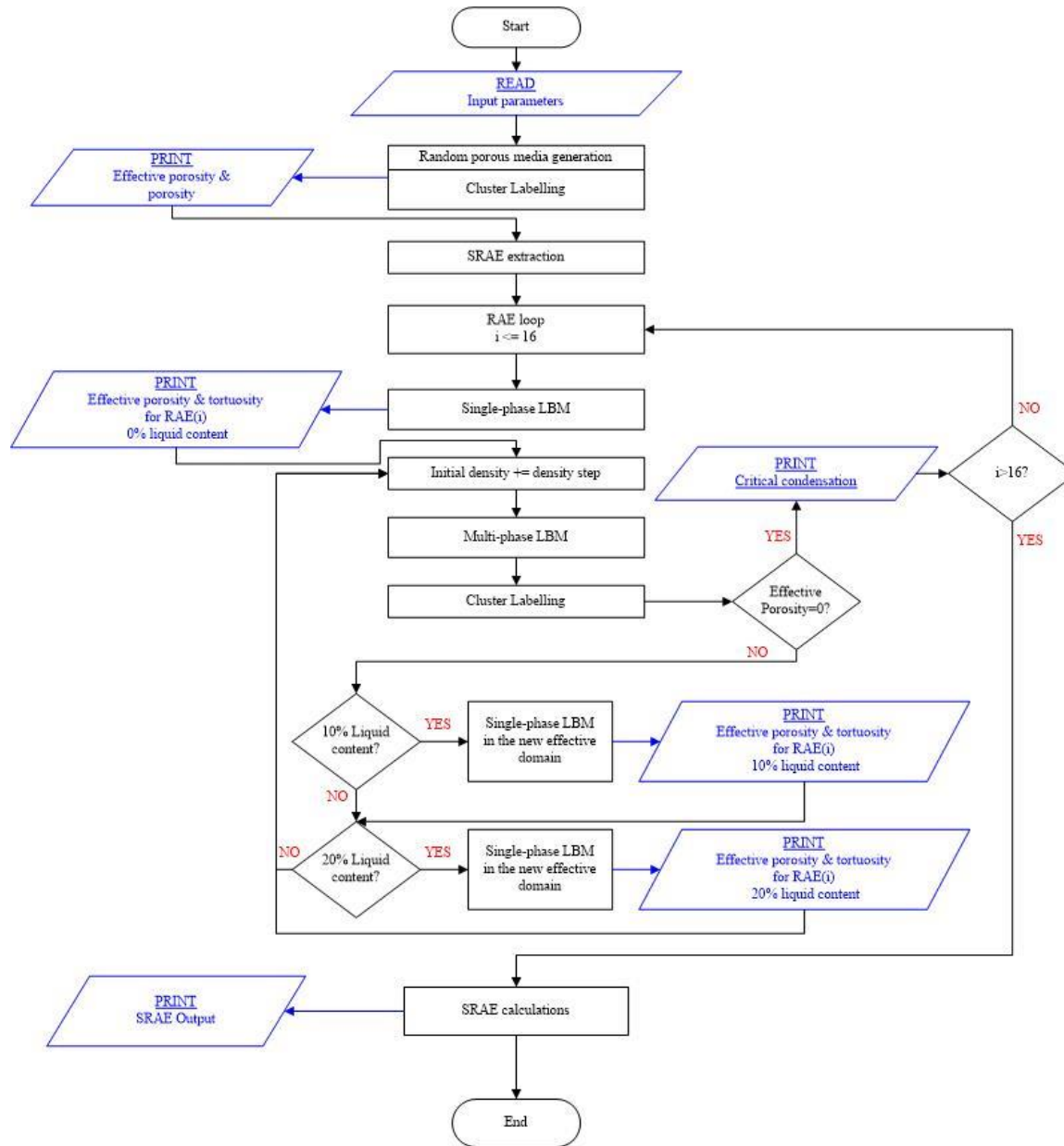


Figure 2.2. Flowchart of the serial code for a single trial.

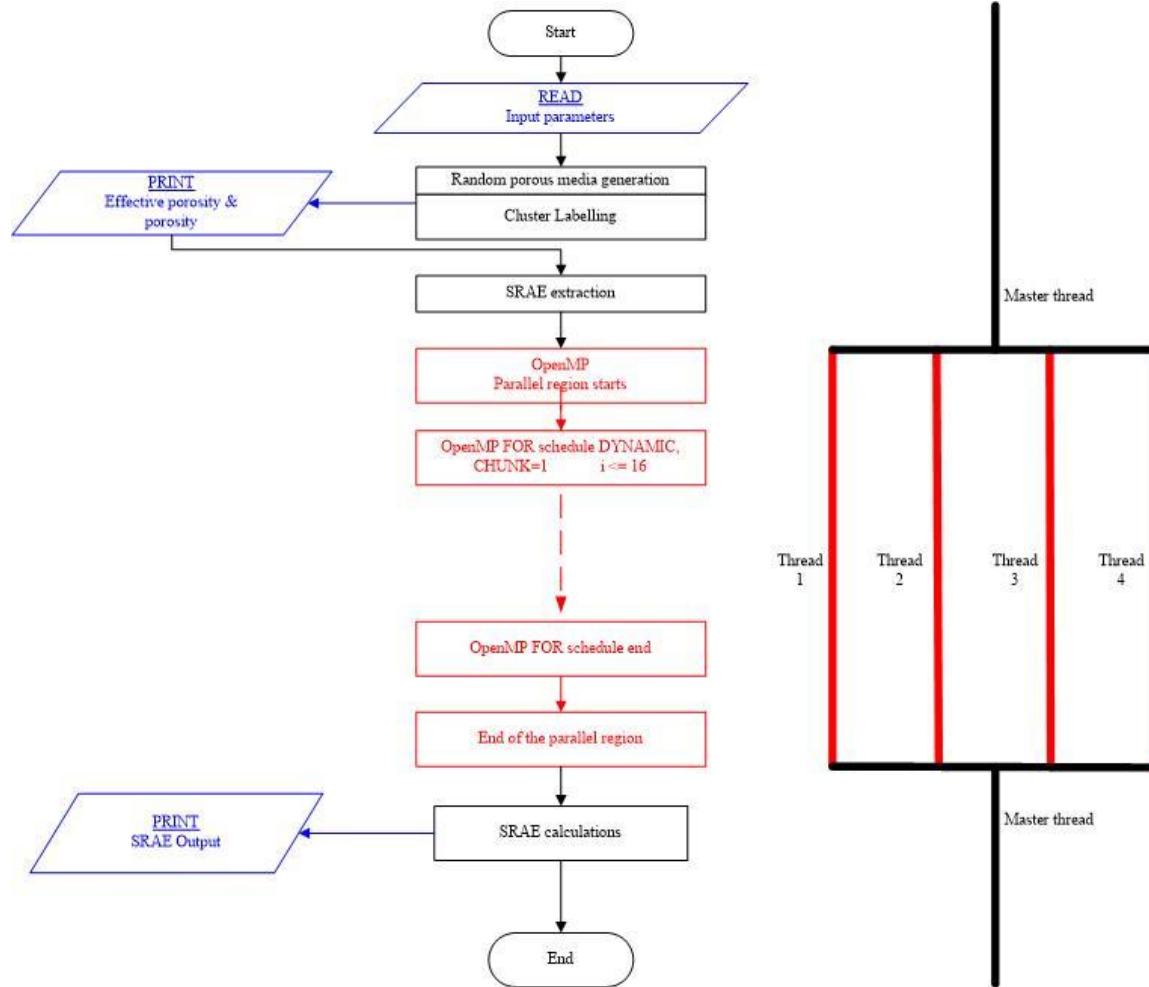


Figure 2.3. OpenMP implementation to the serial code. Flowchart of the parallel code for a single trial and demonstration of the fork-join model with 4 threads. Flowchart of the serial code for a single trial.

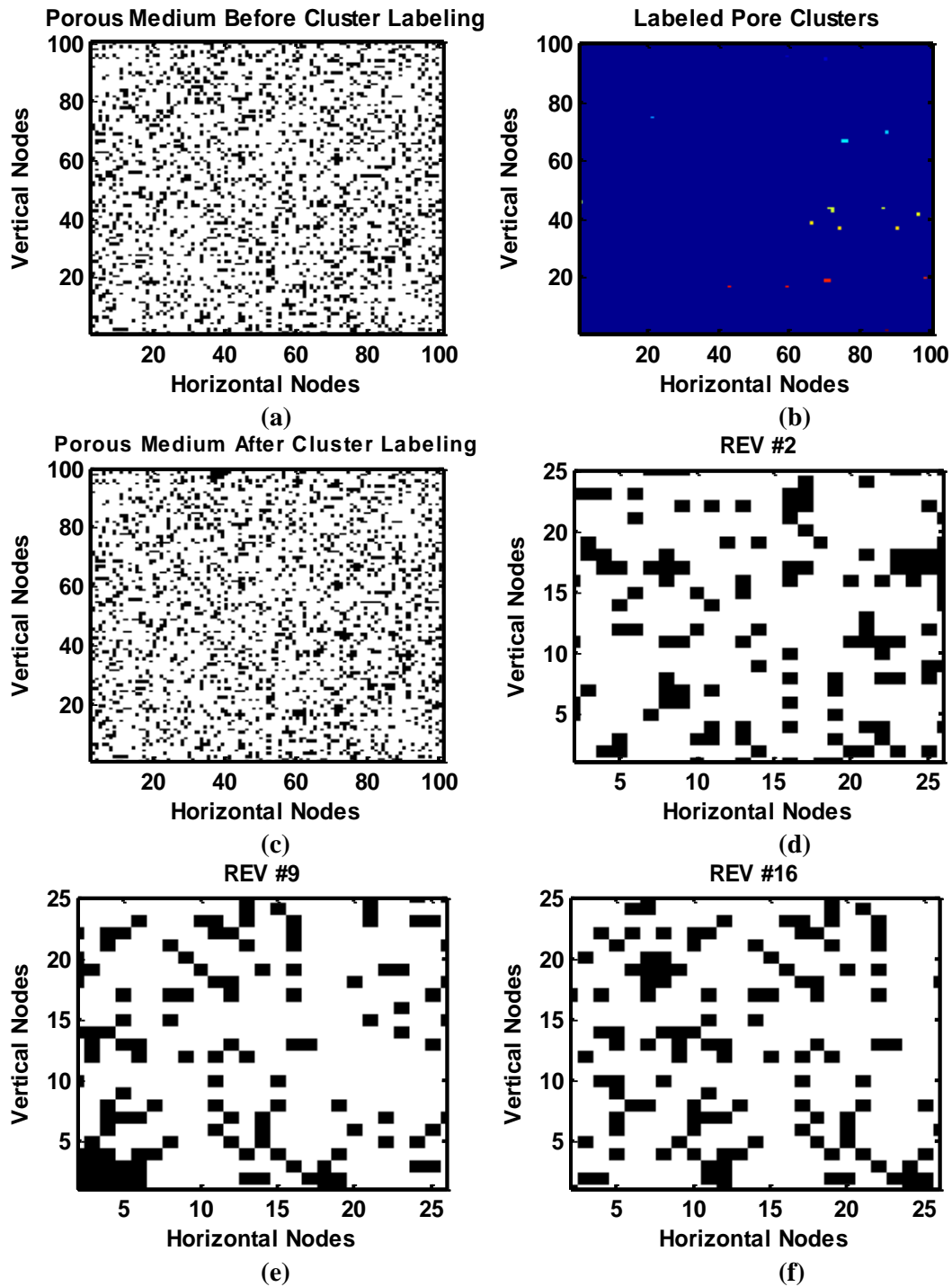
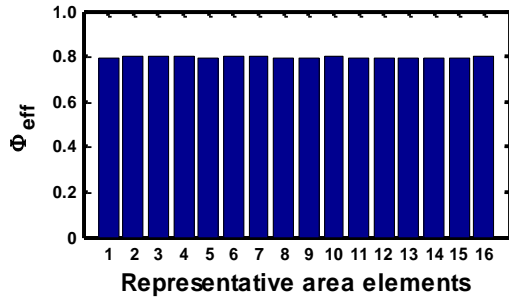
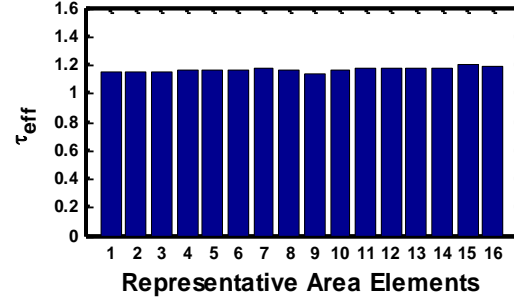


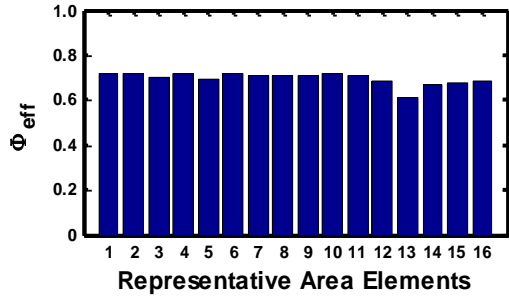
Figure 2.4. Path-percolation model for initial porous medium generation (a) domain before cluster labelling (b) cluster labelling (c) effective domain (d) - (f) three random RAEs.



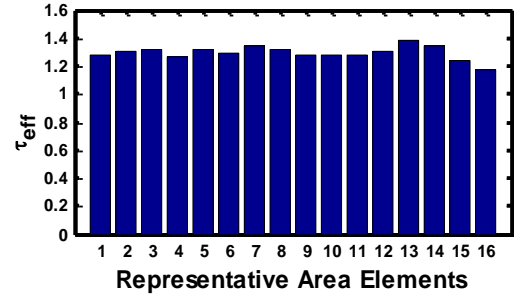
(a)



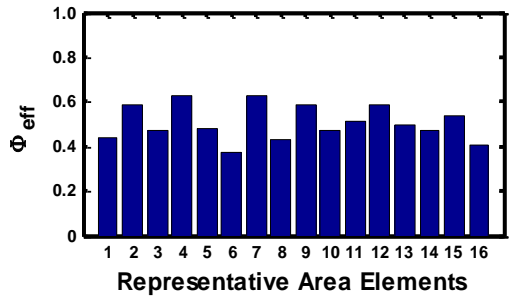
(b)



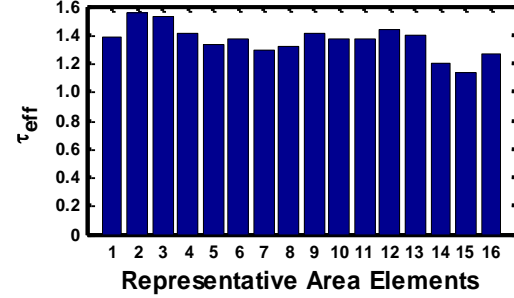
(c)



(d)



(e)



(f)

Figure 2.5. Effective porosity & tortuosity calculations for RAEs of an example trial with 80% porosity and 0% condensation (a) Φ_{eff} with 0% condensation (b) τ_{eff} with 0% condensation (c) Φ_{eff} with 10% condensation (d) τ_{eff} with 10% condensation (e) Φ_{eff} with 20% condensation (f) τ_{eff} with 20% condensation.

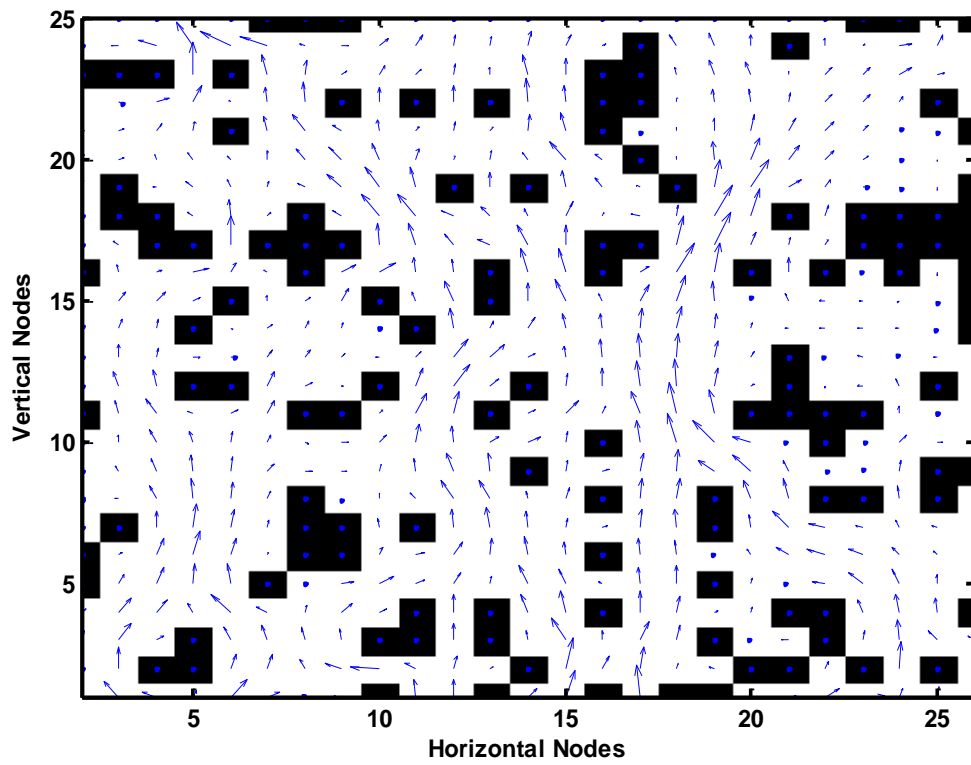


Figure 2.6. Velocity vectors along RAE #2. Tortuosity is 1.153163.

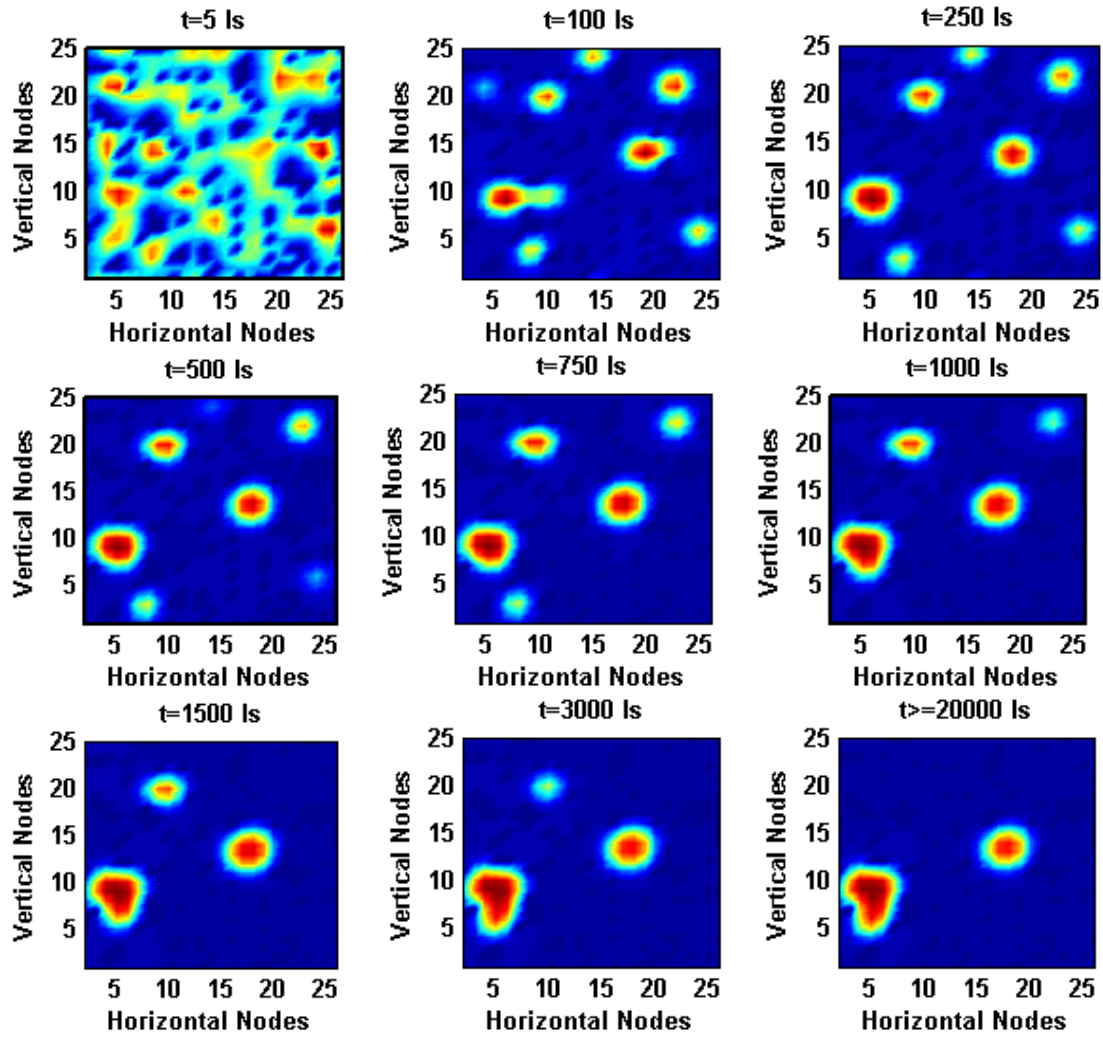


Figure 2.7. Evolution of phase separation of a 10% condensed two-phase fluid in REV #2.

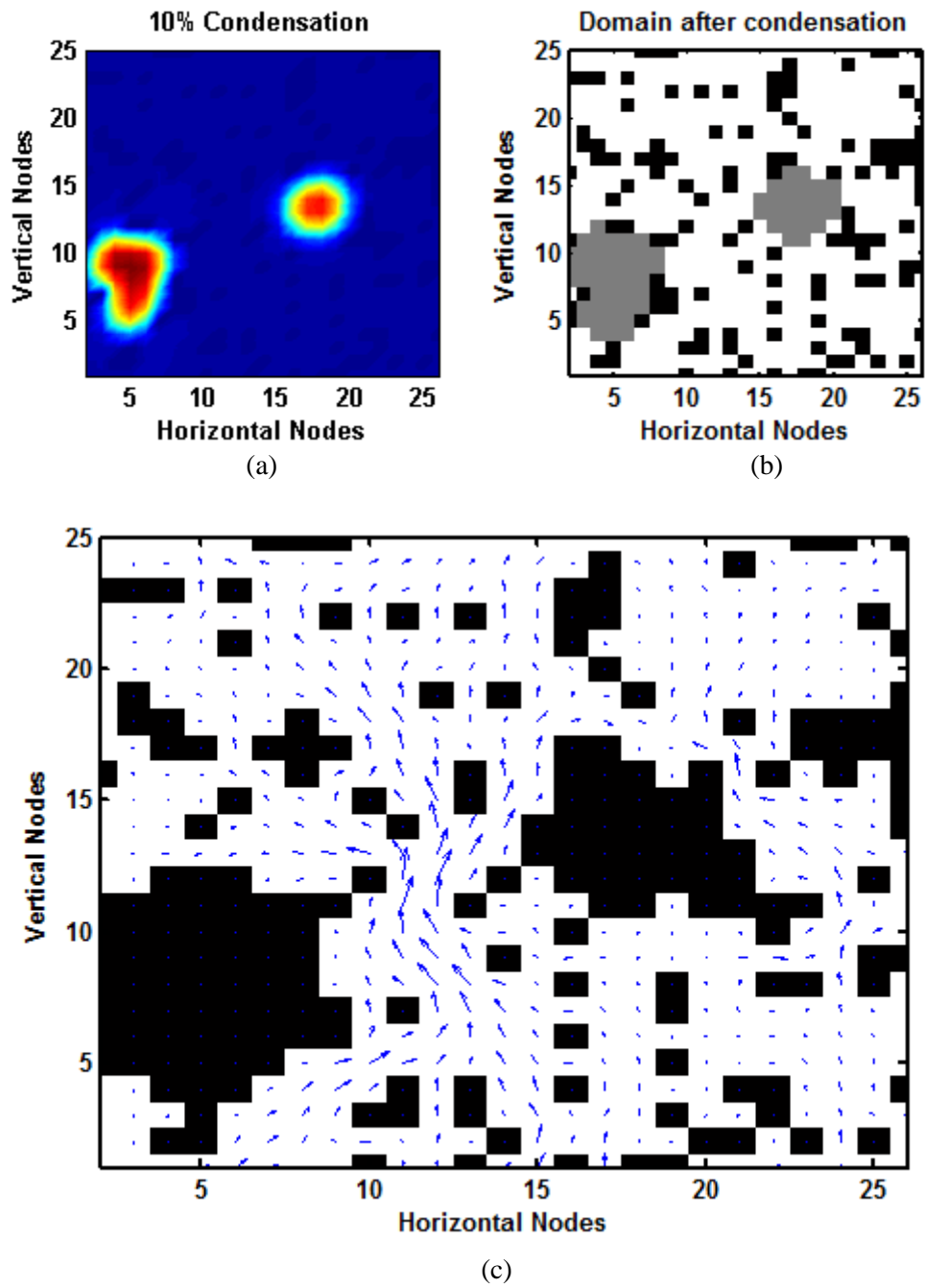


Figure 2.8. Vapor phase mass transfer with a 10% condensation (a) liquid formation (b) the voids occupied by liquid are shown in gray (c) Mass transfer in vapor phase, the effective tortuosity is 1.310.

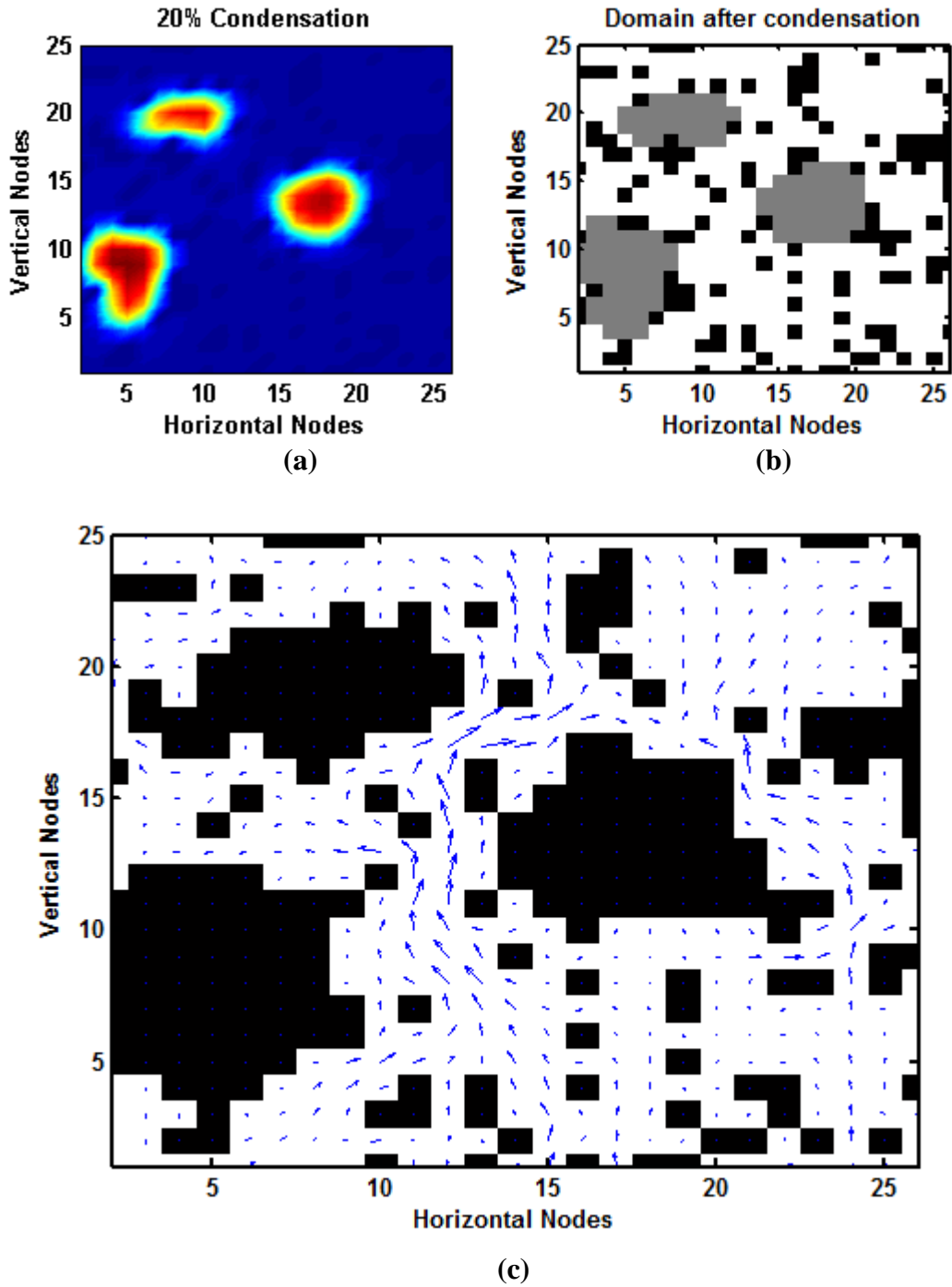


Figure 2.9. Vapor phase mass transfer with a 20% condensation (a) liquid formation (b) liquid formations are shown in gray (c) Velocity field of the vapor phase, the effective tortuosity is 1.552.

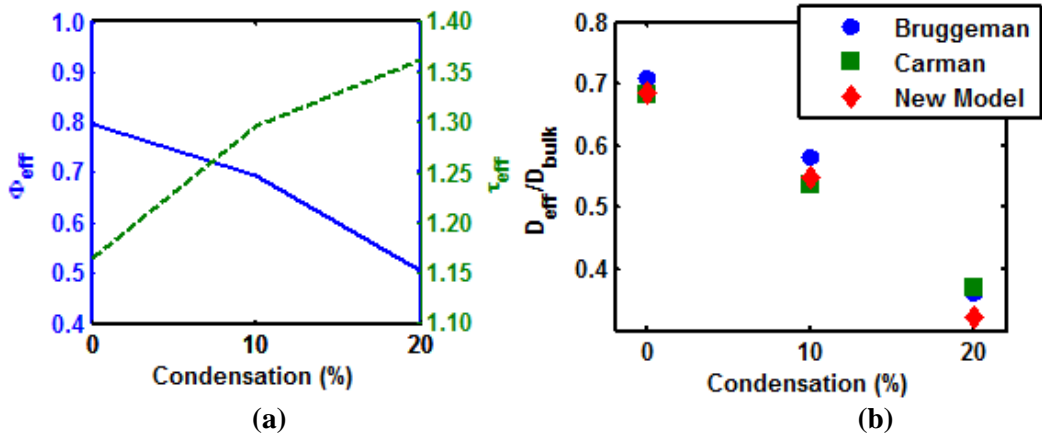


Figure 2.10. Effects of condensation on mass transfer for a single example trial (a) effective porosity and tortuosity vs. condensation (b) diffusion ratio vs. condensation.

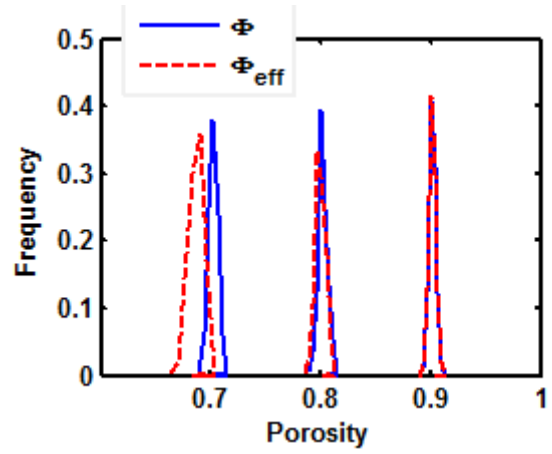


Figure 2.11. Confidence level results for initially generated 100x100 porous media with 70%, 80%, and 90% porosity.

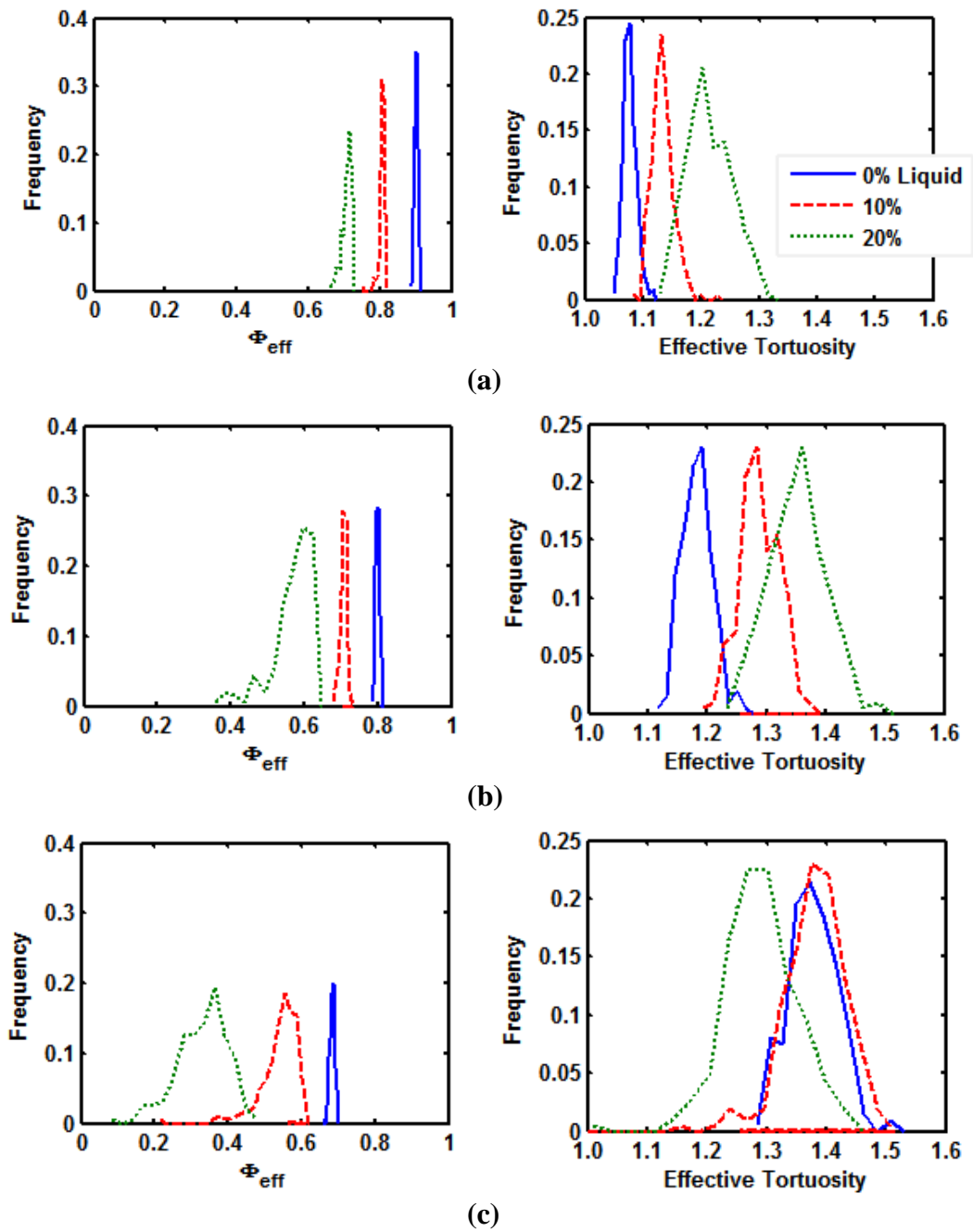


Figure 2.12. Confidence level results for SRAEs with (a) 90%, (b) 80%, and (c) 70% porosity. Figures on the left and right are probability distributions of effective porosity and tortuosity, respectively.

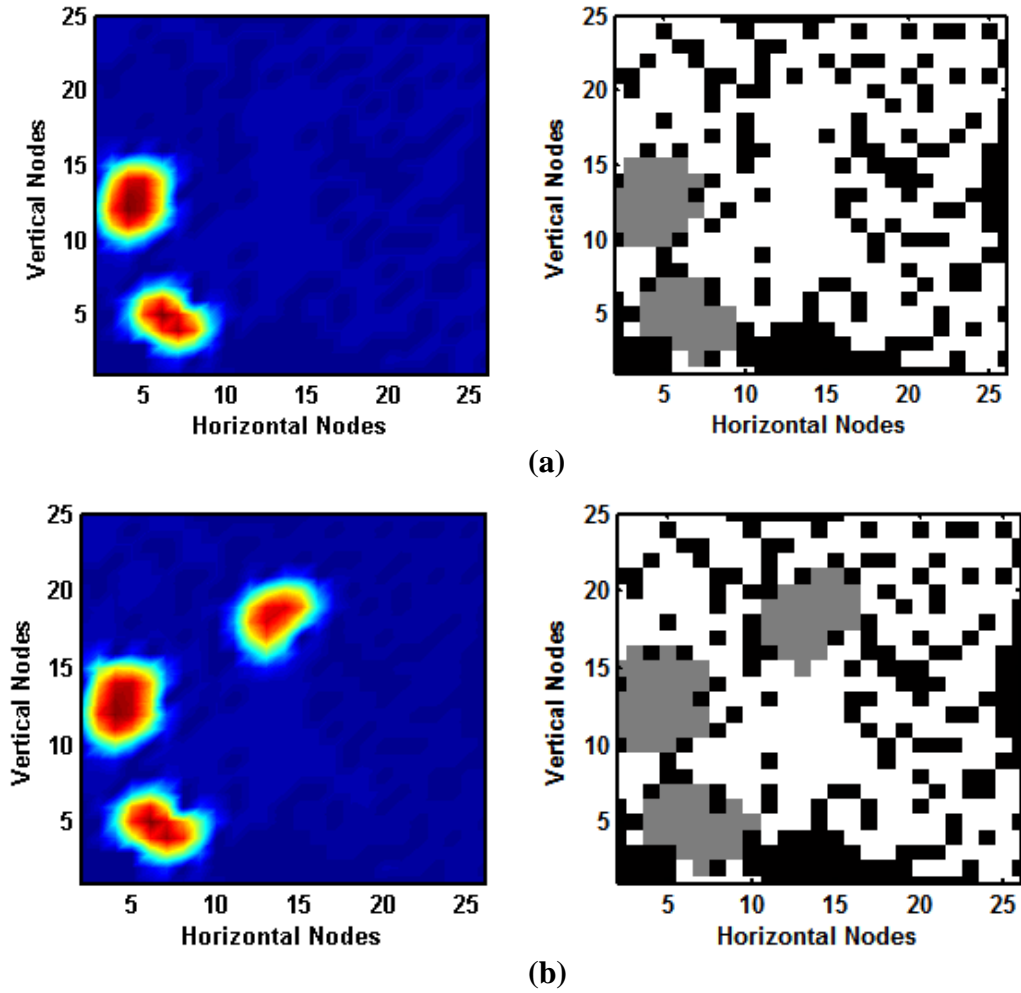
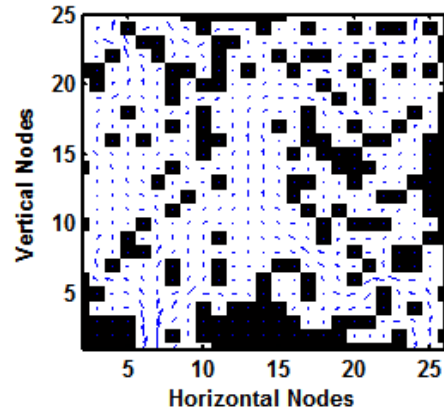
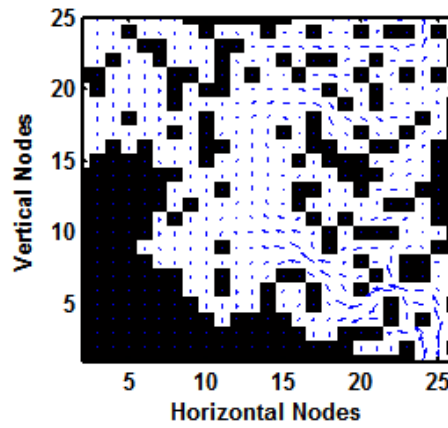


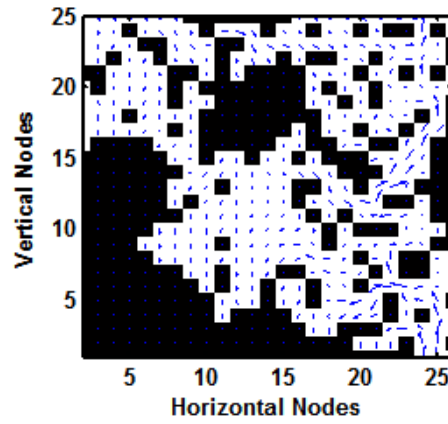
Figure 2.13. Liquid formation in an example RAE for 70% target porosity (a) 10%, (b) 20%.



(a)

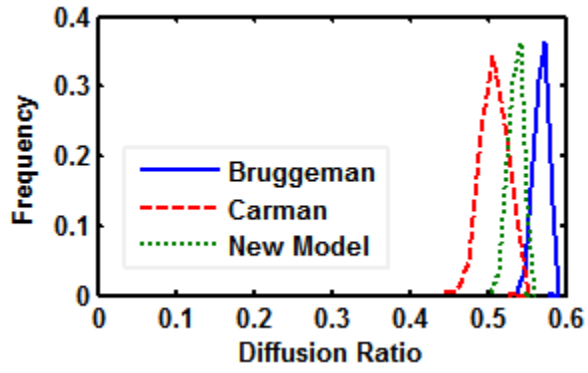


(b)

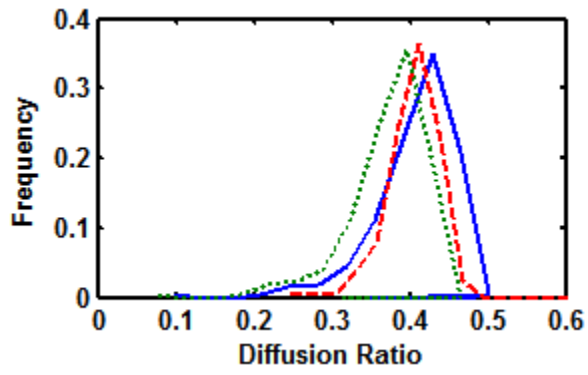


(c)

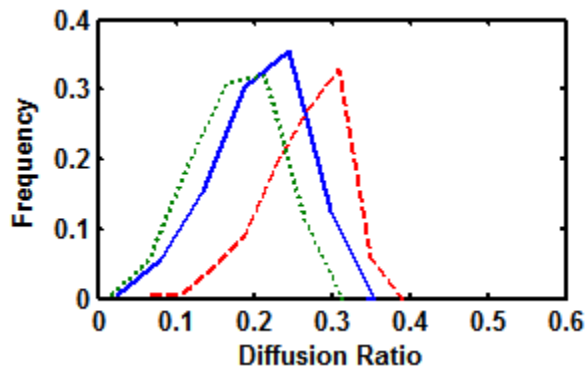
Figure 2.14. Velocity fields in effective domains with (a) 0%, (b) 10%, (b) 20% condensation. Computed tortuosities are 1.403323, 1.447953, and 1.28602, respectively.



(a)



(b)



(c)

Figure 2.15. Diffusion ratio probability distributions with a medium with (a) 0%, (b) 10%, (c) 20% liquid formation.

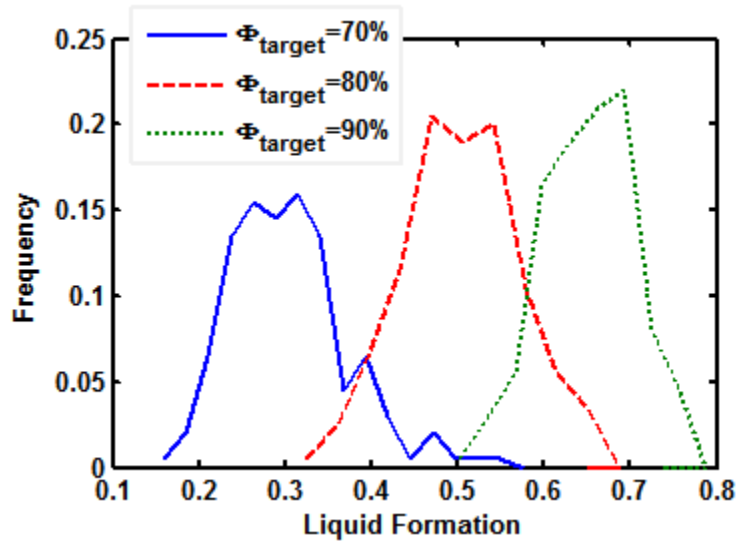


Figure 2.16. Critical liquid formation probability distributions with a medium with 70%, 80%, and 90% target porosity.

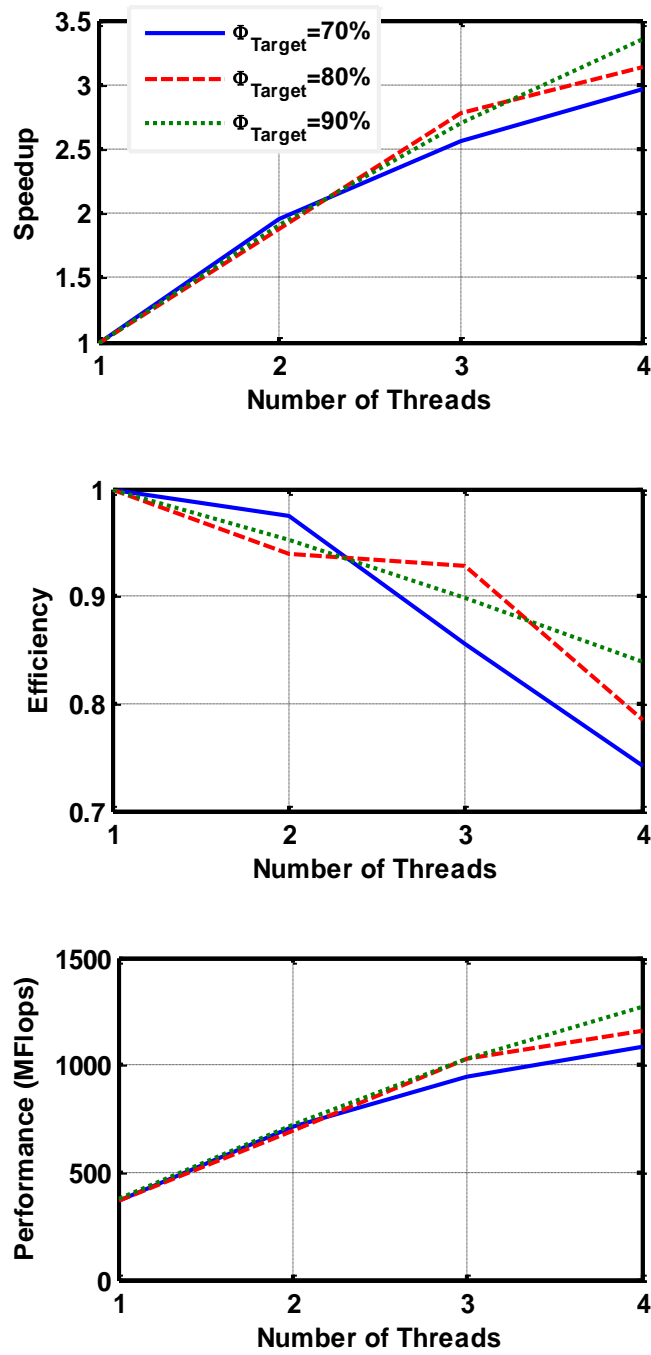


Figure 2.17. Performance analysis for parallel application.

CHAPTER III
SINGLE- AND MULTI-PHASE FLOW ANALYSIS IN
INHOMOGENEOUS RANDOM POROUS CHANNELS: I. SINGLE-
PHASE, LOW-TORTUOSITY FLOW WITH DOUBLE PATH-
PERCOLATION THEORY

Abstract

In this chapter, a statistical model, called the double-path-percolation theory, was introduced to investigate the diffusion behavior of gases in low-tortuosity systems. In addition to the inhomogeneous random low-tortuosity porous media simulations, as its name implies, this new model also simulates paths in both solid and void regions between the inlet and outlet of the channel, hence transport analysis can be performed in both regions. Confidence level studies with 95%, 97%, and 99% were performed to obtain statistical effective porosity results. A single-component single-phase Lattice-Boltzmann model with two-dimensions and nine velocity components was developed to obtain the velocity distributions in the simulated porous media, and tortuosity was determined to be between 1.0005 and 1.0663 for the channels with a wide range of effective porosities. A new effective diffusion model was developed as a function of the effective porosity. The results were compared with that of high-tortuosity systems. Except the high effective-porosity-media, a diffusion ratio difference of 0.2 was observed between these two sorts of porous channels. In addition, a software was developed for the double-path-percolation and Lattice-Boltzmann models, and the performance was improved by three different parallel implementations; Posix Threads, OpenSHMEM, and MPI. The best performance was achieved by the Posix Threads code with four cores, and a speedup of 3.962 was achieved. This new model is unique through its statistical approach, and solid-cluster labelling process.

Introduction

The double-path-percolation theory was developed to simulate random, inhomogeneous porous channels with both void and solid paths between the inlet and the outlet. The original idea of the path-percolation theory was introduced by Jung et al. [2] to statistically investigate the electrical property variations in randomly generated porous media. Path-percolation theory differs from percolation theory by its statistical approach, and it also introduces a process called cluster labelling process. Cekmer et al. [47] adapted the path-percolation theory to examine the diffusion behavior of gasses in inhomogeneous porous channels. Their model was developed to provide void channels for gas flow. In the current study, the diffusion behavior of gases in randomly generated porous channels with a tortuosity of nearly unity was investigated. A two-dimensional lattice-Boltzmann model was developed to obtain the velocity distribution throughout the randomly generated channels and the tortuosity was determined. A new diffusion model was developed, and compared with the one developed by Cekmer et al. [47]. Furthermore, three different high-performance parallel codes were developed using Posix threads, OpenSHMEM, and MPI to enhance computational performance. All three systems were implemented in two particular sections of the code, and the speedup and performance were measured.

The main motivation of this work is to investigate the differences in diffusion behavior of gases between low- and high- tortuosity systems with the same effective porosity. The techniques and the statistical results of the current study can be used in any porous media application involved with mass and momentum transfer with low-tortuosity-flows. The internal structure of a porous channel has a significant effect on diffusion, hence the developed effective

diffusion model will be a better approximation for the macroscopic porous media simulations involving low-tortuosity systems. The increased performance of the developed software with three different parallel implementation proves that this computational model has a potential to utilize better confidence levels for the statistical results, and enables a path for extension into three dimensional simulations. Since, the double-path-percolation theory can be utilized to simulate a porous medium with both solid and void paths, the results of this work can be applied in any porous medium application area with both solid and void parts of the channels involved with transport phenomena.

In the current work, the introduced double-path percolation theory is unique because of its statistical approach based on the law of large numbers. The path-percolation theory brings a new aspect to the well-known percolation theory by the cluster labelling process, which significantly reduces the runtime of the developed program. The double-path percolation model differs from the path-percolation theory by a new process called the solid-cluster-labelling. Void paths for the gas molecules are obtained by void-cluster labeling process of path-percolation theory. This double-path-percolation model therefore simulates solid paths for energy and electron transport in solid parts of an inhomogeneous porous medium as well.

Methodology

The current work initiates with a random porous media generation technique, which is called the double-path-percolation theory. The confidence-level study was introduced first to construct a statistical base for the simulations. Then, the necessary aspect ratio of the dimensions of the channels to provide both void and solid paths were determined. Three different target porosities were applied, and the effective porosity ranges were analyzed to complete the

determination of the necessary properties of the initially generated random porous media. Furthermore, representative elementary area selection was performed to provide small representative areas to solve the momentum balance equation. The outcome of the study was used to develop a new effective diffusion model. On the other hand, the developed in-house program was improved by three parallel programming systems, and the performance analysis was performed.

Double-path-percolation theory

The double-path-percolation theory is a statistical model used to simulate inhomogeneous random porous channels. Aspect ratio is defined as the ratio of the horizontal and vertical nodes, and has an important effect on double-path-percolation model. A sample simulation with an aspect ratio of 10 is explained here before the application of the statistical confidence-level study. The horizontal node number was arbitrarily set to 300, then the vertical node number became 30. The target porosity, which is the desired porosity of the simulated medium, was set to 60%. After determining the node numbers and the target porosity, a random inhomogeneous porous medium was generated. To accomplish this, an in-house program was developed to randomly assign numbers between 0 and 100 to each node. Depending on the target porosity, the program determines the phase of the each node. If the assigned number is lower than the target porosity, the phase of the node becomes void, otherwise solid. A simple demonstration of the procedure is shown in Figure 3.1. In this figure, randomly generated numbers are on the left, and the assigned phases are on the right. Numbers on three nodes are greater than target porosity, hence they were assigned as solid, and the others as void. Solid and void nodes are represented by black and white, respectively.

An initially generated random porous medium is presented in Figure 3.2(a). The resulting porosity is 0.5944. To provide a domain for a fluid flow simulation, the porous medium generated was transformed into a channel by assigning a flow inlet and outlet to bottom and top boundaries, respectively. Then, the pore-cluster labeling process was applied to group the interconnected pores into clusters as seen in Figure 3.2(b). The orphan pores, which were not connected to both inlet and outlet, were eliminated and a new domain was obtained as presented in Figure 3.2(c). The porosity of the domain was reduced to 0.2687.

To this point, the procedure is the same as that of the single-path-percolation theory [47], in which void paths were provided for fluid flow in the channel. Furthermore, solid paths are needed, although no transport phenomena in solid was considered in this work. However, the double-path-percolation theory can be used in systems which involve transport phenomena in solid regions. As an example, there are porous layers of a polymer electrolyte fuel cell, through which electron and heat transport occur. Electrons are produced in the porous catalyst layer of the system, and they conduct through the carbon based fibers of the porous gas diffusion layer, from the anode to the cathode side of the fuel cell. Heat conduction is another consideration in these electrochemical systems [52]. However, the main target here is obtaining low-tortuosity flow channels by eliminating the solid obstacles in the channel. To accomplish this, solid cluster labeling process is utilized to group the interconnected solid nodes together, as seen in Figure 3.2(d). The orphan solid clusters were eliminated after the solid-cluster labeling process, and the effective domain is presented in Figure 3.2(e). The final domain obtained after pore- and solid-cluster labeling processes is called the effective domain, and the porosity of the domain is called the effective porosity, which is 0.4662 for this simulation. The final form of the domain was then

stretched in vertical direction by aspect ratio to fit a square, as seen in Figure 3.2(f). The stretching is performed to obtain square domains for lattice-Boltzmann analysis.

A confidence-level study is needed to obtain statistical results of porosity and effective porosity. To do this, the law of large numbers [2, 42, 47] was utilized. A confidence-level is defined as the reliability of any estimate, and formulated as:

$$CL = Pr \left\{ \left| \frac{k}{n} - p \right| \leq \varepsilon \right\} \quad (3.1)$$

In Eq. (3.1), CL stands for the confidence level. Pr is the probability of the event in the brackets. The target porosity is represented by p , whereas n and k are the total history number and the number of generating a single pore, respectively. Total history number is mathematically defined as the multiplication of the total node number in the domain and the trial number. Hence, it depends on the size of the domain and the number of needed repetitive simulations for a specified target porosity. The division in the parenthesis gives the simulated porosity. Error, ε , is defined as the critical error between the simulated and target porosity, and set to 1×10^{-3} in this work. Eq. (3.1) means that the confidence level is equal to the probability of the difference between the simulated and target porosities to be less than or equal to the specified error. Eq. (3.2) is obtained after applying the law of large numbers, and was used with an error function table to determine the necessary history number [42, 47].

$$\frac{CL}{2} = \text{erf} \left(\varepsilon \sqrt{\frac{n}{pq}} \right) \quad (3.2)$$

In Eq. (3.2), q is equal to $1 - p$. The effects of aspect ratios of 5, 10, and 15 on statistical results were analyzed here with confidence levels of 95%, 97%, and 99%. Furthermore, the results with target porosities of 55%, 60%, and 65% were also investigated. A simple application

of confidence-level study is described here. The total history number is needed within a confidence level of 99% for a 60% porous medium and an aspect ratio of 10. Then, the left hand side of Eq. (3.2) becomes $0.99/2=0.495$. An error function table is used to obtain the inside parameter of the error function (Table 3.1).

$$\operatorname{erf}\left(\varepsilon \sqrt{\frac{n}{pq}}\right) = 0.495 \quad \therefore \quad \varepsilon \sqrt{\frac{n}{pq}} = 2.5767$$

Since, the target porosity is 0.60, then $p = 0.60$ and $q = 0.40$. Error was determined 1×10^{-3} . The total history number becomes 1,593,452. The horizontal node number was decided to be 300, hence vertical node number became 30, since the aspect ratio was 10. The trial number is the total history number divided by the total node number. Hence, 277 simulations are needed to provide a 99% confidence level to simulate porous media with 60% porosity within an error range of 1×10^{-3} . The results of the confidence level analysis are presented in the “Results and Discussion” section.

Lattice-Boltzmann method

The lattice-Boltzmann equation is a first order partial differential equation, hence the developed code for the lattice-Boltzmann model (LBM) is not as complex as the codes, in which Navier-Stokes equations were used. However, it is still a computationally intensive method. To reduce the runtime of the code, a representative area element (RAE), which represents the entire domain, is needed for each simulation. The RAE must represent the effective porosity and the tortuosity of the generated porous channel, hence a problem rises by the unknown effective tortuosity of the entire domain. To overcome this problem, a method called the two-point statistics is utilized [43, 44, 47]. Instead of using a single RAE, a statistical representative area element (SRAE) set with a certain number of RAEs is constructed. The first step is the RAE size

determination, the detailed procedure can be found in the study by Cekmer et al. [47]. The second step is determination of the necessary RAE number in an SRAE set. To accomplish this, a confidence-level study was utilized. The procedure is the same as the confidence level studies in path-percolation theory, except that the total history number is now the multiplication of the trial number, which was determined in the previous section, the total node number of a single RAE, and the number of RAEs in an SRAE set. The ensemble average in an SRAE for any property can be calculated as follows:

$$\hat{X} = \frac{1}{N} \sum_{m=1}^N X_m \quad (3.3)$$

In Eq. (3.3), X_m is any property of the m^{th} representative area element in a set, N is the total element number, and \hat{X} is the ensemble average. X is set to be effective porosity and tortuosity in this work. The detailed analysis is explained in the results section.

Ludwig Boltzmann derived the lattice-Boltzmann equation in 1872 [3], and introduced the probability density function, $f(\vec{x}, \vec{p}, t)$, as the probability of a molecule to be at position \vec{x} at time t with momentum \vec{p} . In numerical lattice-Boltzmann models, there are two mechanisms that describe the movement of molecules; streaming and collision. The streaming process is simply the movement of a molecule from one node to another. The collision step counts the molecules, which enters or leaves the considered node via a collision with another molecule.

A D_2Q_9 square lattice with two dimensions and nine velocity components is used in this study. A simple demonstration of a D_2Q_9 lattice is presented in Figure 3.3(a). All the nodes in the representative porous channels are treated as D_2Q_9 lattices. The unit lattice velocities are as follows:

$$\begin{aligned}
c_{0,x} = 0, c_{0,y} = 0, & & c_{1,x} = 1, c_{1,y} = 0, & & c_{2,x} = 0, c_{2,y} = 1 \\
c_{3,x} = -1, c_{3,y} = 0, & & c_{4,x} = 0, c_{4,y} = -1, & & c_{5,x} = 1, c_{5,y} = 1 \\
c_{6,x} = -1, c_{6,y} = 1, & & c_{7,x} = -1, c_{7,y} = -1, & & c_{8,x} = 1, c_{8,y} = -1
\end{aligned} \tag{3.4}$$

The streaming and collision mechanisms are shown in Eqs. (3.5) and (3.6), respectively.

$$f_k(x + \Delta x, y + \Delta y, t + \Delta t) = f_k(x, y, t + \Delta t) \tag{3.5}$$

$$f_k(x + c\Delta t, y + c\Delta t, t + \Delta t) - f_k(x, y, t) = -\mathbf{\Omega}[f_k(x, y, t) - f_k^{eq}(x, y, t)] \tag{3.6}$$

where, c , x , y , and t represent speed of sound, horizontal coordinate, vertical coordinate, and time, respectively. The details of the determination of collision matrix, $\mathbf{\Omega}$, and the equivalent distribution factor, f_k^{eq} , can be found in [47]. Periodic boundary conditions were applied on the top and bottom boundaries, and the side walls are reflective. The unit lattices at the boundaries are shown in Figure 3(b), where the velocity vectors shown by dashed lines are unknowns, and the solid lines were calculated from streaming process. After solving the equation system (3.5) and (3.6) with the boundary conditions, the probability density function is obtained, and the lattice density, and horizontal and vertical components of a lattice velocity can be determined by Eqs. (3.7), (3.8), and (3.9), respectively.

$$\rho = \sum_{k=0}^8 f_k \tag{3.7}$$

$$u = \frac{1}{\rho} \sum_{k=0}^8 c_{k,x} f_k \tag{3.8}$$

$$v = \frac{1}{\rho} \sum_{k=0}^8 c_{k,y} f_k \tag{3.9}$$

Tortuosity is a measure of the actual path travelled by a particle divided by the shortest distance between the same points. Numerical or effective tortuosity can be calculated using Eq. (3.10).

$$\tau_{eff} = \frac{\int_A V dA}{\int_A v dA} \quad (3.10)$$

To develop an effective diffusion model using the outcome of this work, a well-known diffusion model was used. The Carman model estimates the diffusion ratio as a function of porosity and tortuosity [11], as seen in Eq. (3.11).

$$D_{eff} = D_{bulk} \frac{\Phi}{\tau} \quad (3.11)$$

A new effective diffusion model for low-tortuosity flow was developed, and compared with the one developed by Cekmer et al. [47] by single-path-percolation theory for high-tortuosity flows as shown in Eq. (3.12).

$$D_{eff} = D_{bulk} \Phi_{eff}^{1.6556} \quad (3.12)$$

The results are explained in the “Results and Discussion” section.

Parallel Implementation

An in-house program was developed to utilize the double-path-percolation and Lattice-Boltzmann models to investigate the single-phase mass transfer in randomly generated porous media. Three different application programming interfaces, Posix Threads (Pthreads), OpenSHMEM, and MPI were implemented on the serial code, and the performances were compared.

A simple flowchart of the serial code for a single-phase trial is shown in Figure 3.4. The program reads the input parameters, and generates a random porous medium. Then, it calls the void and solid cluster labelling subroutines, and prints the porosity and the effective porosity of the entire domain. The next step is the SRAE selection process. The program optimally extracts the best RAEs to construct an SRAE. To do this, the entire domain was scanned starting from the

upper left corner, and all possible RAEs are examined as shown in Figure 3.5(a). First, the porosity of the small domain is computed, and the relative error between the porosities of the small and large domains is determined. A critical error was assigned as 1×10^{-2} . If the error is smaller than the critical error, then the void and solid cluster labelling subroutines are called, and the second criterion is examined. This criterion dictates that the relative error between the effective porosities of the smaller domain and the entire channel should be smaller than 1×10^{-2} to let the RAE be a potential member of the SRAE. If both criteria are obeyed, then the RAE is saved. After, the entire domain is scanned, and every possible RAE is examined, the selected potential RAEs are ranked in terms of their relative effective porosity error, and the ones with the least errors are chosen to be the members of the SRAE.

After the SRAE selection process, the code starts LBM to solve momentum balance equation for each RAEs of the SRAE set. Finally, effective porosity and tortuosity of the SRAE are computed.

Two parts of the code were made parallel by four systems. First part is the SRAE extraction. This section was parallelized as seen in Figure 3.5(b). In this figure, an SRAE extraction process with 5 threads is demonstrated. The domain is divided into five sections, and these sections are allocated by five processors. Then, all threads start scanning simultaneously. After they store the potential RAEs, the best options are chosen. In OpenSHMEM and MPI codes, a MASTER thread ranks the RAEs, and sends the best options to the other threads. In Pthreads implementation, the selected RAEs are stored in a three dimensional matrix in shared memory. A single thread is charged to rank the selected RAEs. The ranked SRAE set is stored in the shared memory.

The second parallel part of the code is the LBM simulation. After a single thread selects the RAEs of an SRAE set, each thread starts sharing the RAEs, and applies the LBM. Then, they print the related effective porosity and tortuosity values. Finally, the effective porosity and the tortuosity of an SRAE are calculated by Eq. (3.3).

Two parameters were used to determine the performance of using parallel programming in this work. The first of these is called speedup (S), and determined by dividing the runtime of the serial code, (T_1), by the runtime of the parallel code with n_c threads, (T_{n_c}), as shown in Eq.

(3.13) [49]:

$$S = \frac{T_1}{T_{n_c}} \quad (3.13)$$

The second parameter is the performance, which is defined as the ratio of the total floating point operations and the runtime. The performance in MFLOPs is computed by Eq. (3.14) for this particular code.

$$\text{Performance} = 4.74925 \times 10^3 \sum_{i=1}^{N_{RAE}} \Phi_{eff}(i) / \text{Execution Time} \quad (3.14)$$

where, N_{RAE} is the number of RAEs in an SRAE set, and $\Phi_{eff}(i)$ is the effective porosity of RAE number i . As a hardware, a personal computer with 4 processors with 2.40 GHz speed, each performs 4 floating-point operation (Flop) per cycle was used. The peak performance was calculated as follows:

$$P_{peak} = \frac{2.40 \text{ GHz}}{1 \text{ core}} \times \frac{4 \text{ Flop}}{\text{cycle}} \times 4 \text{ cores} = 38.4 \frac{\text{GFlop}}{\text{sec}} \quad (3.15)$$

The performance analysis was discussed in the following section.

Results and Discussion

The double-path-percolation theory was introduced in the first part of this work. This model is used to construct inhomogeneous porous media for low-tortuosity flow systems. Confidence-level analyses was utilized first to provide statistical results, and the effective porosities of the randomly constructed domains were determined. A confidence level of 99%, an aspect ratio, and a target porosity with a wide range of resulting effective porosity was selected for momentum transfer analyses. The study continued by a statistical representative area element selection, and a single-component, single-phase lattice-Boltzmann model was applied to the system to determine the effective tortuosity of the flow system. The following sections summarize the results for each step.

Confidence-levels of 95%, 97%, and 99% were applied using the law of large numbers to determine the porosity and effective porosity of the generated porous channels with the aspect ratios of 5, 10, and 15. Target porosities of 55%, 60%, and 65% were examined on the channels generated by double-path-percolation model. Figure 3.6 presents the results for three cases with aspect ratio – target porosity pairs of 5/0.55, 10/0.65, and 15/0.60. In each plot, porosities were divided into subgroups, and each domain's porosity was added to the subgroup, which it belongs to. The vertical axis represents the occurrence frequency of each subgroup of porosities. Then, the probability distributions against porosity were plotted in this figure. As observed in all three plots in Figure 3.8, the occurrence frequency of the group with the desired (or target) porosity is the highest in 99% confidence level. Furthermore, the possible resulting porosity range of the simulations are the narrowest when confidence level is 99%. Although, only three cases were presented in Figure 3.8, this result holds for all 9 cases with three aspect ratios, three target

porosities, and three confidence levels. Hence, 99% of confidence level will be pursued in the remaining part of this study.

The goal of the current work is to develop an alternative effective diffusion model for low-tortuosity flow and to obtain an equation for effective diffusion coefficient as a function of bulk diffusion coefficient and effective porosity. Thus, the tortuosity term in the Carman model was eliminated, and the effect of tortuosity was included as a constant power of effective porosity in the new model. Therefore, further LBM computations for momentum transport can be eliminated in more advanced future studies involved with mass diffusion in porous media. Furthermore, it is thought that it would be useful to demonstrate the ability to show computationally that two media with the same effective porosity may have significantly different diffusion ratios. To do this, it is crucial to provide information of flow characteristics for low-tortuosity porous media with a great range of effective porosity. The resulting effective porosity distributions of all three target porosities were plotted for the aspect ratios of 5, 10, and 15, as presented in Figure 3.7, to consider the most appropriate aspect ratio - target porosity pair. As observed in the figure, porous media generated with a target porosity of 65% results an effective porosity of 100% for all three cases with different aspect ratios. Porous media with a target porosity of 55% with an aspect ratio of 5, generates effective porous domains with an effective porosity of lower than about 30%, and this case generate domains with an effective porosity of 0%, with a chance of 60%, which is the occurrence frequency of the effective porosity of 0%. This frequency reduces to 10% for the case with an aspect ratio of 10, and the effective porosity takes values between 0% and 40%. In the case with an aspect ratio of 15, the occurrence frequency of a domain with an effective porosity of 0% reduces to about zero, and the effective

porosity takes values between 0% and 50%. When the target porosity is set to 60% with an aspect ratio of 5, it is observed that the resulting effective porosity range is relatively wide comparing with the other cases. However, there is a 15% chance of the case with a resulting domain with an effective porosity of 100%. When aspect ratio increases, the resulting effective porosity chance of 100% decreases.

To cover all the possible effective porosity ranges in the new diffusion model, the cases with both 55% and 60% target porosities with an aspect ratio of 15 can be performed. However, porous channels with an aspect ratio of 15 will provide very short paths for the fluid molecules. Two resulting porous channels for the cases with the aspect ratios of 5 and 15, and a target porosity of 60% are demonstrated in Figure 3.8. Therefore, path-percolation model with a 99% confidence level, a target porosity of 60%, and an aspect ratio of 5 was selected for the new effective diffusion model. Hence, 88 porous channels with dimensions of 300x60 were generated, and the momentum transfer in each domain was simulated using D_2Q_9 lattice-Boltzmann model to obtain the effective tortuosity. Perhaps the most precise way to simulate low-tortuosity flow in inhomogeneous porous media is obtaining the digitized micro-computed tomographies of the actual domains, and applying LBM for mass transfer (e.g. using a D_2Q_5 lattice for mass transport). The introduced model with the selected aspect ratio is an alternative approach for diffusion studies in inhomogeneous random low-tortuosity porous media that is much less computationally expensive. It can be useful if the tortuosity of the actual geometries are qualitatively predictable or exactly known. Furthermore, the void- and solid-cluster labelling processes can also be applied on the real geometries to reduce the runtime of the simulation.

The size of a single RAE is determined to be 55×11 [47], and a confidence level study was performed to obtain the necessary RAE number in an SRAE set. The result is presented in Table 3.2, and the RAE number in a single SRAE set is determined as 30.

In LBM simulations, the rectangular RAEs were stretched in vertical direction to obtain squares. This process was performed to compare the single- [47] and double-path-percolation results for square channels. Figure 9 presents a sample demonstration of the entire procedure. A random inhomogeneous porous medium was generated as seen in Figure 3.9(a). The target and resulting porosities are 0.6000 and 0.6002, respectively. The void and solid cluster labelling processes were applied on the domain, and the effective domain was obtained as shown in Figure 3.9(b). The resulting effective porosity was determined as 0.6659. SRAE set was constructed with 30 RAEs. LBM was applied to all representative areas in the SRAE set. Velocity distribution in two of the RAEs are shown in Figure 3.9(c) and (d). The effective porosity and tortuosity of the set was computed as 0.6623 and 1.0017, respectively.

The statistical results of this work are shown in Figure 3.10. These results were obtained after simulating 88 trials as seen in Table 3.2. Effective porosity results were plotted against the computed effective tortuosity values, as shown in Figure 3.10(a). Relatively low tortuosity values were observed (below 1.02), regarding to single-path-percolation results, which were lying between 1 and 3 [47]. When effective porosity increased, tortuosity slightly decreased. The Carman model was applied on the data using Eq. (3.19), and the diffusion ratio was plotted against the effective porosity as shown in Figure 3.10(b). A data fit was applied to develop an effective diffusion model to be used in low-tortuosity flow in porous media. The new model is shown in Eq. (3.16).

$$D_{eff} = D_{bulk} \Phi_{eff}^{1.0122} \quad (3.16)$$

As expected, tortuosity has a lower effect on effective diffusion coefficient. Figure 3.10(c) demonstrates the difference between two models for high- and low-tortuosity flows by single- and double-path-percolation theories. This figure tells that the diffusion behavior of a gas in two porous channels with the same effective porosity would be significantly different than each other, because of the tortuosity effects. In high-tortuosity systems, an increase in tortuosity decreases the diffusion ratio much more than that of the low-tortuosity systems. There is approximately 20% difference in diffusion ratios in these systems, especially for low effective porosities. This difference slightly reduces with the increased effective porosity, and they overlap ($D_{eff}/D_{bulk} = 1.0$) when the effective porosity becomes 1, where the tortuosities and effective porosities become equal for two systems. As a summary, about 20% more gas is diffused in low-tortuosity flows, simulated by double-path-percolation theory, than high-tortuosity flows, simulated by single-path-percolation theory, for a great range of effective porosity. For the example simulation shown in Figure 3.9, the diffusion ratio was computed as 0.5964, using the new model. It must be noted that these results are 99% confident in precision within an error limit of 1.0×10^{-3} as explained in the “Methodology” section.

For the performance analysis of the single-phase parallel codes, PAPI time counters [53] were placed in the specific parts of the code, and a runtime analysis was performed for all implementations. Figure 3.11 shows the speedup and performance results for all parallel implementations. The best performance was observed with Pthreads implementation with 4 processors as observed in Figure 3.11. A maximum performance of 2.8 GFLOPs was achieved,

whereas the maximum speedup was 3.962. Hence, Pthreads implementation was utilized to obtain the statistical results in this study.

A two-dimensional model was developed in the current study, hence it has several potential sources of errors. First of all, the missing third dimension would affect the resulting effective porosity and tortuosity values, since new paths for the fluid molecules will be opened and both effective porosity and tortuosity will be increased. Finally, hardware with more than 4 processors will definitely provide better results, since the availability of higher confidence level studies are provided. All these issues are subject of the ongoing study.

Conclusions

A novel model called the double-path-percolation theory was developed to simulate low-tortuosity fluid flows through inhomogeneous random porous channels, and introduced in this study. The double path-percolation model is different than existing models through its stochastic approach, and introduction of solid cluster labelling. A single-component single-phase Lattice-Boltzmann model was applied to investigate the diffusion behavior of gases in the low-tortuosity channels. Tortuosity was analyzed for the media with a great range of effective porosity, and had values between 1.0005 and 1.0663. The impacts of effective porosity and tortuosity on effective diffusion in porous media were also investigated, and compared with the high-tortuosity flows. It was concluded that the effective tortuosity has a negligible effect on mass diffusion in the channels generated by double-path-percolation theory. A new effective diffusion model was developed to predict the effective diffusion coefficient as a function of effective porosity. In this model, the diffusion ratio increases with the effective porosity with a power of 1.0122.

Furthermore, three high performance systems were implemented on two sections of the code, and the performances were examined to determine the optimal application programming interface for this particular work. The best performance of 2.8 GFLOPs, was achieved by the Pthreads implementation with four processors, and the gained speedup was computed as 3.962.

The introduced porous channel simulation technique can be utilized in any porous medium application involved with transport phenomena in solid and void paths, and the results of the current work can be applied in any mass diffusion study with low-tortuosity porous channels.

Appendix

Table 3.1. History calculations for double-path-percolation model.

Confidence Level	$\text{erf}\left(\varepsilon\sqrt{\frac{n}{pq}}\right)$	$\varepsilon\sqrt{\frac{n}{pq}}$	p	n	Nodes trials	Nodes trials	Nodes trials	
95%	0.475	1.9604	0.55	951,184		83	166	248
			0.60	922,360	240x48	81	161	241
			0.65	875,321		76	152	228
97%	0.485	2.1707	0.55	1,166,205	Aspect ratio=5 170x54	80	160	240
			0.60	1,130,866		78	156	233
			0.65	1,071,966		74	148	221
99%	0.495	2.5767	0.55	1,643,248	Aspect ratio=10 300x60	92	182	273
			0.60	1,593,452		88	177	266
			0.65	1,510,460		84	168	252
					Aspect ratio=15		270x18	233
							300x20	266

Table 3.2. History calculations for single-phase Lattice-Boltzmann model in double-path percolation theory.

Confidence Level	$\text{erf}\left(\varepsilon \sqrt{\frac{n}{pq}}\right)$	$\varepsilon \sqrt{\frac{n}{pq}}$	p	n	Aspect ratio	Nodes	Trials	RAE size	RAE # in a size
99%	0.495	2.5767	0.60	1,593,452	5	300x60	88	55x11	30

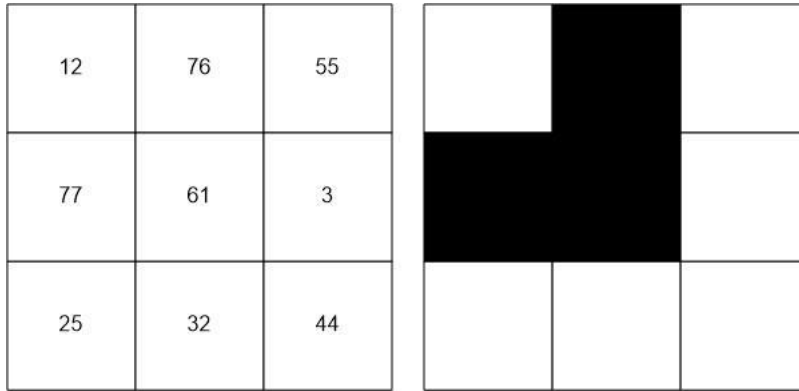


Figure 3.1. Random inhomogeneous porous medium generation.

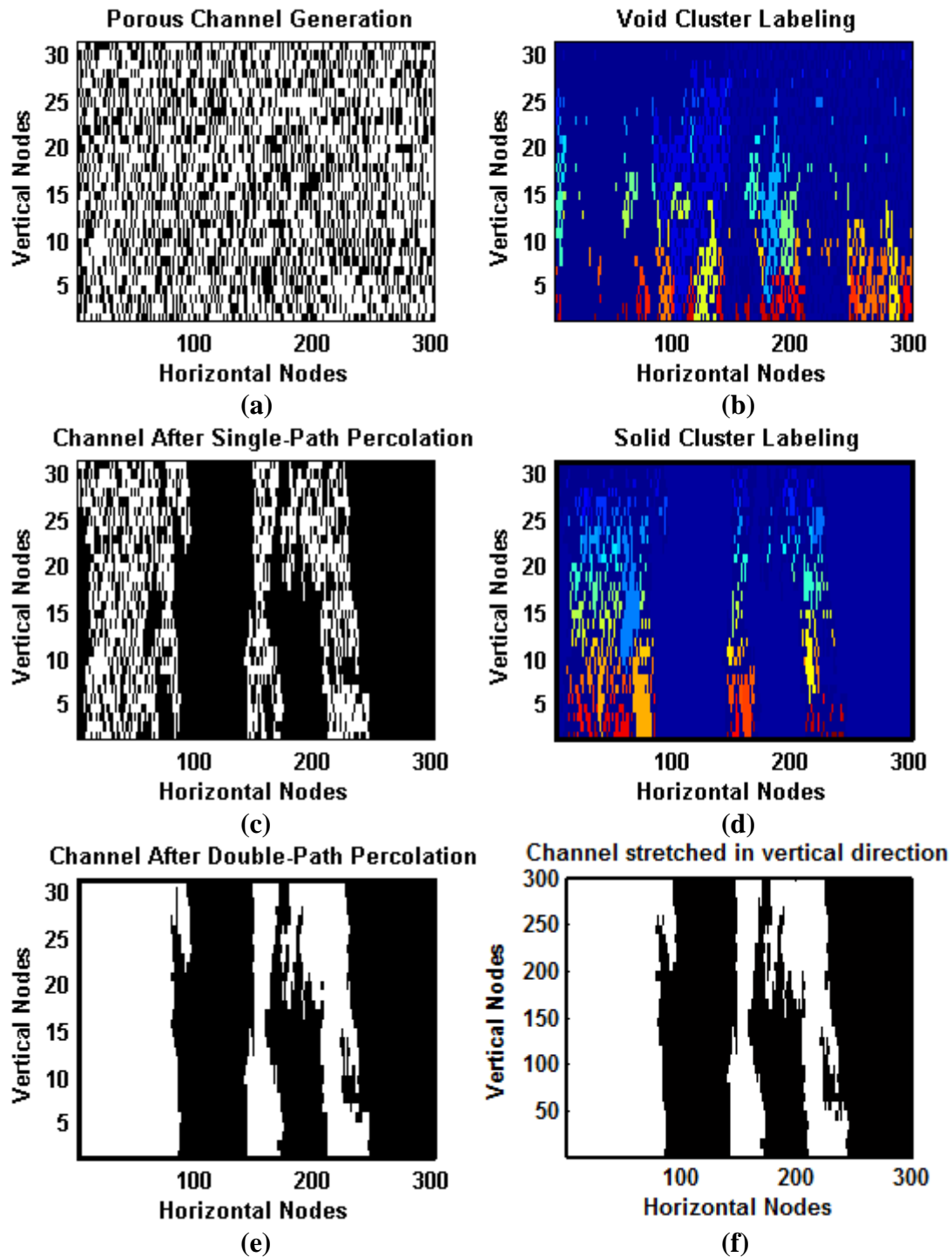


Figure 3.2. Random porous medium with an aspect ratio and target porosity of 10 and 60%, respectively.

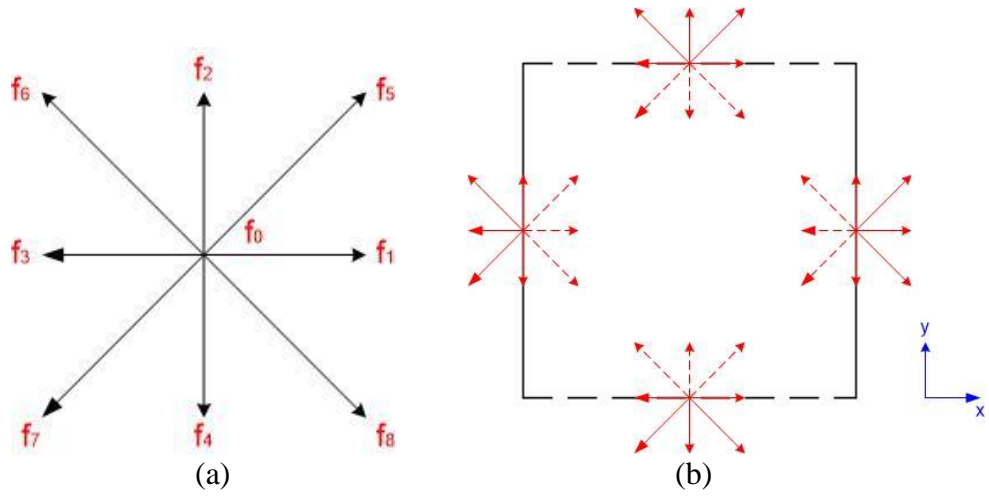


Figure 3.3. A D_2Q_9 lattice (a) a square lattice with nine velocity components (b) lattices at the boundaries with the unknown (dashed) components.

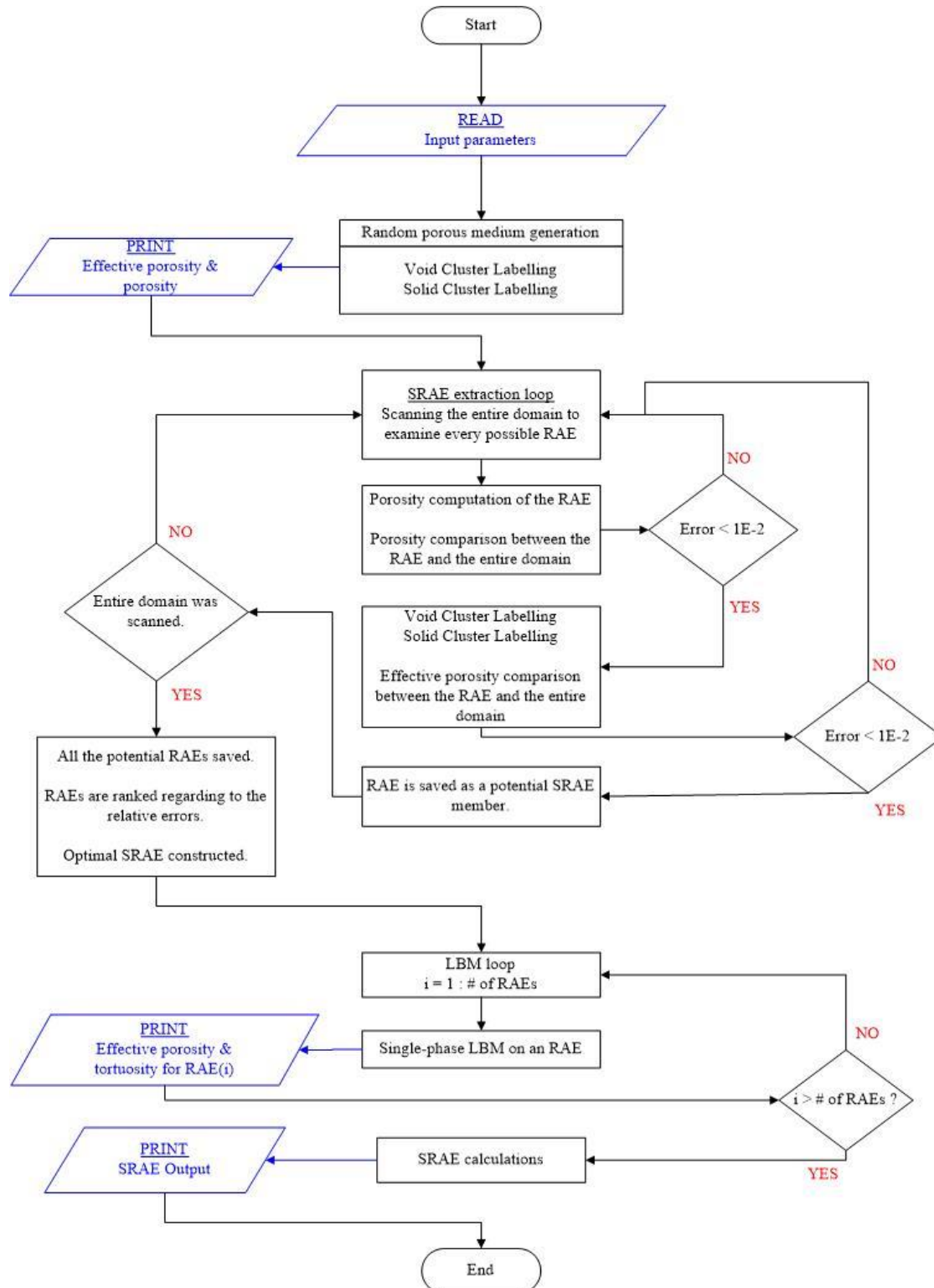


Figure 3.4. Flowchart of the single-phase serial code for a single trial.

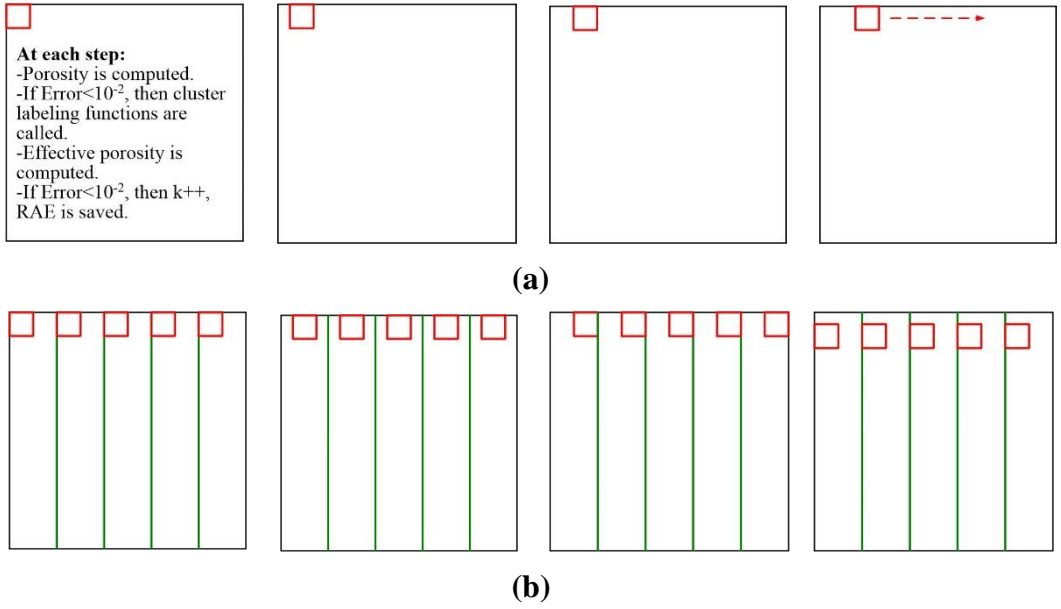


Figure 3.5. SRAE extraction by (a) the serial code, and (b) the parallel code with 5 processors.

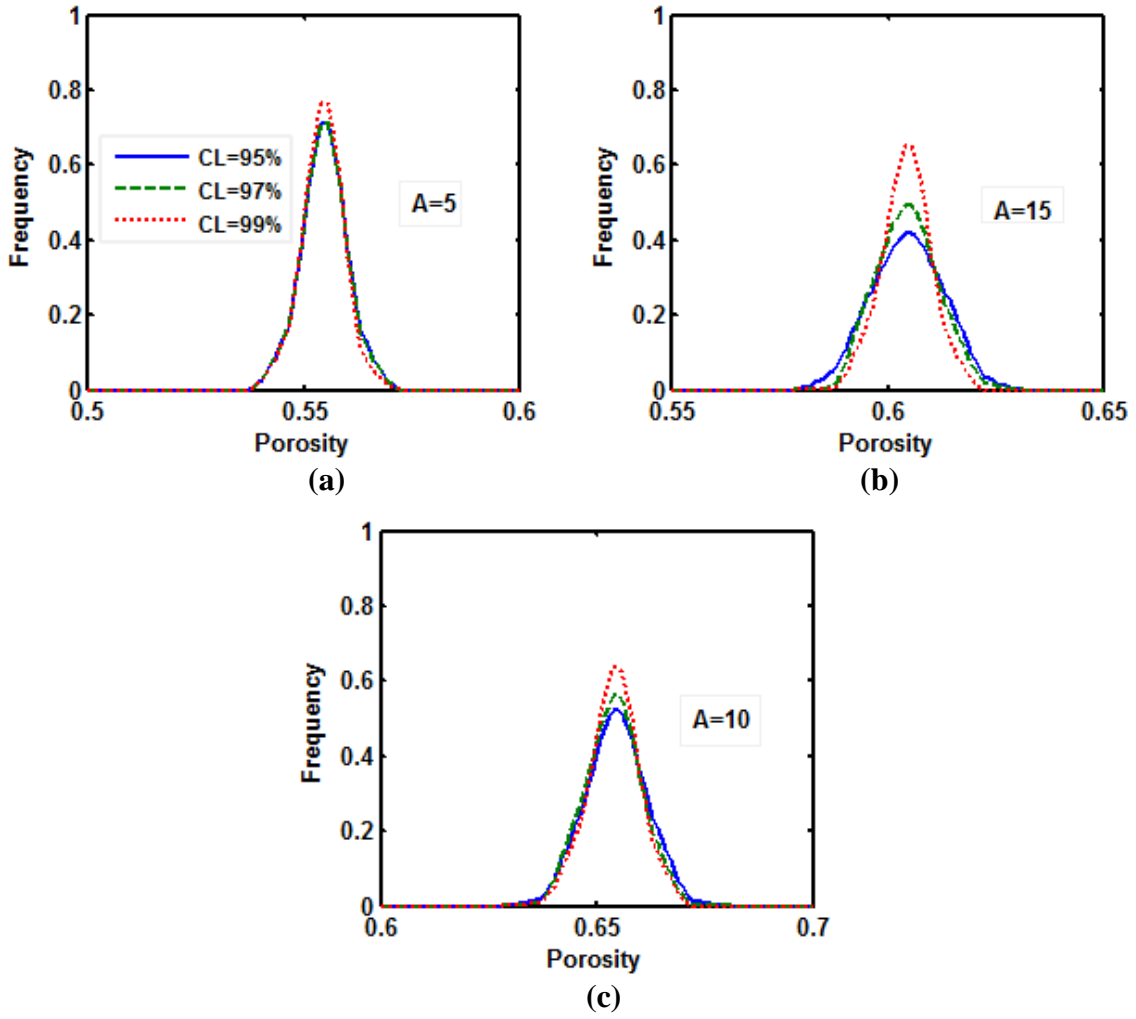


Figure 3.6. Results of the confidence level study for porosity. Target porosities and aspect ratios are (a) 55%, A=5, (b) 60%, A=15, and (c) 65%, A=10.

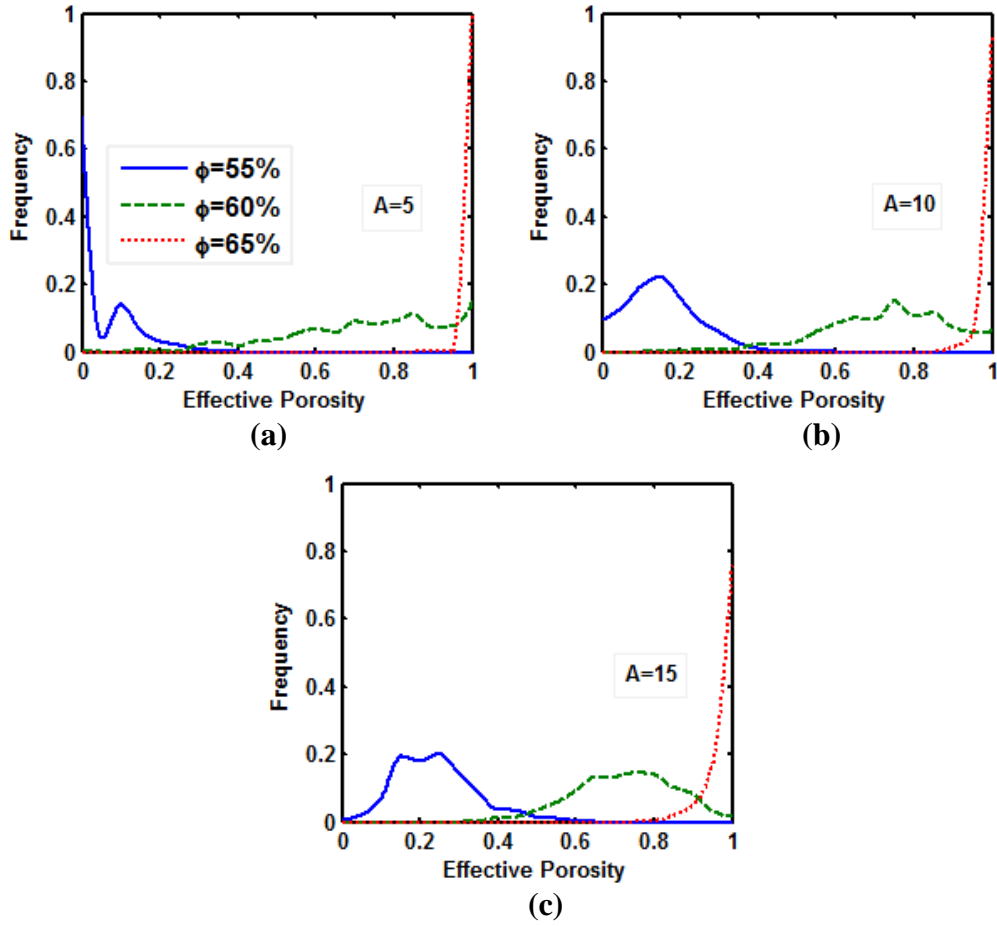


Figure 3.7. Results of the confidence level study for effective porosity with all three target porosities. The aspect ratios are (a) $A=5$, (b) $A=10$, and (c) $A=15$.

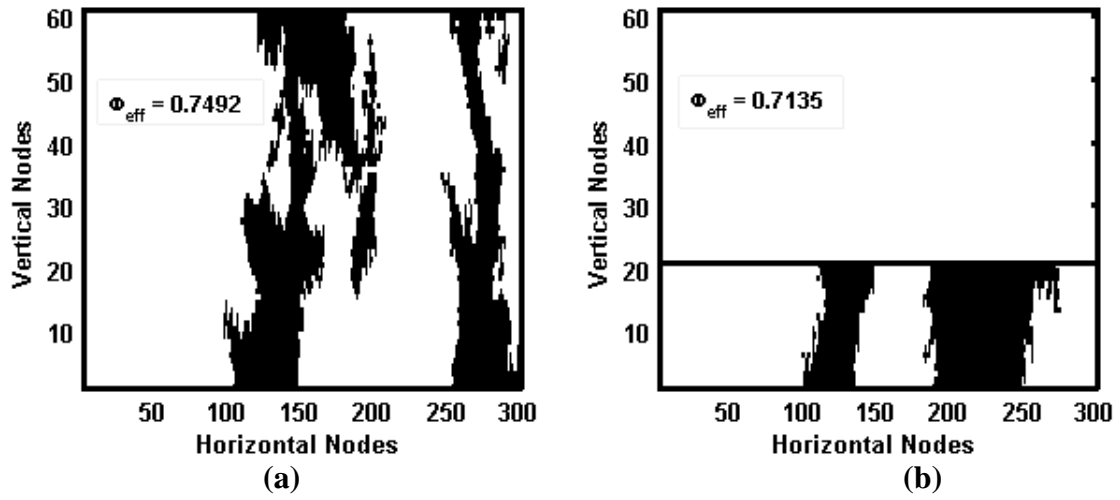
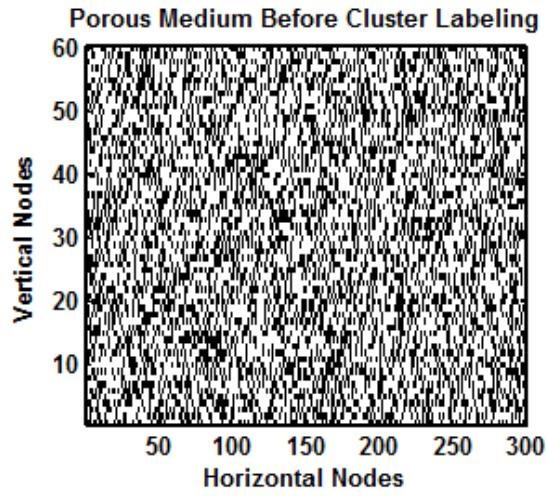
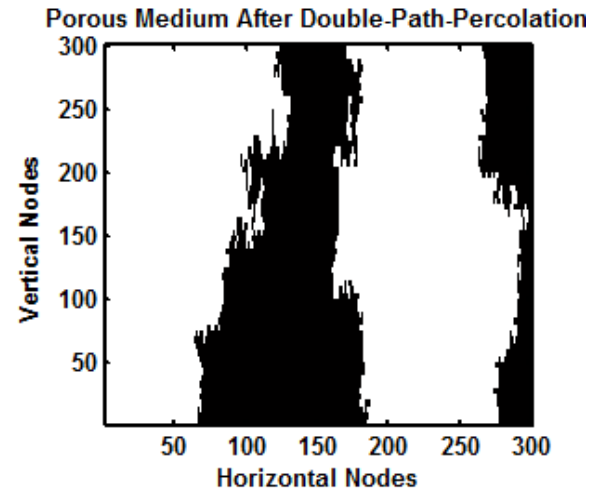


Figure 3.8. Two random porous channels generated by double-path-percolation theory. The aspect ratios are: (a) $A=5$, and (b) $A=15$.

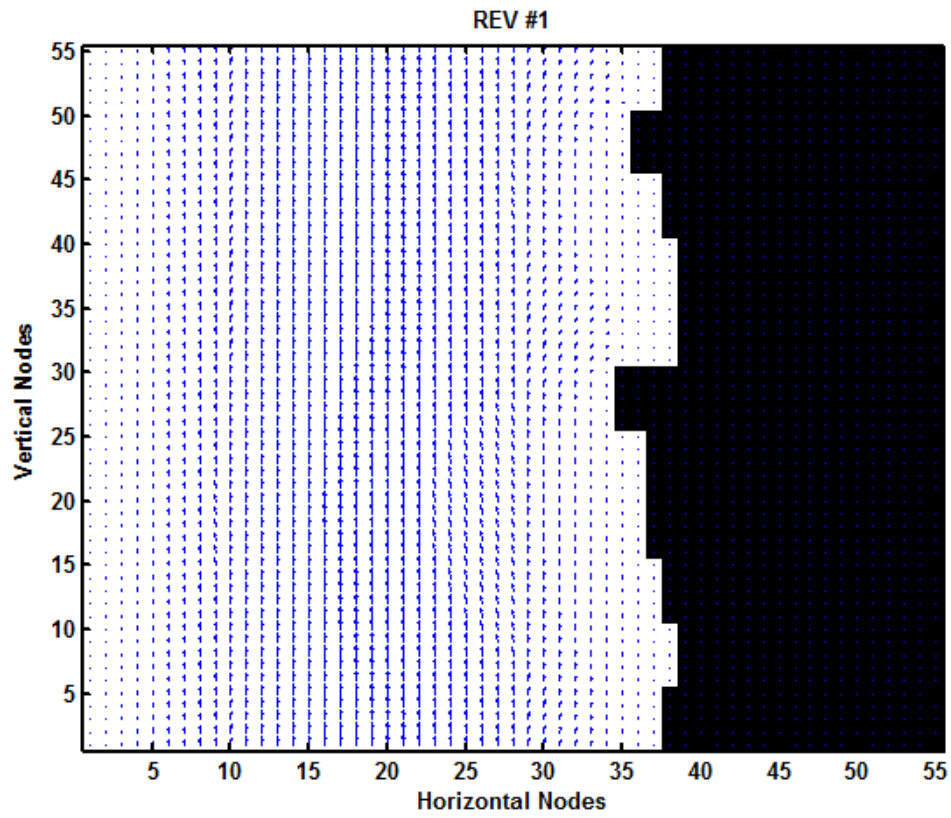
Figure 3.9. A sample double-path-percolation and LBM procedure; (a) initially generated porous domain, target porosity = 0.6000, resulting porosity= 0.6002, (b) effective domain with an effective porosity of 0.6659, LBM results for (c) RAE #1 ($\Phi_{eff} = 0.6661, \tau_{eff} = 1.0010$) and (c) RAE #20 ($\Phi_{eff} = 0.6975, \tau_{eff} = 1.0028$).



(a)



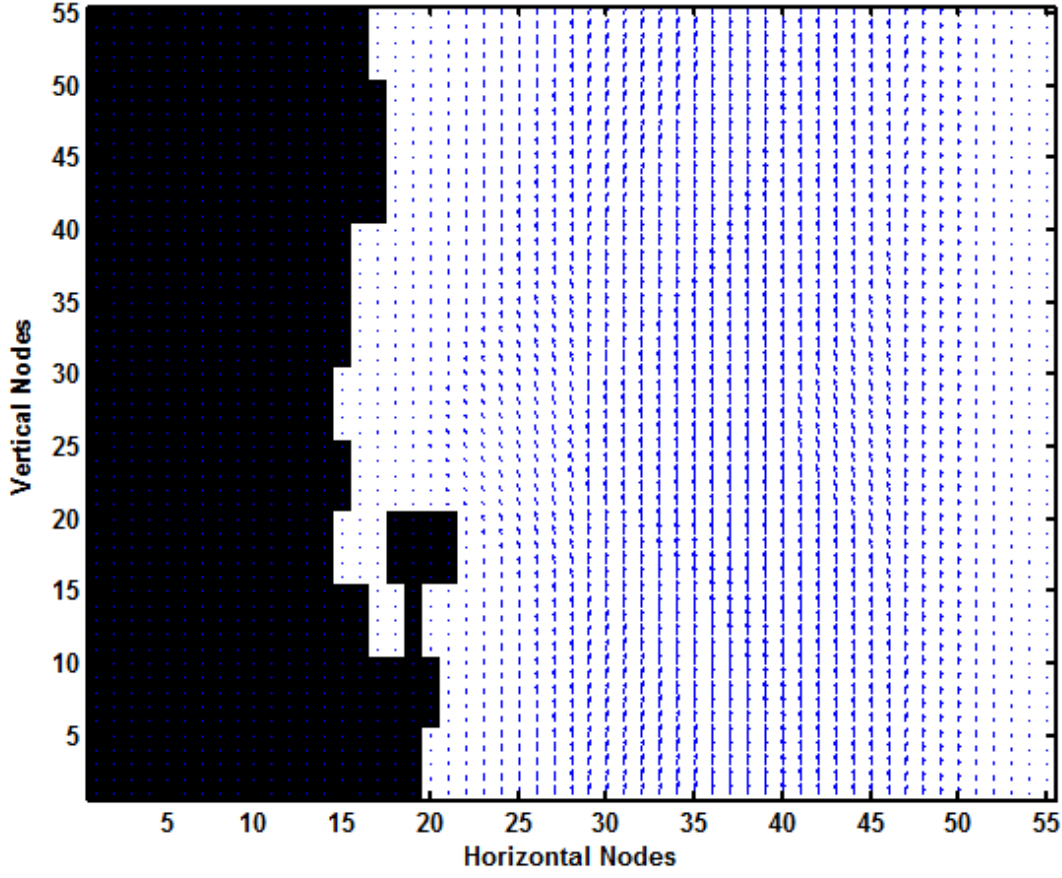
(b)



(c)

Figure 3.9. Continued.

REV #20



(d)
Figure 3.9. Continued.

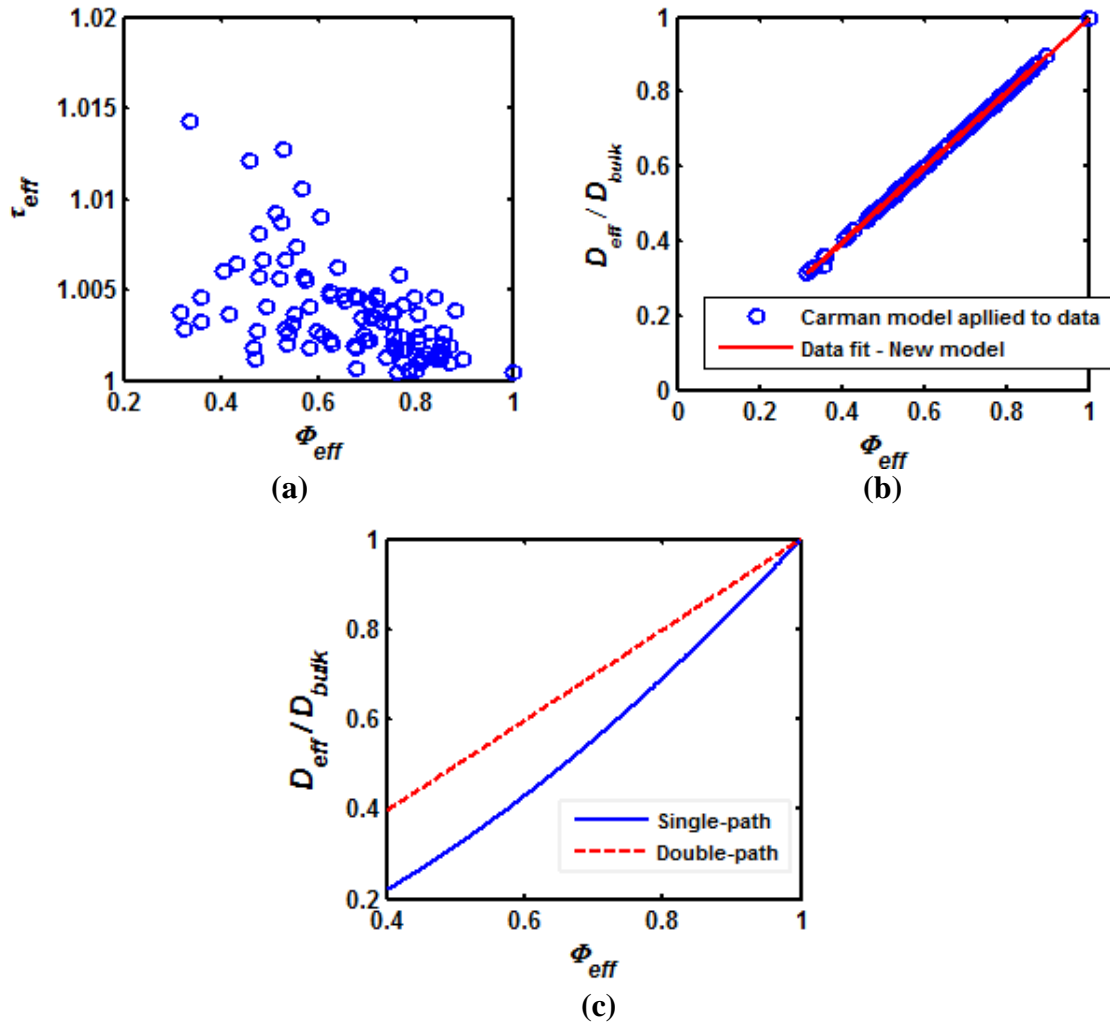
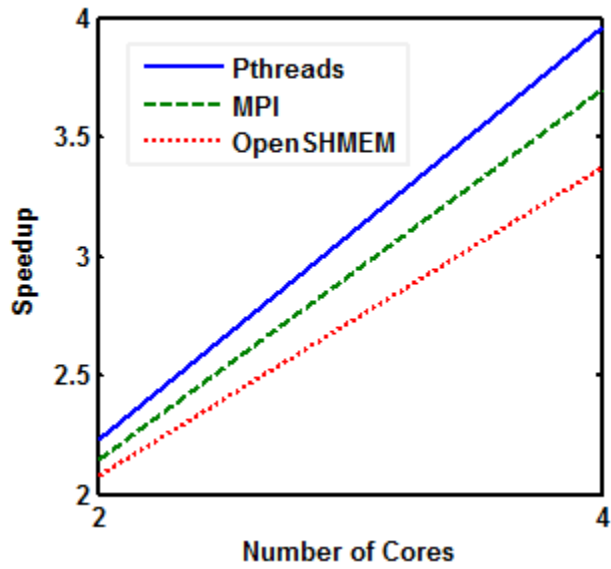
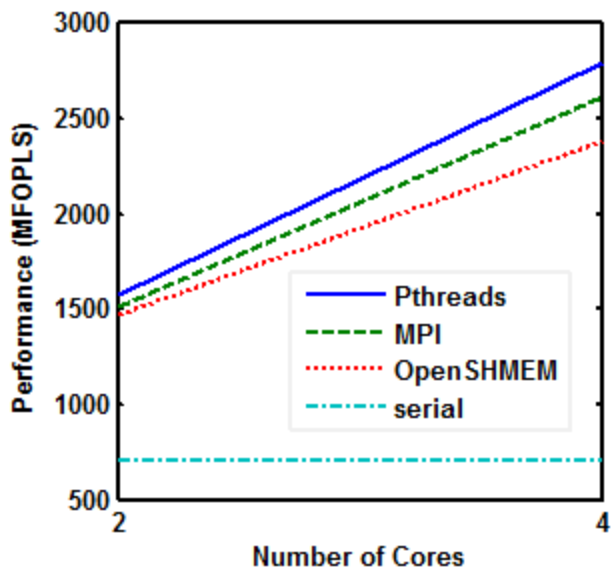


Figure 3.10. Double-path-percolation results – (a) Tortuosity vs. effective porosity vs. porosity, (b) new diffusion model, (c) comparison with high-tortuosity (single-path-percolation) model.



(a)



(b)

Figure 3.11. Speedup and performance achieved by three different high performance systems.

CHAPTER IV
SINGLE- AND MULTI-PHASE FLOW ANALYSIS IN
INHOMOGENEOUS RANDOM POROUS CHANNELS: II. EFFECTS OF
HYDROPHOBIC SOLID STRUCTURES ON MASS TRANSFER WITH
SINGLE- AND DOUBLE-PATH-PERCOLATION THEORIES

Abstract

In this study, statistical single- and double-path-percolation theories were applied to simulate high- (above 1.0700) and low-tortuosity (between 1.0005 and 1.0700) porous channels, respectively. Single-path-percolation theory was used to simulate void paths in the channel for the fluid molecules, and double-path-percolation theory was used to simulate both void and solid paths. Single- and multi-phase Lattice-Boltzmann models were developed to investigate the effects of 0%, 10%, and 20% liquid saturation on gas transport in the channels. In low-tortuosity systems, effective tortuosity was increased with the liquid volume for all effective porosity ranges. For a high-tortuosity high-porosity medium, tortuosity was increased with the liquid formation. When the effective porosity was decreased significantly, fewer pathways were left in the channels. If a pathway was plugged by the liquid molecules, the effective porosity would reduce more. The remaining paths were mostly almost vertical, and it caused a decrease in effective tortuosity. Although there are differences in the effects of liquid content on effective tortuosity as a function of effective porosity, a general trend was observed in impact of liquid formation on effective diffusion coefficient in porous channels, which states that the existence of liquid molecules reduces the amount of gas diffused. Furthermore, 0%, 50%, and 100% of the solid surface inside the channel was set hydrophobic, and the effects were examined with 10% and 20% condensate cases. The hydrophobic content in the channel slightly decreased the effective diffusion coefficient in low-tortuosity systems, since the tortuosity was increased. However, in high-tortuosity systems it has a negligible effect on tortuosity and gas diffusion. Finally, an in-house pthreads program was developed to work with higher computing

performance using parallel programming. A speedup and a peak performance of 3.763 and 2.788 GFLOPs were achieved, respectively, using a hardware with four physical processors.

Nomenclature

a	A parameter to include intermolecular attractive force into the van der Waals equation of state, ($m^6 \text{ Pa/mol}^2$)
b	A parameter to include the effects of non-negligible molecule volume into the van der Waals equation of state, (m^3/mol)
CL	Confidence level
c	Unit lattice velocity, (m/s)
D_{bulk}	Bulk diffusion coefficient, (m^2/s)
D_{eff}	Effective diffusion coefficient, (m^2/s)
F	Intermolecular force, (N)
F_{ads}	Adsorption force between solid and liquid particles, (N)
f	The probability distribution function
f^{eq}	Equivalent distribution function
G	Intermolecular interaction strength
G_{ads}	Intermolecular adsorption strength
k	Lattice index
N_{RAE}	Number of the representative area elements in a statistical representative area element set
n	Total history number
n_m	Number of moles of the fluid

P	Pressure of the fluid, (Pa)
Pr	Probability of any event to occur
p	The probability of a pore to occur in a node
q	The probability of a solid to occur in a node
R	Gas constant of the fluid, (J/mol K)
S_{ads}	A switch parameter that can be 0 or 1.
T	Temperature of the fluid, (K)
t	Time, (s)
U	Velocity, $u = \sqrt{u^2 + v^2}$, (m/s)
u	Velocity in horizontal direction, (m/s)
V	Volume of the fluid, (m ³)
v	Velocity in vertical direction, (m/s)
w	Weighting factor of the lattice components
\bar{X}	Arithmetic average of any property
x	Horizontal distance, (m)
y	Vertical distance, (m)

Greek Letters

ε	Error between the true and estimated probabilities of an event
ρ	Density of the fluid, (kg/m ³)
ρ_0	An arbitrary parameter, (kg/m ³)
τ	Tortuosity
τ_{eff}	Effective tortuosity

ϕ	Porosity
ϕ_{eff}	Effective porosity
ψ	Intermolecular interaction potential
ψ_0	An arbitrary parameter

Introduction

This work contains two main components. In the first part, random inhomogeneous porous channels were simulated by two methods. The first method is called the single-path percolation theory, which was developed by Jung et al. [2] to investigate the electrical property variations in spatially-disordered inhomogeneous media, using a statistical approach based on the law of large numbers [42]. The path-percolation model was modified to examine the diffusion behavior of gases in randomly generated inhomogeneous porous channels by Cekmer et al. [47]. With the developed two-dimensional model, inhomogeneous porous media were randomly generated depending on the initial porosity, and effective porosities were determined by eliminating the orphan pores, which do not contribute to mass transport. A Lattice-Boltzmann model (LBM) was utilized to solve the momentum balance equation, and statistical effective tortuosity values were determined using the velocity distribution throughout the porous channels. The single-path-percolation theory was also used in Chapter II to examine the multi-phase mass transfer in random porous channels. In this work, effective porosities and tortuosities were determined for different liquid-solid-vapor configurations using a combined path-percolation and single-component multi-phase LBM. Although tortuosity was observed to be increased or decreased with liquid formation in the channel, the effective diffusion coefficient was always reduced with increased condensate. In the same study, a parallel programming application was

used to achieve higher computing performance with a reduced runtime. Four processors were used in a fork and joint model in LB simulations, and a performance and a speedup of 1.275 GFLOPs and 3.3553 achieved, respectively. A new path-percolation model called the double-path-percolation was developed in Chapter III to simulate low-tortuosity flow systems. In this work, a new diffusion model was developed for low-tortuosity systems, and compared with that of statistical single-path-percolation model. A single-component single-phase LBM was applied on low-tortuosity channels, and the code was improved using three different high-performance computing systems; Posix threads (Pthreads), OpenSHMEM, and MPI. A speedup of 3.962 with a performance of 2.8 GFLOPs were achieved with four processors in Pthreads implementation.

In the current study, the effects of surface-fluid interactions on multi-phase mass transfer were investigated for high- and low-tortuosity systems by single- and double-path-percolation models, respectively. A single-component multi-phase LBM was developed using the van der Waals equation of state to include the effects of intermolecular attractive forces as introduced by Shan and Chen [27], and He and Doolen [28]. Furthermore, the adhesive interaction force between the fluid molecules and the surface was also included in the model as introduced by Martys and Chen [29], to simulate the effects of hydrophobic surface on multi-phase mass transfer. In addition, Pthreads codes were developed for the combined path-percolation – Lattice-Boltzmann models, and the same hardware in [54, 55] was used with four processors each with 2.40 GHz speed. This study is therefore an extension to the previous statistical works done by Cekmer et al. [47, 54, 55].

Its statistical approach based on the law of large numbers with the novel cluster labeling process make this work different than the previous inhomogeneous porous medium studies. The

statistical outcome of this work can be used in any low- and high-tortuosity inhomogeneous porous medium system involved with multi-phase flow with hydrophilic and hydrophobic solid structures. Furthermore, the methods introduced here can be applied on any porous system involved with transport phenomena in both its solid and void regions, as in gas diffusion layers (GDL) of a polymer electrolyte fuel cell (PEFC), in which there is species transport through void regions, whereas electrons travel through solid paths [52].

Methodology

In the first part of this study, a confidence level analysis for an inhomogeneous random porous medium construction is conducted using statistical single- and double-path-percolation theories. This was followed by a statistical representative area element (SRAE) extraction procedure with two-point statistics. Then, a typical LBM simulation was explained in detail for three different liquid formation amount in the channel; 0%, 10%, and 20%, and three solid structure cases with a hydrophobic content of 0%, 50%, and 100%. The detailed procedure of constructing a random domain by single- and double-path-percolation theories with their separate cluster labelling processes can be found in Chapters I and III, respectively, and was not repeated here.

Confidence-Level Calculations

The model initiates with a confidence-level study to obtain statistical results with a 99% confidence level. The confidence level, CL , expresses the reliability of any estimate and the following relation is derived to relate the confidence level to the estimated and resulting parameters in terms of an error function [42]:

$$\frac{CL}{2} = \text{erf}\left(\varepsilon \sqrt{\frac{n}{pq}}\right) \quad (4.1)$$

where, p and q are the estimated probabilities of generating a pore and a solid in a single node, respectively. Thus q becomes $1-p$ since there are only two probabilities of the phase assigned to a node. The difference between the true and estimated probabilities of an event, which is the porosity in this case, is called the error and represented by ε . The error is set to 1×10^{-3} in this work. The only unknown, n , is the total history number, and calculated by Eq. (4.1) and an error function table [42]. Mathematically, the history number is the multiplication of the node number, which is the size of the domain, and the trial number, which is the needed number of simulations to reach the desired porosity within the specified error range.

The confidence-level study was performed for double path-percolation theory, in which the target porosity of the inhomogeneous domain is 60% [54]. Hence, p and q become 0.60 and 0.40, respectively, whereas CL and ε are 0.99 and 1×10^{-3} , respectively. Using an error function table lets us calculate the RHS of Eq. (1) as 2.5767, which makes n 1,593,452. A domain size of 300×60 was determined, hence the trial number becomes 88. The results for the initial porosity can be found in [54]. In this work, the result of the confidence-level study was also used in hydrophobic solid particle injection as explained in the Results and Discussion section. The trial number determined here was also applied to single-path-percolation simulations to compare the results of these low- and high-tortuosity flow systems.

For the LBM simulations, the entire domain was not used. Instead, an SRAE set was constructed by selecting many representative area elements (RAEs), and the LBM was applied on all these RAEs in an SRAE set as explained in the following sections. Another confidence-

level study is needed for the LBM simulations. To do this, an RAE size of 30x6 was selected. This time, the history number (1,593,452) becomes the multiplication of the trial number (88), RAE size (180), and RAE number in an SRAE set. Thus, the RAE number in a set becomes 100.

Hydrophobic Solid Addition

Unique to the previous path-percolation works [47, 54, 55], the surface-fluid interactions were included in this combined path-percolation – multi-phase LB model in this work. To do this, after the generation of the initial domain, and the cluster labelling process, in other words; after obtaining the effective domain, hydrophobic solid particle injection was performed. A subroutine was developed to inject hydrophobic particles on the surface of the solid regions, which is in contact with gas. Two examples with target porosity of 60% and hydrophobic content of 50% for both percolation models are explained here. To provide a clear and simple demonstration, the domain size was selected 100x100 for single- and 100x20 for double-path-percolation model to keep the aspect ratio of 5 as explained in Chapter III.

In single-path-percolation model which simulates paths only in the void region, the first step is generating a random porous domain as shown in Fig. 4.1(a). The porosity of the initial domain is 59.96%. The cluster labeling process is performed to eliminate the orphan pore clusters, which are not connected to both inlet (the bottom boundary) and outlet (the top boundary) of the channel. The interconnected pore clusters are shown in Fig. 4.1(b), whereas the effective domain in Fig. 4.1(c). The resulting effective porosity is 37.91%. In Fig. 4.1(d), the hydrophobic solid particle spraying is presented. The resulting hydrophobic content on surface is 50.96%. Another consideration of the hydrophobic implementation is the active hydrophobic area. The parts of the hydrophobic solids, which are not in contact with void will be passive as

presented in Fig. 4.2. The active hydrophobic area is computed 54.23% of the total hydrophobic solid area.

Low-tortuosity porous channel generation is done by double-path-percolation theory. There are a few differences between these two percolation models. First, the aspect ratio in double-path-percolation model, which is defined as the ratio of the horizontal to the vertical length of the channel is not 1 as in single-path-percolation model. Instead, it was selected 5 to enable two transport paths; one in solid and the other in void regions. Furthermore, there are two additional steps in the double-path-percolation model. The first one is the solid cluster labeling process, which groups the interconnected solids into clusters, and eliminates the orphan solid nodes. The next difference is the stretching process. The aim of this work is to compare the multi-phase mass transport behavior in both systems with the same size. That is why the aspect ratio is set to 1 again by stretching the channel in vertical direction, after generating the low-tortuosity porous domain. The entire process is demonstrated in Fig. 4.3. The initial porous medium with a porosity of 59.15% was generated. The void and solid cluster labelling processes were applied, and an effective porous domain with a porosity of 37.55% is obtained. After the hydrophobic particle spraying, 51.23% of the solid particles became hydrophobic, with an active area of 30.03% of the total hydrophobic area.

A difference of 24.2% in active hydrophobic area was observed in these two examples with approximately the same effective porosity and hydrophobic content. The statistical results are discussed in the “Results and Discussion” section.

SRAE Selection Process

In the multi-phase transport simulation part of this study, LBM was applied on the system for many times as explained in “Pthreads Implementation” section. Since, the Lattice-Boltzmann model is a computationally intensive method, although it is not as intensive as Navier-Stokes based models, an alternative method is needed. To do this, a tool called the two-point statistics was used in the current work [43, 44, 47]. Instead of applying LBM on the entire domain, smaller representative domains were extracted. An RAE is a domain smaller in size, which represents the entire domain in terms of porosity, effective porosity, and hydrophobic solid content. An SRAE is a set of RAEs, which were optimally extracted from the entire domain [55]. To determine the properties of the SRAE set, the following equation is used:

$$\hat{X} = \frac{1}{N_{RAE}} \sum_{m=1}^{N_{RAE}} X_m \quad (4.2)$$

where, X can be set as porosity, effective porosity, and tortuosity, \hat{X} is the ensemble average of any of these properties, X_m is the property of the m^{th} RAE, and N_{RAE} is the total element number in a set, which is 100 in the current work. In summary, every single SRAE set is considered as a single virtual representative domain of the entire channel, and its properties are calculated by Eq. (4.2).

A Multi-Phase Lattice-Boltzmann Model

A D₂Q₉ lattice was used in this study, and the equations for the single-component single-phase LBM is the same as that of Cekmer et al. [47], except that a single-relaxation time was applied in collision process, instead of multi-relaxation matrix:

$$f_k(x + c\Delta t, y + c\Delta t, t + \Delta t) - f_k(x, y, t) = -\frac{1}{\tau} [f_k(x, y, t) - f_k^{eq}(x, y, t)] \quad (4.3)$$

$$f_k(x + \Delta x, y + \Delta y, t + \Delta t) = f_k(x, y, t + \Delta t) \quad (4.4)$$

where, x and y are the horizontal and vertical positions, f is the probability density function, k is the lattice index, t is time, c is the unit lattice velocity, and τ is the single-relaxation factor [4, 5, 56]. The van der Waals equation of state was used to include the long-range intermolecular attractive forces to simulate multi-phase flow in porous channels. To do this, a single-component multi-phase LBM was developed [5, 27]. In this isothermal multi-phase model, the intermolecular attractive force causes a phase separation between liquid and vapor. Initially, the porous channel was occupied by a two-phase fluid with a non-zero thermodynamic quality. Hence, there is no phase change included in the model, only a phase separation after the phase change is considered. The model initiates with a phase separation right after the phase change.

The non-ideal van der Waals equation of state is applied to account the intermolecular attractive forces in the model:

$$P = \frac{nRT}{V - nb} - a \left(\frac{n}{V} \right)^2 \quad (4.5)$$

In Eq. (4.5), n , R , T , V , and P are number of moles, gas constant temperature, volume, and pressure of the fluid, respectively. Furthermore, the second term on RHS accounts for intermolecular attractive forces, and nb represents the non-negligible volume of molecules, which were neglected in the current study. He and Doolen [28] derived a simpler form of the van der Waals EOS to determine the pressure distribution throughout a channel:

$$P = \frac{\rho}{3} + \frac{G}{6} \Psi^2 \quad (4.6)$$

The interaction potential is represented by Ψ , and computed by the following equation in an isothermal process [27]:

$$\Psi = \Psi_0 \exp\left(\frac{-\rho_0}{\rho}\right) \quad (4.7)$$

where, Ψ_0 and ρ_0 are constants. G is the interaction strength. The intermolecular attractive force can be calculated by Equation (4.8), where c_k and w_k are the lattice velocity and weighting factor of the k^{th} velocity component, respectively.

$$F = -G\Psi(x, t) \sum_{k=1}^8 w_k \Psi(x + c_k dt, t) c_k \quad (4.8)$$

Finally, an adhesive interaction force was added to the model to include the effects of hydrophilic and hydrophobic solid surface on mass transport. Two new parameters are needed for the model, which are the adsorption strength, G_{ads} , and a solid switch, S_{ads} , respectively. S_{ads} can take values 0 and 1. If the neighbor of the working node is solid, then it becomes 1, otherwise 0. The adhesive interaction force between the void and solid nodes is shown in Eq. (4.9) [29].

$$F_{ads} = -G_{ads}\Psi(x, t) \sum_{k=1}^8 w_k S_{ads}(x + c_k dt, t) c_k \quad (4.9)$$

The controlling parameter to determine the contact angle between the solid and void is the adsorption strength. Eqs. (4.10-4.11) are the G_{ads} equations for 180° and 0° contact angle, respectively [5].

$$G_{ads} = G \quad (4.10)$$

$$G_{ads} = G\Psi \quad (4.11)$$

Ψ is computed 2.8 by Eq. (4.7), using the average liquid density obtained in the previous work [55]. G is taken -120, hence G_{ads} becomes -341.7 and -120.0 for a 0° and 180° of contact angles, respectively, which are similar to the results by Sukop [5]. A sample simulation is shown in Fig. 4.4. In this example, a low-tortuosity porous domain with an effective porosity of 0.45 was

constructed by double-path-percolation model, and the best representative element was selected for this sample demonstration. The same RAE with a surface with 0% and 100% hydrophobic contents were simulated. Then, multi-phase LBM was applied and 33% of a condensation was obtained. In Fig. 4.4 (a), all the surface was set hydrophilic (0° contact angle), and it is observed that the entire surface attracts the liquid molecules, and the channel stayed open for gas transport with an effective porosity of 29.77%. As presented in Fig. 4.4(b), the surface is 100% hydrophobic (180° contact angle), and the liquid molecules plugged the channel, and caused a zero effective porosity.

To simulate the liquid formation and the hydrophobic solid surface impact on effective gas diffusion coefficient, a simple procedure is pursued. After generating the effective channel by a percolation-theory, SRAE extraction process is performed. For each RAE of the set, a single-phase LBM is applied to obtain the effective porosity and tortuosity of the dry channel. Then, a multi-phase LBM is utilized. The controlling parameter for the amount of the liquid volume is the initial density of the fluid. The density is set to an appropriate value at the beginning and the multi-phase LBM subroutine is executed. If the desired condensate amount, which is 10% and 20% in the current work, is reached, then the nodes occupied by the liquid molecules are treated as solid. The void cluster labelling process is performed to obtain the new effective porosity of the domain. Then, the single-phase LBM function is called to determine the tortuosity for the gas-phase flow. If the desired liquid amount is not reached, the code increases the density, and repeats the procedure again, starting from the single-phase LBM. It ends, after all the information is obtained, and passes to another RAE. The detailed information about this process can be found in [55].

The statistical results are explained in the “Results and Discussion” section.

Pthreads Implementation

A widely-used high-performance computing system called Pthreads was implemented on two separate parts of the path-percolation – multi-phase LBM code. Pthreads provides multiple threads to run in a single memory space [49]. A Pthreads program initiates with a single thread, additional threads are created as needed, and destroyed if a sequential part of the code is reached.

The first parallel part of the code is the SRAE extraction. Instead of using only one processor to scan the entire domain to extract potential RAEs for an SRAE set, four of them are charged. Each thread has its own territory in the domain. The domain matrix, its porosity, effective porosity, and hydrophobic content are read by the threads from the shared memory. The threads scan the region of the domain they are responsible, perform the cluster labelling process and the related computations in their private memories, and store the selected potential RAEs in a matrix in the shared memory. Then, all the generated threads are destroyed and a single thread is charged to rank the selected RAEs, and construct the SRAE set. The SRAE matrix is stored in the shared memory.

The second parallel part of the code is the LBM simulations. All the RAEs are distributed to the threads, and each thread is responsible for its own RAE group. When all the computations are completed, and the effective porosity and tortuosity values for each condensate level are obtained, each thread prints the results in a file [54]. The performance increase was analyzed in the “Results and Discussion” section.

Effective Diffusion in Porous Channels

The effective tortuosity, τ_{eff} , has an important role in mass diffusion in porous media. It is defined as the ratio of the actual path travelled by a particle and the shortest distance between the same points. The computational effective tortuosity is computed by the following equation, where U is the velocity vector, and v represents the velocity component in the flow direction:

$$\tau_{eff} = \frac{\int_A U dA}{\int_A v dA} \quad (4.12)$$

Carman's diffusion model is used to investigate the effects of liquid formation and hydrophobic solid surface on mass transport in inhomogeneous porous channels [11].

$$D_{eff} = D_{bulk} \frac{\Phi}{\tau} \quad (4.13)$$

Two new effective diffusion models for low- and high-tortuosity flows were developed by Cekmer et al. [47, 54] by double- and single-path-percolation theories, and shown in Eqns. (4.14) and (4.15), respectively.

$$D_{eff} = D_{bulk} \Phi_{eff}^{1.0122} \quad (4.14)$$

$$D_{eff} = D_{bulk} \Phi_{eff}^{1.6556} \quad (4.15)$$

The results are explained in the following section.

Results and Discussion

The current study was initiated with random inhomogeneous porous media generation by single- and double-path-percolation models. The first step was the confidence-level study to determine the necessary node and trial numbers. A confidence-level of 99% was selected, and porous domains with a size of 300x300 were generated by these two models. A trial number of 88 was calculated as a result of the confidence level study.

The statistical confidence level results for porosity, hydrophobic content, and active hydrophobic area are presented in Fig. 4.5. Fig. 4.5(a) is the result for the initial porosity of the generated domain. As seen in the figure, the probability range of the desired porosity, which is 60%, is wider in the double-path-percolation model. In confidence level study, 99% confidence level was assigned to the double-path-percolation model, and the size of the domain was set 300x60, whereas the trial number was 88. As explained in the Methodology section, 300x60 domain was stretched by a factor of 5 in vertical direction to compare the results for two square domains generated by single- and double-path-percolation theories. For the single-path-percolation theory, the trial number was kept at 88, whereas the node number became 300x300. Hence, the confidence level was increased. Therefore, the probability of generating a porous medium with the desired porosity is higher in single-path than double-path-percolation model. In the figure in the middle, the probability distributions for hydrophobic solid particle spraying is presented. The desired hydrophobic content is 50%. Again, the probability distribution range is a little wider in double-path-percolation model because of the same reason, which is the confidence level is a little higher than 99% in single-path-percolation model. The figure on the right represents the probability curves for the active hydrophobic area divided by the total hydrophobic area. It is clearly seen that for the same amount of hydrophobic solid content, the active hydrophobic area is much (about 25%) larger in the porous channels generated by single-path-percolation theory. Hence, it is expected that the effects of hydrophobic surface would be less in double-path-percolation results. Another conclusion is that in the single-path-percolation model, by which relatively high-tortuosity porous channels are generated, the same hydrophobic

effect can be obtained using less hydrophobic material on the surface than that of double-path-percolation model.

The first statistical single-path-percolation result is shown in Fig. 4.6, where the effective tortuosity probability ranges are plotted against the occurrence frequency for three different cases. In Fig. 4.6(a), the effective tortuosity probability range for 0%, 10%, and 20% liquid formations in a channel with a porosity higher than 75% was plotted for the cases with 0%, 50%, and 100% hydrophobic surface. It is observed that the tortuosity was increased slightly when the liquid formation was increased from 0% to 10% for the case with 0% hydrophobic surface. Although the results are very similar, the maximum occurrence frequency is observed around 1.4 for 10% liquid formation, whereas it can take any values between 1.2 and 1.6 with almost the same occurrence frequency when the channel is dry. When there is 20% liquid in the channel, tortuosity is increased significantly. If the hydrophobic content on the surface is increased to 50%, tortuosity with 20% liquid decreases, and it takes slightly higher values than the cases with lower liquid formation for the case with 100% hydrophobic surface. The results are different for the domains with porosities between 60% and 75% as seen in Fig. 4.6(b). It must be noted that the results for 0% liquid formation are the same, since there is no effect of hydrophobic surface on pure gas flow. This time, the tortuosities in the channels with 10% and 20% liquid have smaller values than that for dry channel. The liquid molecules plugged some of the paths for the gas flow, and the effective porosity was reduced. Detailed information about the tortuosity reduction with increased liquid formation in low-porosity channels can be found in the article by Cekmer et al. [55]. When hydrophobic content is increased, tortuosity values becomes slightly smaller, and the probability ranges get narrower. In Fig. 4.6(c), tortuosity distribution versus the

occurrence frequency is plotted for the domains with porosities lower than 0.60 for 0%, 50%, and 100% hydrophobic solid surface in porous channels. The effects of hydrophobic surface on tortuosity is similar with the previous case. The only difference is the effects of the porosity. The tortuosity values become smaller, hence the probability range curves are shifted to left. With a liquid formation of 20%, tortuosity has values below 1.5.

The statistical results of the effects of liquid formation and hydrophobic surface on effective tortuosity for double-path-percolation model are presented in Fig. 4.7. The general trend is that the effective tortuosity is increased with the hydrophobic content on the solid surface throughout the channels. The reason is that the hydrophobic surface repels the liquid to the void regions. The results for the channels with a porosity above 75% are shown in Fig. 4.7(a). In a channel with hydrophilic surface, the liquid formation does not affect the tortuosity significantly. The impact of liquid volume increases with the hydrophobic content, especially for 20% condensate. With the decreased porosity, these impacts become more observable. When the effective porosity of the domain is below 60%, the effective tortuosity probability ranges become wider, and the curves shift to right with hydrophobic content.

The impact of the hydrophobic content on the solid surface on effective tortuosity can be seen more clearly in Fig. 4.8, in which the tortuosity probability is plotted against the occurrence frequency for the porous channels generated by single-path-percolation model. When the porosity is above 75%, the hydrophobic content decreases the tortuosity. This effect is much obvious for the case of a channel with 20% condensate as seen in Fig. 4.8(a). For the smaller porosities, no general trend is observed in high-tortuosity systems generated by single-path-percolation theory as seen in Figs. 4.8(b-c). However, in low-tortuosity systems, the increased

hydrophobic solid amount increases the effective tortuosity for all effective porosity ranges as shown in Figure 4.9.

Effective diffusion models shown in Eqs. (4.13-4.15) were used to investigate the effects of condensation and surface characteristics on diffusion ratio, which is defined as the ratio of the effective and bulk diffusion coefficients. The statistical results for the domains with a porosity above 75% are shown in Fig. 4.10. The results for low-tortuosity effective diffusion model developed by Cekmer et al. [54] overlap with those of Carman's equation, especially for the cases with 0% and 50% hydrophobicity. When the surface is set to be 100% hydrophobic, then these two models differ slightly. On the other hand, the high-tortuosity flow diffusion model developed by Cekmer et al. [47] has differences with Carman's model for dry media. When condensation occurs, these two models almost overlap. Liquid formation in the channel reduces the diffusion ratio as expected. Furthermore, the diffusion ratio in the domains with the same porosities generated by single- and double-path-percolation models show a difference of approximately 0.20, and this discrepancy reduces with hydrophilic content on the surface. The difference between the diffusion coefficients of low- and high-tortuosity channels increase with effective porosity as shown in Fig. 4.11. In this figure, the same results are presented for the channels with a porosity between 60% and 75%. Although the hydrophobic solid addition to the surface increases the tortuosity, the reduction in the diffusion ratio is not observed in high-tortuosity systems, but it reduces with the increased hydrophobic content in low-tortuosity domains. This result is observed much clearly in Fig. 4.12, which presents the results for the domains with a porosity higher than 75%. The reduction of diffusion ratio with increased condensate can also be observed in this figure.

A high-performance computing system Pthreads was implemented to the code to achieve a better computing performance. Four processors were used to make the code parallel. Figure 4.13 presents the speedup and performance results. A speedup and a performance of 3.7627 and 2.7876 GFLOPs were achieved, respectively. Although the hardware used is sufficient for the current study, a better one can be used with more than 4 physical cores. Alternatively, a graphical processing unit can be used via CUDA (Compute Unified Device Architecture) to use multiple threads to improve the computing performance, and to apply a better confidence level for more accurate results.

It should be noted that the results here are for a two-dimensional model which can easily be implemented in three dimensions with additional computational cost. The outcomes of a three-dimensional model would be more accurate than the current two-dimensional work, since the effective porosity and tortuosity values will be higher than the current results due to additional pathways into z-direction for transport.

Conclusions

Statistical based path-percolation theories were utilized to investigate the multi-phase mass transport with hydrophobic surface effects in randomly generated inhomogeneous porous channels. A multi-phase Lattice-Boltzmann model with fluid-fluid and surface-fluid interactions was developed to investigate the effects of liquid formation and surface characteristics on mass transport. The conclusions are listed as:

- Single-path-percolation model was used to simulate high-tortuosity (above 1.07) flow channels.

- Double-path-percolation model was used to simulate low-tortuosity (between 1.0005 and 1.0700) flow channels.
- In both low- and high-tortuosity systems, increased liquid volume increases the tortuosity.
- In high-tortuosity low-porosity systems, added liquid content decreases the tortuosity.
- In both low- and high-tortuosity channels, liquid formation decreases the effective diffusion coefficient and gas transport for all effective porosity ranges.
- Hydrophobic surface addition in channel increases the effective tortuosity, and slightly decreases the effective diffusion coefficient in low-tortuosity domains.
- The effects of hydrophobic content on gas diffusion is negligible in high-tortuosity porous channels.

Furthermore, a parallel program using Pthreads is developed for the current work, and a performance of 2.788 GFLOPs was achieved using four processors. The maximum speedup was 3.763. The methods and the statistical outcome of this study can be used in any porous medium application involved with single- and multi-phase mass transport.

Appendix

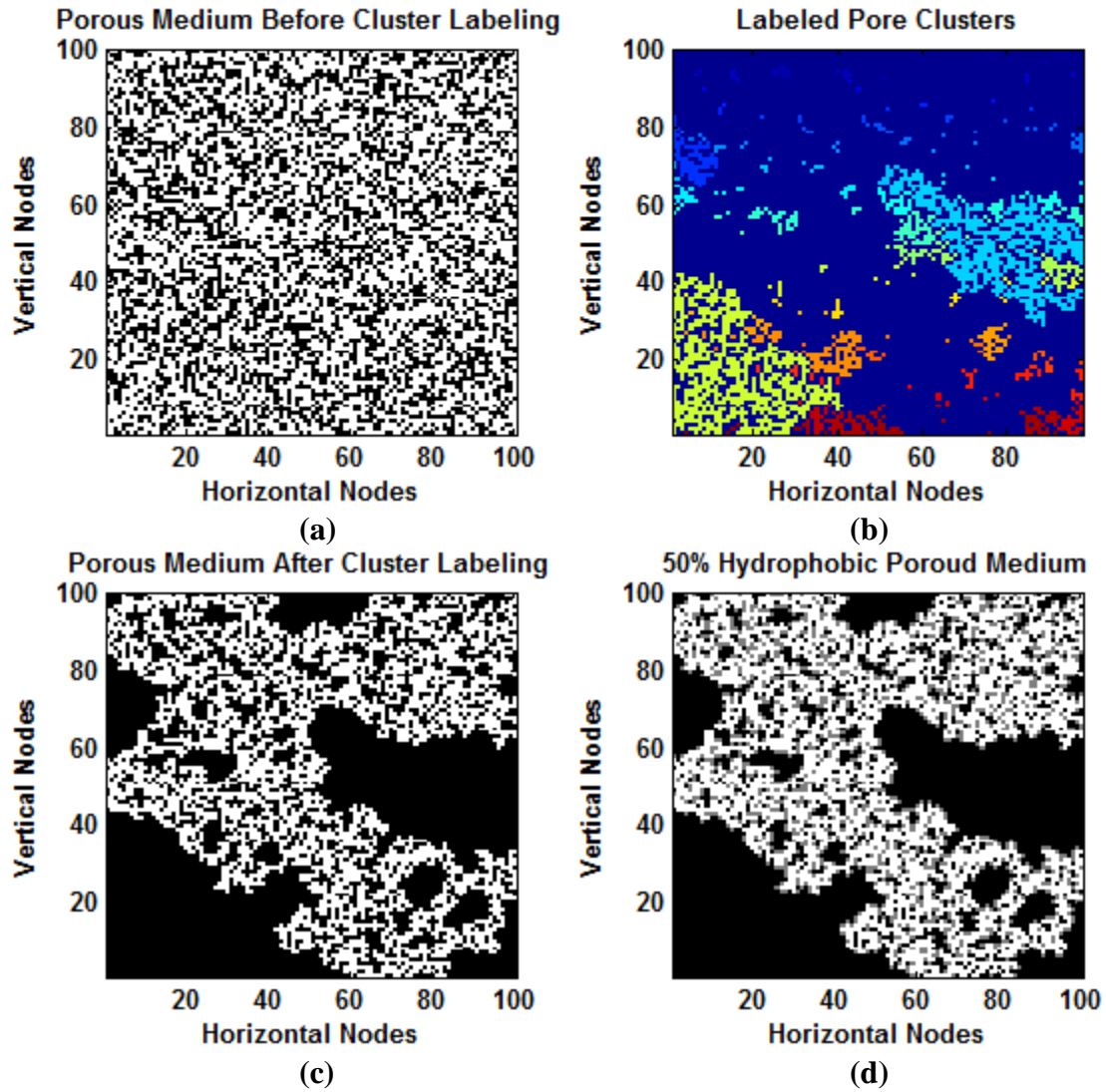
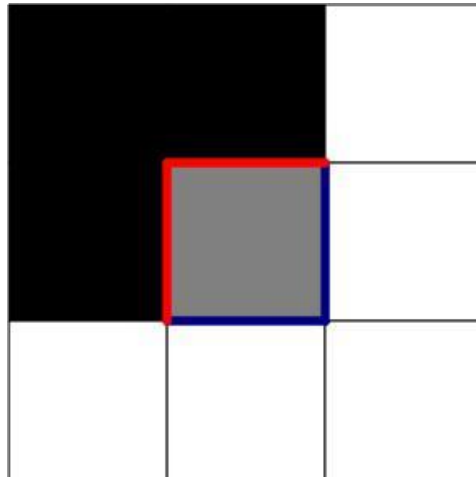


Figure 4.1. An inhomogeneous random domain with 52.5% hydrophobic content by single-path-percolation model. The active hydrophobic area is 54.0% of the total.



- Void
- Hydrophilic solid particle
- Hydrophobic solid particle
- Active hydrophobic area
- Passive hydrophobic area

Figure 4.2. A simple schematic of an active hydrophobic solid content in a representative inhomogeneous porous medium. The active hydrophobic area is 50%.

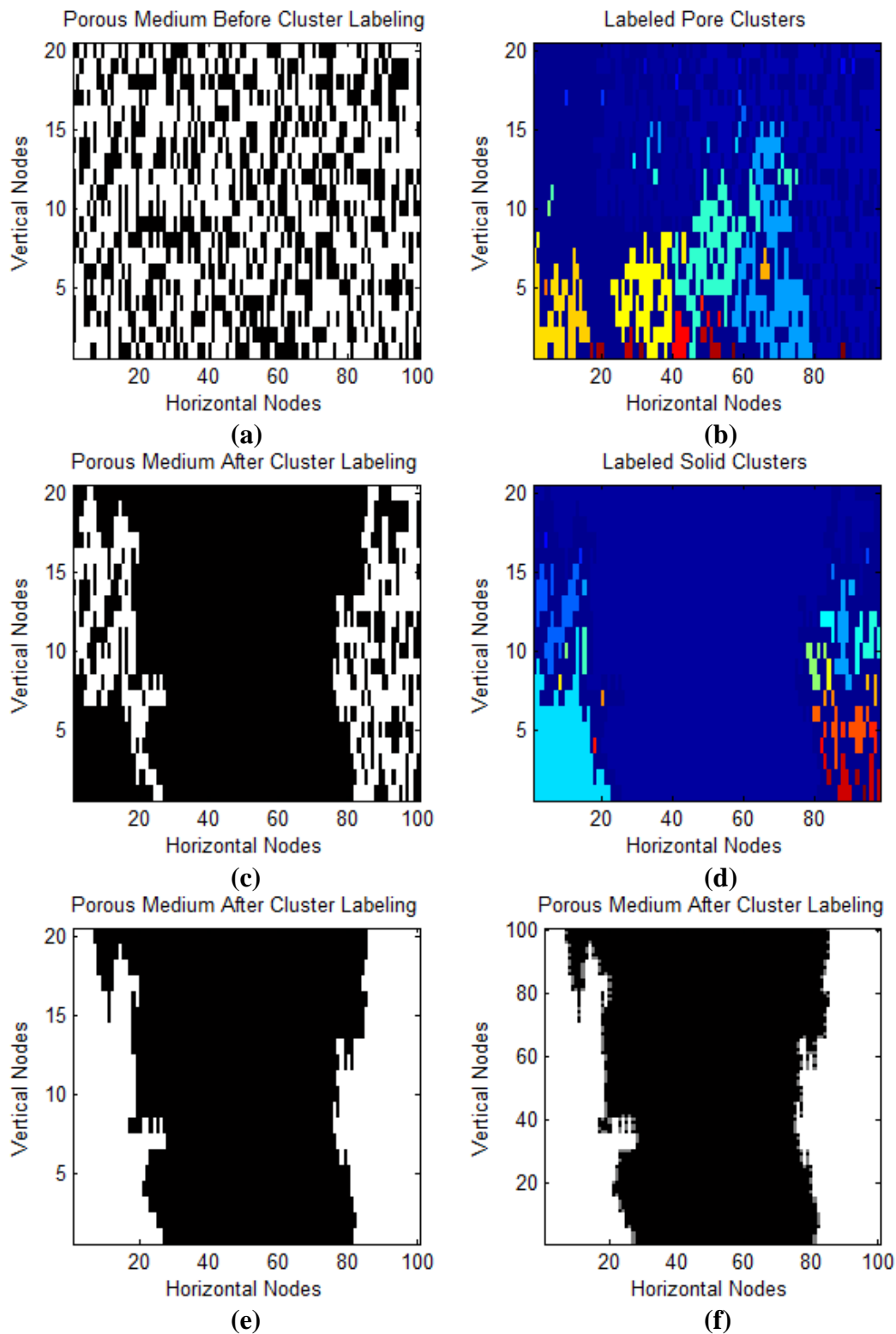


Figure 4.3. An inhomogeneous random domain with 51.23% hydrophobic content by double-path-percolation model. The active hydrophobic area is 30.03% of the total.

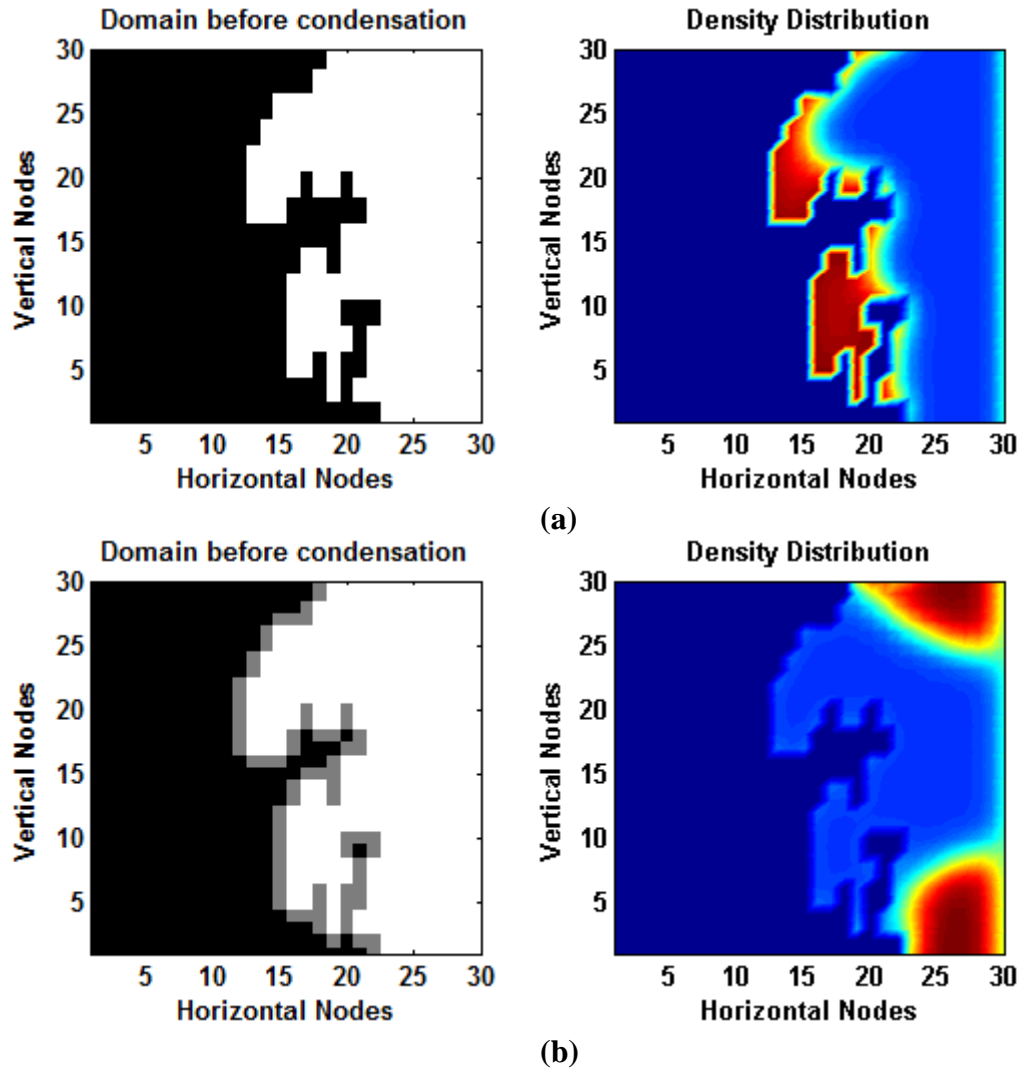


Figure 4.4. 33% liquid formation in a channel with (a) 100% hydrophilic, (b) 100% hydrophobic surfaces.

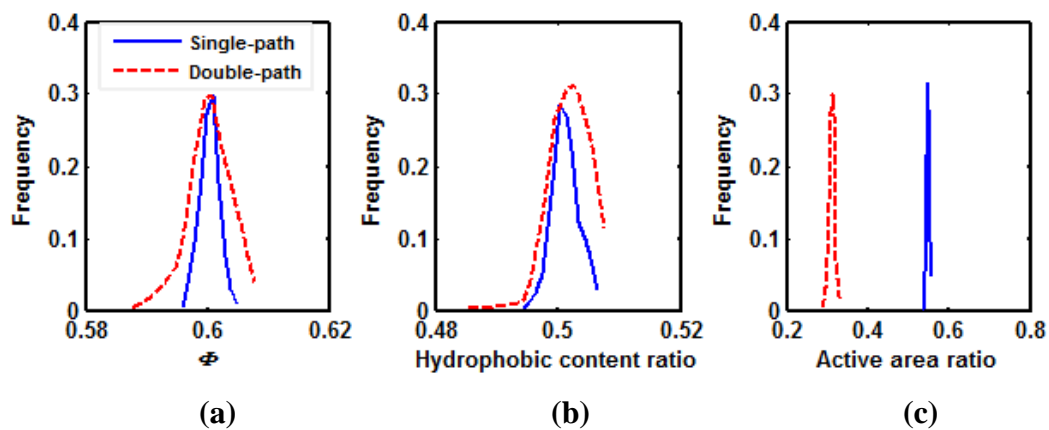


Figure 4.5. Confidence level results for (a) porosity, (b) hydrophobic solid content ratio on the surface, (c) active hydrophobic area ratio.

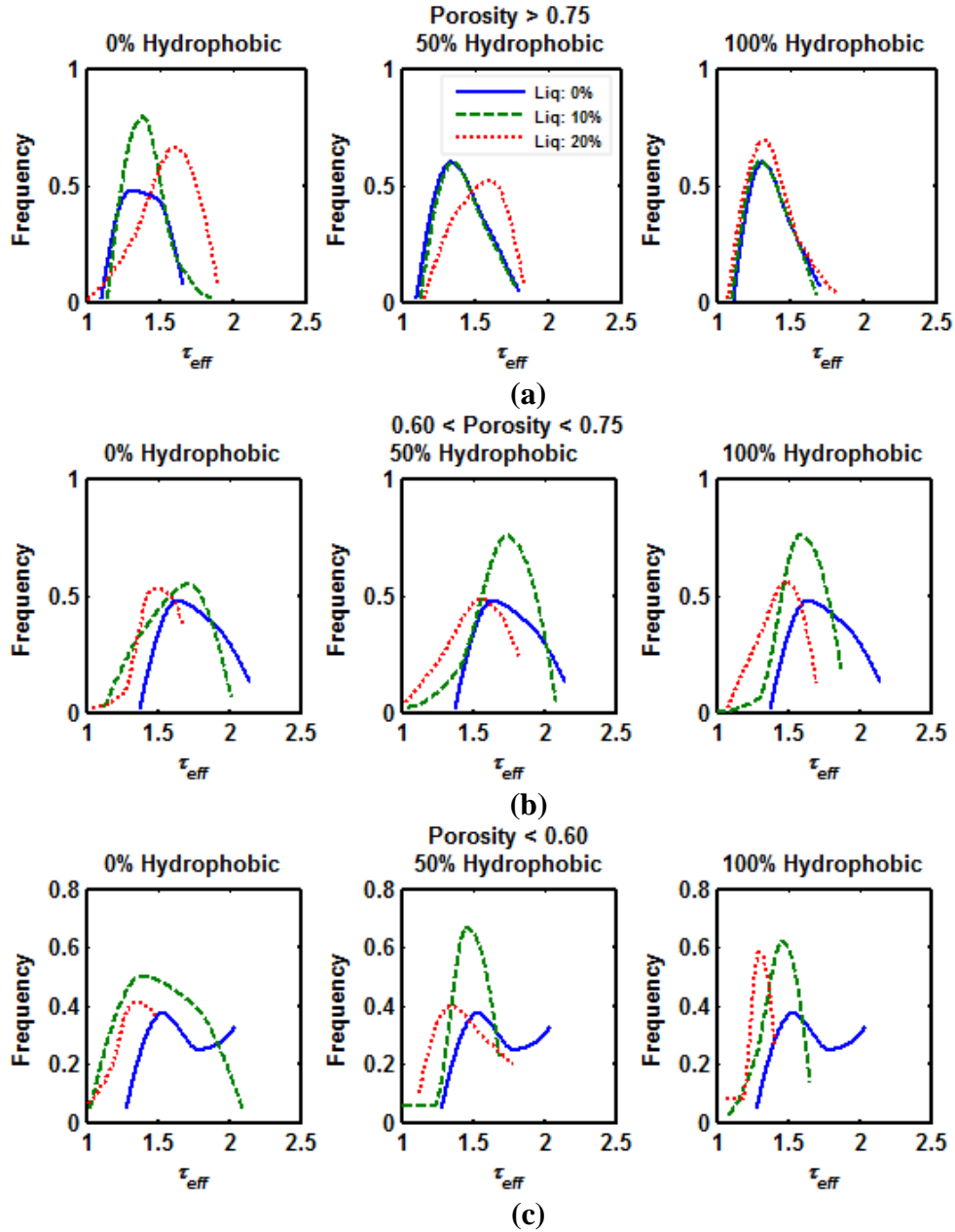


Figure 4.6. Single-path-percolation model - Confidence level results for effective tortuosity for 0%, 50%, and 100% hydrophobic surface for the domains with porosities (a) higher than 75%, (b) between 60% and 75%, (c) lower than 60%.

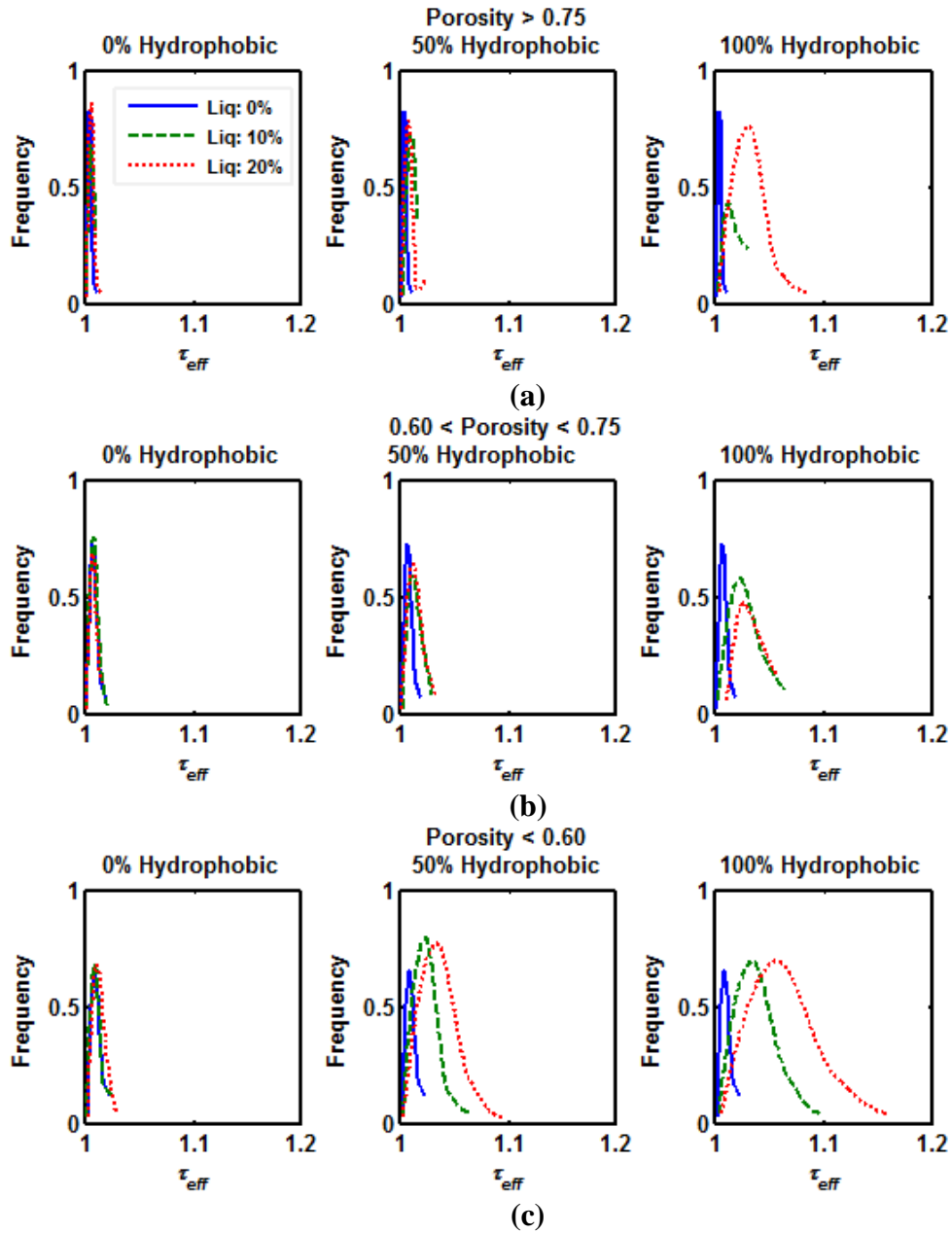


Figure 4.7. Double-path-percolation model - Confidence level results for effective tortuosity for 0%, 50%, and 100% hydrophobic surface for the domains with porosities (a) higher than 75%, (b) between 60% and 75%, (c) lower than 60%.

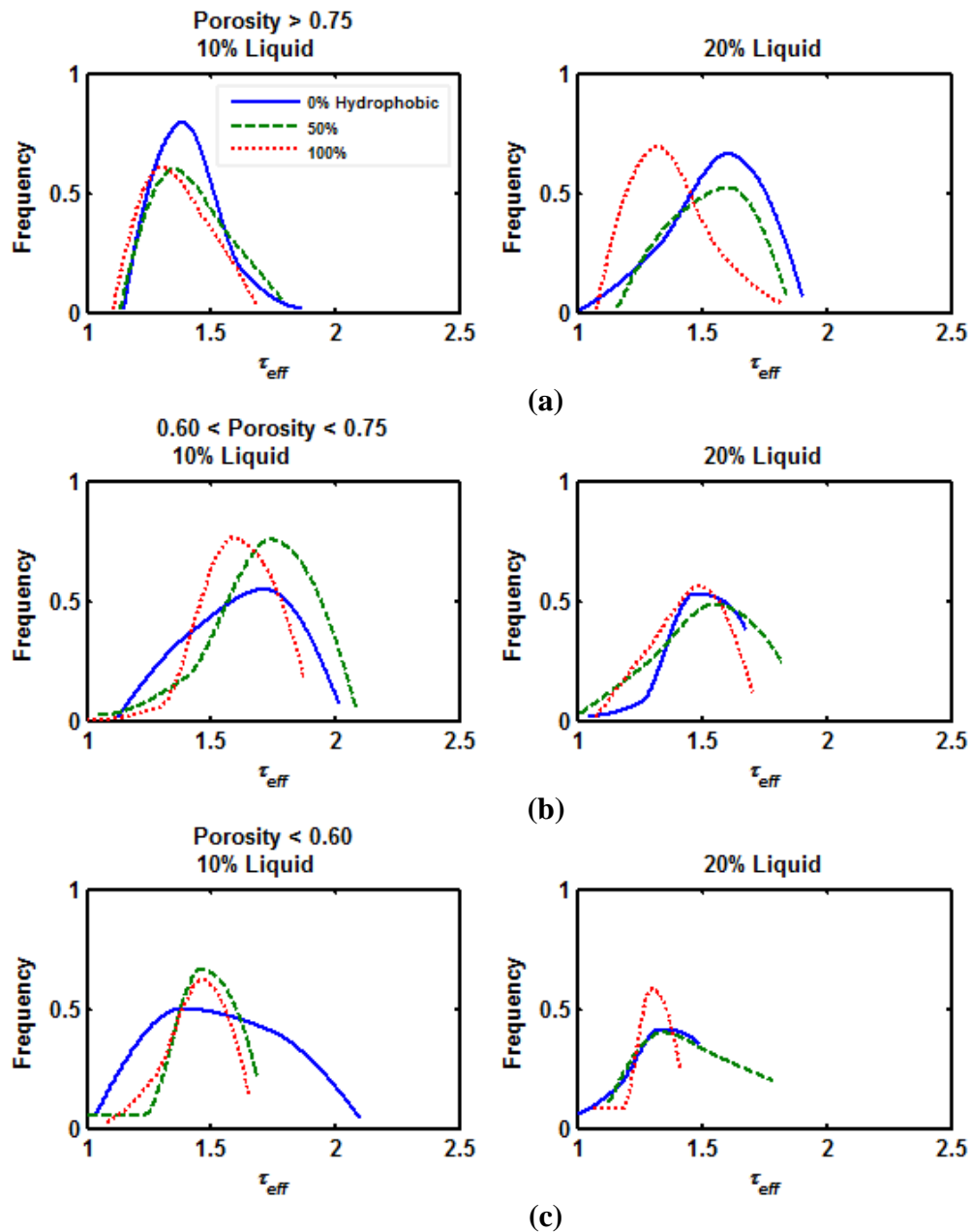


Figure 4.8. Single-path-percolation model - Confidence level results of effective tortuosity for 10%, and 20% liquid formation for the domains with porosities (a) higher than 75%, (b) between 60% and 75%, (c) lower than 60%.

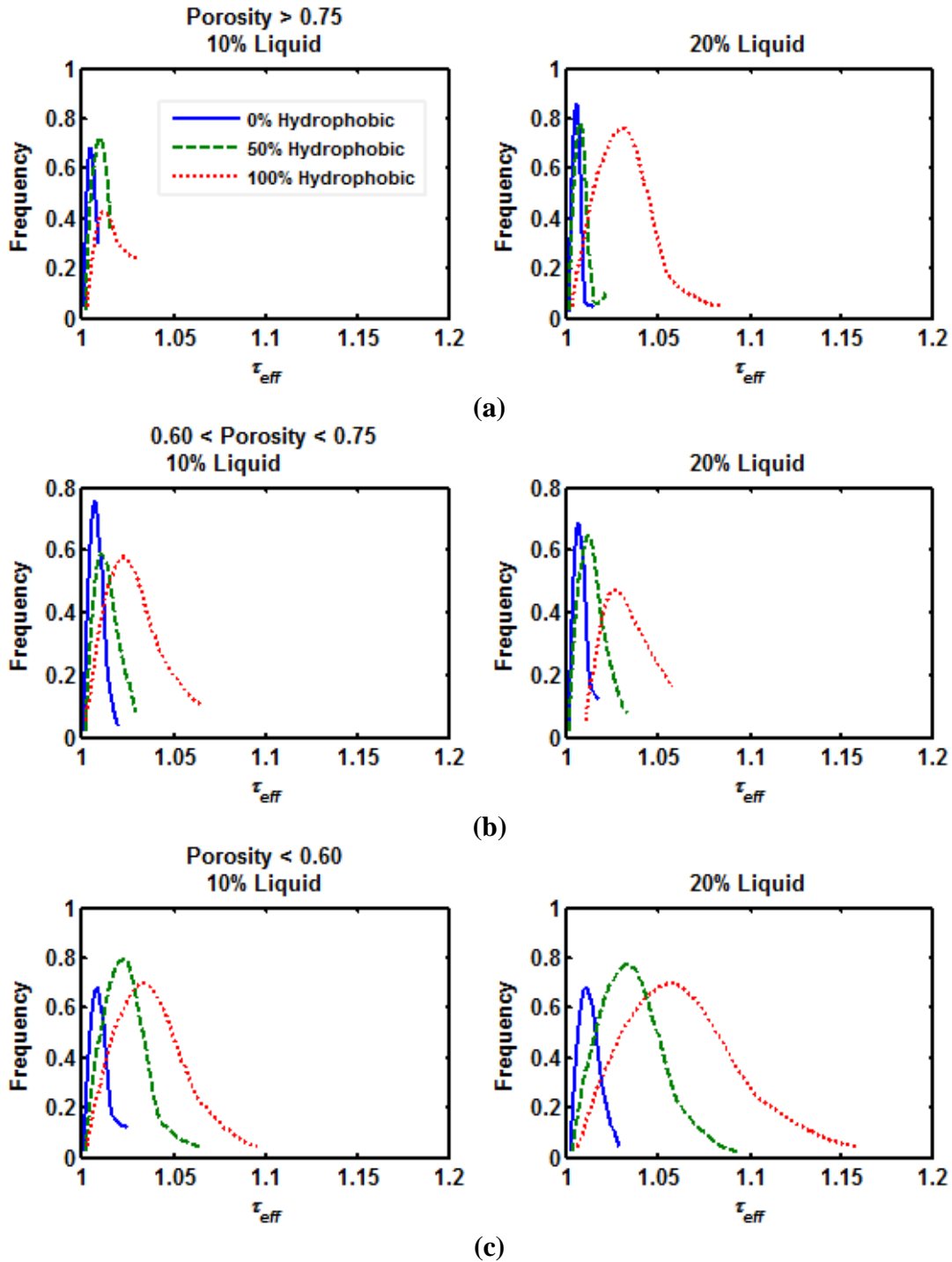


Figure 4.9. Double-path-percolation model - Confidence level results of effective tortuosity for 10%, and 20% liquid formation for the domains with porosities (a) higher than 75%, (b) between 60% and 75%, (c) lower than 60%.

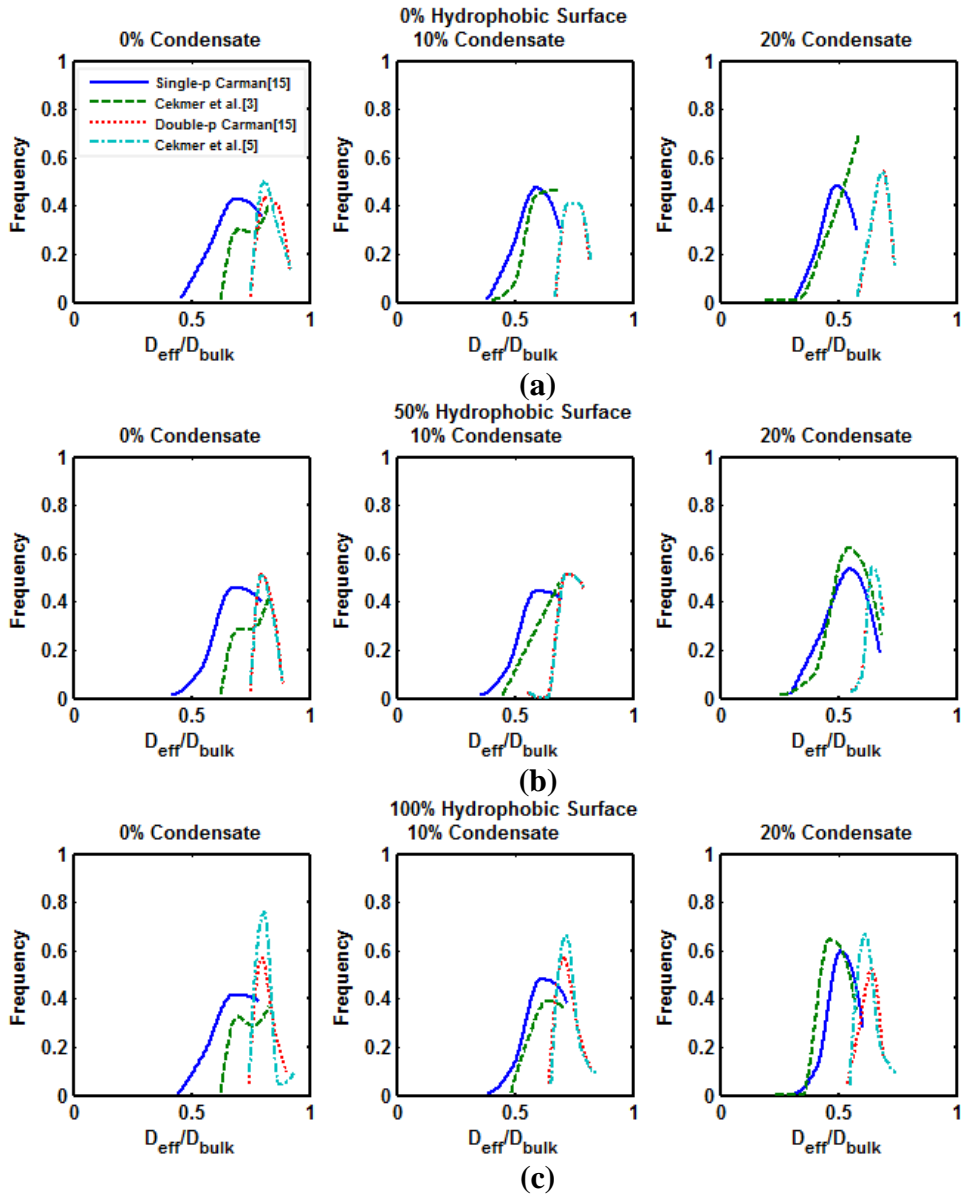


Figure 4.10. Confidence level results for diffusion ratio for the domains with porosities above 75%. Hydrophobic surface content is (a) 0%, (b) 50%, (c) 100%.

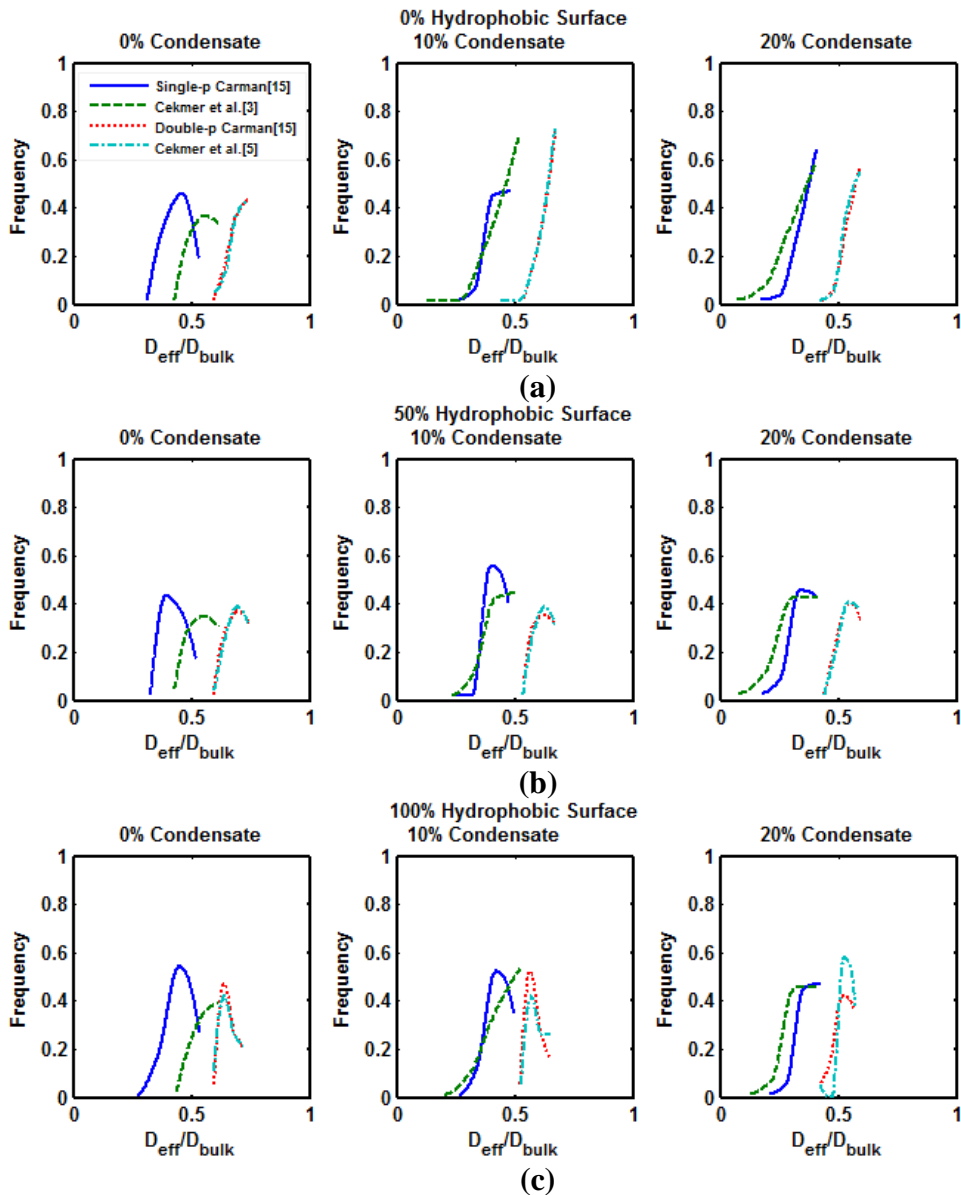


Figure 4.11. Confidence level results for diffusion ratio for the domains with porosities between 60% and 75%. Hydrophobic surface content is (a) 0%, (b) 50%, (c) 100%.

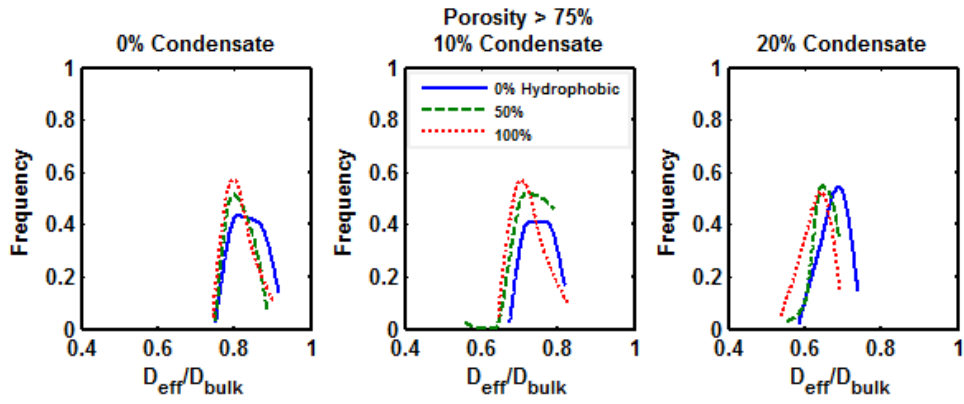


Figure 4.12. Double-path-percolation model, diffusion ratio confidence level results with 0%, 50%, and 100% hydrophobic surface for the domains with porosities above 75%.

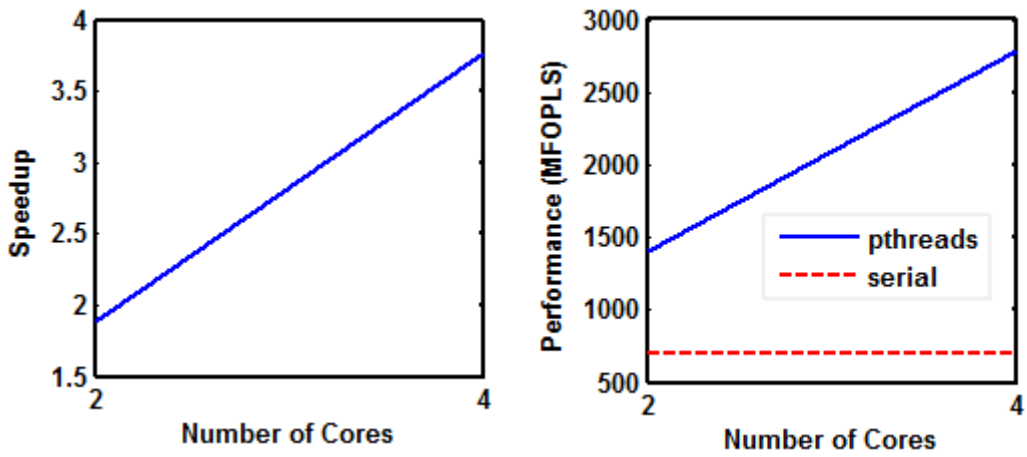


Figure 4.13. Speedup and performance achieved by pthreads implementation.

CHAPTER V
SINGLE- AND MULTI-PHASE FLOW ANALYSIS IN
INHOMOGENEOUS POROUS CHANNELS: III. MICRO-COMPUTED
PEFC GAS DIFFUSION LAYER GEOMETRIES

Abstract

In this computational study, a statistical approach was pursued to investigate multi-phase mass transport using micro-computed tomographies of gas diffusion layer (GDL) samples used in polymer electrolyte fuel cells. A Mitsubishi Rayon Corp. MRC-105 and a Sigracet SGL-25BA were examined. A 5% of PTFE loading was performed numerically. A multi-phase Lattice-Boltzmann model with surface-fluid interactions was developed in two dimensions. The cluster labeling process was applied to reduce the runtime. The effects of liquid formation on mass transfer in the GDL samples was examined. To do this, channels with 10% and 20% condensate were simulated, and the changes in effective porosity, tortuosity, and diffusion ratio were analyzed. Effective porosity was decreased with the liquid amount as expected. The effective tortuosity was increased significantly with 10% liquid formation, but its increase got slower with further liquid formation. For the case with 20% liquid formation, the resulting effective tortuosities overlapped with the case of 10% condensate in MRC-105, and it was slightly decreased in SGL-25BA simulations. The diffusion ratio is decreased with liquid amount in the simulations for both samples. Furthermore, the critical liquid formation, beyond which all the paths for the gas molecules plugged the channel, takes values between 40% and 88% for both samples. The statistical approach based on the law of large numbers differs this work from the previous studies.

Nomenclature

a A parameter to include intermolecular attractive force into the van der Waals equation of state, ($m^6 Pa/mol^2$)

b	A parameter to include the effects of non-negligible molecule volume into the van der Waals equation of state, (m^3/mol)
CL	Confidence level
c	Unit lattice velocity, (m/s)
D_{bulk}	Bulk diffusion coefficient, (m^2/s)
D_{eff}	Effective diffusion coefficient, (m^2/s)
F	Intermolecular force, (N)
F_{ads}	Adsorption force between solid and liquid particles, (N)
f	The probability distribution function
f^{eq}	Equivalent distribution function
G	Intermolecular interaction strength
G_{ads}	Intermolecular adsorption strength
k	Lattice index
N_{RAE}	Number of the representative area elements in a statistical representative area element set
n	Total history number
n_m	Number of moles of the fluid
P	Pressure of the fluid, (Pa)
Pr	Probability of any event to occur
p	The probability of a pore to occur in a node
q	The probability of a solid to occur in a node
S_{ads}	A switch parameter that can be 0 or 1.

t	Time, (s)
U	Velocity, $u = \sqrt{u^2 + v^2}$, (m/s)
u	Velocity in horizontal direction, (m/s)
V	Volume of the fluid, (m^3)
v	Velocity in vertical direction, (m/s)
w	Weighting factor of the lattice components
\hat{X}	Arithmetic average of any property
x	Horizontal distance, (m)
y	Vertical distance, (m)

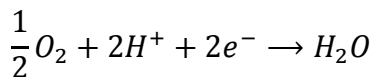
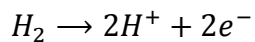
Greek Letters

ε	Error between the true and estimated probabilities of an event
ρ	Density of the fluid, (kg/m^3)
ρ_0	An arbitrary parameter, (kg/m^3)
τ	Tortuosity
τ_{eff}	Effective tortuosity
ϕ	Porosity
ϕ_{eff}	Effective porosity
ψ	Intermolecular interaction potential
ψ_0	An arbitrary parameter

Introduction

A polymer electrolyte fuel cell (PEFC) consists of a polymer electrolyte, anode and cathode catalyst layers, gas diffusion layers (GDL), and bipolar plates with flow channels [52].

The following electrochemical reactions occur in anode and cathode electrodes, respectively, neglecting the elementary steps:



Hydrogen gas is oxidized in the anode electrode, and disintegrates into its protons and electrons. The protons pass through the proton exchange membrane, and reach to the cathode electrode, whereas the electrons are conducted to cathode by an external circuit. In cathode electrode, oxygen is reduced by gaining electrons, and water is formed.

The GDL is placed at the interface between the catalyst layer and the current collectors. In polymer electrolyte fuel cells, usually a carbon based porous medium is used and basically two types are common on this purpose: woven carbon cloth and fiber structure bonded with a graphitized thermoset resin [52]. Two discrete forms of carbon-fiber-based diffusion media are adapted to PEFCs especially due to their high porosity ($\geq 70\%$) and good electrical conductivity; non-woven papers and woven fabrics (or cloths). Two possible treatments are applied to these base materials to improve performance and durability of fuel cells. First, polytetrafluoroethylene (PTFE) treatment is applied to increase and stabilize hydrophobicity. Generally, between 5% and 30% PTFE is used in PEFC diffusion media. Second, an MPL consisting of carbon or graphite particles mixed with a polymeric binder (usually PTFE), is used to improve water management, to reduce electrical contact resistance with adjacent catalyst layer.

There are many previous works, in which the diffusion characteristics of GDL samples were investigated. Zamel et al. [30] experimentally determined the effective diffusion coefficient of a $O_2 - N_2$ gas mixture, using a Loschmidt diffusion cell. As diffusion media, TORAY carbon

paper samples with a porosity between 63% and 75%, with and without PTFE loading were used. It was found that the previous effective diffusion models overpredict the diffusion coefficient by at least four times. Chan et al. [31] also used a Loschmidt cell to investigate the effective diffusion coefficient of an O₂ – N₂ mixture in TORAY TGP-H-120 and TGP-H-060 series with 0%, 30%, and 60% PTFE loading, and without microporous layer. Gas diffusion in SolviCore Type A and B, and Sigracet 10 and 25 series GDL with different PTFE loadings and MPL coatings were also analyzed. It was concluded that no existing effective diffusion model could predict the diffusion coefficient with significant Knudsen contribution. A new effective diffusion coefficient correlation was developed using a TORAY TPGH-120 type carbon paper with and without Teflon treatment and with varying porosities by Zamel et al. [37]. Fick's second law of diffusion was solved by Fluent, using a finite volume method. Effective diffusion correlations for in-plane and through-plane diffusion was obtained as a function of porosity. Photothermal deflection measurement of effective gas diffusion coefficient of a porous medium with 70% porosity, using an in-house Loschmidt cell with a photothermal-deflection probe was performed by Rohling et al. [32]. CO₂ – O₂ gas mixture was used as binary gas pair, and the effective diffusion coefficient was determined as $4.39 \times 10^{-6} \text{ m}^2 \text{ s}^{-1}$. In their experimental study [33], LaManna and Kandlikar investigated the effects of MPL coatings, GDL thickness, and PTFE loading on effective water vapor diffusion coefficient in PEFC gas diffusion layers. In addition to SGL and Toray series samples, two types of Mitsubishi Rayon Corporation Grafil U-105 series GDL with 7% PTFE loading were also used. A significant resistance to diffusion was introduced by MPL coatings and PTFE loading, whereas the thickness had a negligible effect on diffusion.

In the current study, statistical path-percolation theory [2, 47, 54, 55, 57] and Lattice-Boltzmann model (LBM) were applied on digitized micro-computed tomographies of Sigracet SGL-25BA and Mitsubishi Rayon Corp. MRC-105 to investigate single- and multi-phase mass transfer. A 5% of PTFE loading was performed on both samples in the simulations. No MPL coating was simulated. Gas flow in two cases with 10% and 20% saturated channels in addition to a dry medium was analyzed. The liquid formation in porous channels was simulated by a multi-phase LBM [5, 27] as done in the work by Cekmer et al. [55]. The simulations with surface-liquid interactions for both samples with 5% hydrophobic PTFE loading were also performed by multi-phase LBM with surface interactions [5, 29, 55]. Effective porosity, tortuosity, and dimensionless diffusion ratio, which is defined as the ratio of the effective and bulk diffusion coefficients, were determined. Dimensionless diffusion ratio instead of effective diffusion coefficient was selected for the statistical outcome to enable the future analysis with various gases. Furthermore, the critical saturation amount, beyond which there is no mass transfer, was determined statistically and compared for both samples.

The statistical approach based on the law of large numbers with a confidence level of 99% differs the current study from the previous works. The cluster labeling process, which is a part of the path-percolation theory, and used to reduce the runtime of the simulations, is also a unique process for diffusion studies. Furthermore, instead of solving the mass balance equation, momentum balance was solved, and effects of tortuosity was included in the effective diffusion coefficient results, using well-known Carman model [11]. The statistical outcome of this work can be used in any macroscopic and mesoscopic PEFC model. Furthermore, the methodology

and the statistical approach of the current study can be applied in any other multi-phase inhomogeneous porous medium system.

Methodology

In the first part, micro-computed x-ray tomographies of two GDL samples were obtained from the work prepared by Brandon Walters and Ben Ache from Micro Photonic Incorporation, Allentown, PA. The tomographies of Mitsubishi Rayon Corp. MRC-105 and Sigracet SGL-25BA are presented in three dimensions in Fig. 1. The 3D images were digitized by an in-house program, and two dimensional slices of these three dimensional structures were extracted to apply the cluster labeling process and LBM. Then, square small representative subdomains were extracted from the 2-D slices, and smaller 2D representative area elements (RAEs) were obtained to construct statistical representative area element set by two-point statistics. The number of the 2-D slices, square subdomains, and RAEs for each subdomain were determined by a confidence level study. After the confidence level study, a PTFE loading process was performed to obtain digitized 2D domains of both GDLs with 5% PTFE. The loading was applied on 2-D slices extracted from the 3-D structures.

To initiate the model, a confidence level study was performed to determine the necessary number of the 2D slices, subdomains in 2D slices, RAE number in a single subdomain, and node numbers of the RAEs. Further information of confidence level studies can be found in [2, 42, 47, 54, 55]. The confidence level [42] is defined as the reliability of any estimate:

$$CL = Pr \left\{ \left| \frac{k}{n} - p \right| \leq \varepsilon \right\} \quad (5.1)$$

where, p is the porosity of the actual geometry, and n is the total history number, which is the multiplication of the number of slices, square subdomains in each slice, RAE number in each

subdomain, and the number of nodes of an RAE. Total void number in the simulation is k . The difference between the porosity of the actual 3-D geometry and the statistical outcome of 2-D simulations is called error, and represented by ε . The actual porosities of the GDL samples are 81.46% and 84.24% for MRC-105 and SGL 25BA, respectively. Pr stands for the probability of the event in the brackets, and CL is an abbreviation for the confidence level. A 99% confidence level within an error limit of 1×10^{-3} was applied in this work. The law of large numbers [42] was utilized in Eq. (5.1), and a simpler equation for the confidence level is obtained:

$$Pr \left\{ \left| \frac{k}{n} - p \right| \leq \varepsilon \right\} = 2 \mathbb{G} \left(\varepsilon \sqrt{\frac{n}{pq}} \right) - 1 = CL \quad (5.2)$$

where, q is $1-p$, and \mathbb{G} is the Gaussian function. Eq. (5.2) can be rewritten in terms of the error function as:

$$\frac{CL}{2} = \text{erf} \left(\varepsilon \sqrt{\frac{n}{pq}} \right) \quad (5.3)$$

The unknown in Eq. (5.3), is the total history number, and tabulated for both samples as shown in Table 5.1 with the number of 2D slices extracted. The node number of the subdomains in a 2D slice with the necessary number of subdomains, RAEs in a subdomain, and the node number of an RAE are also presented in the same table. Hence, $10 \times 10 \times 11 = 1100$ simulations for MRC-105 and $10 \times 9 \times 11 = 990$ for SGL-25BA are needed with the specified node numbers for the subdomains, and RAEs in Table 5.1.

A 5% of hydrophobic PTFE loading on 2-D slices of both samples was performed randomly to include the surface-fluid interactions in the current two-phase model. For the simulations, a subroutine was developed to scatter hydrophobic particles on solid region, which

is in contact with gas. The detailed information can be found in [57]. The active PTFE area is defined as the area of the PTFE, which is in contact with the void regions. It was found in a previous work [57] that the active area is 30.03% and 54.23% of the total PTFE area in high- and low-tortuosity systems.

As explained above, there are 10 2-D slices per each GDL sample to be investigated. These domains are very large in size, and a single LBM simulation has a relatively long runtime comparing to that of smaller RAEs. Furthermore, only the single-phase LBM is applied on these domains just once. The multi-phase LBM with surface interactions are applied on the system for many times, until the program finds the critical liquid formation amount, beyond which no further mass transport occurs. Hence, two reduction steps were applied to obtain the statistical representative area (SRAE) sets [43, 44, 47]. In the first step, 100x100 subdomains were extracted from 2-D slices. These subdomains must represent the 2-D slice that it was extracted from in terms of porosity, effective porosity, and PTFE content. Thus, a subroutine was developed to do this. The program scans the entire domain to find the best options for the subdomains. It starts from the upper left corner of the digitized 2-D slice, investigates every possible 100x100 matrix inside. There are three barriers for each matrix to be a subdomain candidate. The errors between the porosity, effective porosity, and the PTFE content of the entire domain and the smaller matrix investigated must be less than 1.0×10^{-3} . The first barrier is the porosity error. If the smaller domain investigated passes the first barrier, in other words, if the relative error between the porosities of the entire domain and the smaller matrix is less than 1.0×10^{-3} , the program applies the cluster labeling process to compute the effective porosity of the matrix. If the smaller matrix passes the effective porosity barrier, then its PTFE content is

computed. If the difference between the PTFE content of the entire domain and the smaller matrix investigated is less than 1.0×10^{-3} , the program stores the matrix as a potential subdomain candidate, and continues its search for the other candidates. After scanning the entire domain, it ranks the potential subdomain candidates in terms of their effective porosity error. The best options are selected as the subdomains to be investigated.

A single LBM simulation in a 100×100 matrix lasts shorter in runtime, but is still computationally intensive. It must be noted again that the multi-phase LBM is applied many times on each porous domain to find 10%, 20%, and critical liquid formation. The initial density in the system is the controlling parameter. The program initiates the loop for the subdomains with a single-phase LBM to determine the tortuosity in a dry channel. After that, a multi-phase loop is started. It applies the multi-phase LBM using an initial density assigned. When the system reaches a steady-state condition, the program computes the liquid formation amount, and turns back to the starting point of the multi-phase loop. The initial density is increased with an amount of differential density ($d\rho$), and the same process is applied again, till the liquid amount in the system exceeds 10%. Then, the program turns one step back by subtracting $d\rho$ from ρ , adds a smaller $d\rho$ to the density, and applies multi-phase LBM again. It continues this repeating process until the difference between 10% and the liquid amount computed in the system becomes less than 1.0×10^{-3} . When the 10% liquid amount is obtained, a single-phase LBM is applied on the saturated domain to compute the effective tortuosity of the partially saturated domain. The same process is repeated starting with the original $d\rho$ to obtain the effective tortuosity in a domain with 20% liquid formation. After obtaining 20% liquid formation, the final step for the multi-phase analysis begins. The program starts to investigate the critical liquid amount in the

channel, beyond which there is no further gas transport, in other words; the effective porosity becomes zero. It was observed that the program runs the LBM simulation for more than 50 times on the average per a single domain. Hence, another reduction is required to extract 30x30 RAEs for each subdomain. A question would rise at this point: Why the RAEs were not extracted from 2-D slices in the first place? The answer is that the storage of the RAE candidates, which pass all the error barriers, takes too much memory, and the program runs much slower even with very small error barriers. That is why this additional step is required.

There are 11 RAEs in an SRAE set in the current work as a result of the confidence-level study. To determine the effective porosity and tortuosity of an SRAE set, the following equation is used:

$$\hat{X} = \frac{1}{N_{RAE}} \sum_{m=1}^{N_{RAE}} X_m \quad (5.4)$$

where, X is set as effective porosity and tortuosity. The ensemble average of any property of the RAEs is represented by \hat{X} , and the results will represent the properties of the related SRAE set. The RAE number in a set is represented by m , and X_m is the property of the m^{th} RAE. The total element number in a set is N_{RAE} , which is 11 in the current study. In summary, an SRAE set with its averaged effective porosity and tortuosity is considered as a single virtual representative domain of the entire channel. Hence, the multi-phase effects in 990 RAEs for SGL-25BA and 1100 RAEs for MRC-105 were investigated here. A posix threads (Pthreads) implemented code was developed to reduce the runtime and increase the computing performance as explained in a previous work of Cekmer et al. [57]. Four processors instead of one were used in SRAE selection and LBM loops.

For the single-phase LBM simulations, the same method in a previous work of Cekmer et al. [47] was applied with a D₂Q₉ lattice. There are nine velocity components and in a two-dimensional single lattice as shown in Fig. 5.2. Since, the molecular interactions are defined by the collision and streaming processes in Boltzmann's theory [3], the following equations are used for the collision and streaming, respectively:

$$f_k(x + c\Delta t, y + c\Delta t, t + \Delta t) - f_k(x, y, t) = -\frac{1}{\tau} [f_k(x, y, t) - f_k^{eq}(x, y, t)] \quad (5.5)$$

$$f_k(x + \Delta x, y + \Delta y, t + \Delta t) = f_k(x, y, t + \Delta t) \quad (5.6)$$

where, x and y are the horizontal and vertical positions of the molecules in the channel. The lattice component index is represented by k , and it takes values between 0 and 8 as seen in Fig. 5.2. Furthermore, t , c , and τ stand for time, the unit lattice velocity, and the single-relaxation factor, respectively [4, 5, 56]. The probability density function, f , is the probability of a particle to be at a specific position at a specific time, and related with the macroscopic properties as follows:

$$\rho = \sum_{k=0}^8 f_k \quad (5.7)$$

$$u = \frac{1}{\rho} \sum_{k=0}^8 c_{k,x} f_k \quad (5.8)$$

$$v = \frac{1}{\rho} \sum_{k=0}^8 c_{k,y} f_k \quad (5.9)$$

In these equations, ρ represents the density of the fluid, whereas u and v are the velocity components in horizontal and vertical directions, respectively. Thus, after solving the coupled

LB equation shown in Eqs. (5-6), the density and the velocity components can be computed. The effective tortuosity is computed as:

$$\tau_{eff} = \frac{\int_A V dA}{\int_A v dA} \quad (5.10)$$

For multi-phase LBM simulations, the long-range intermolecular attractive forces were included in the collision process using the van der Waals equation of state [5, 27]. In the developed model, the system is assumed to be isothermal. Initially, the fluid inside the GDL has a non-zero thermodynamic quality depending on the initial pressure in the system, and the attractive force between the molecules leads to a phase separation between liquid and vapor. The liquid molecules come together, and form clusters. Some of the clusters disappear if the outside pressure is larger than the pressure inside the liquid cluster, and some of them gets larger by attracting the smaller liquid clusters, until a steady-state condition is reached. After this point, no further interactions are observed in the simulations. The following equation is used to add the intermolecular attractive force into account as introduced by He and Doolen [28]:

$$P = \frac{\rho}{3} + \frac{G}{6} \Psi^2 \quad (5.11)$$

where, G and Ψ are the interaction strength and potential, respectively. The interaction potential is computed as follows [27]:

$$\Psi = \Psi_0 \exp\left(\frac{-\rho_0}{\rho}\right) \quad (5.12)$$

In Eq. (12), Ψ_0 and ρ_0 are constants. To calculate the force caused by the intermolecular interactions, Eq. (5.13) is used.

$$F = -G\Psi(x, t) \sum_{k=1}^8 w_k \Psi(x + c_k dt, t) c_k \quad (5.13)$$

In this equation, c_k and w_k are the lattice velocity and weighting factor of the k^{th} velocity component of the lattice, respectively. To include the effects of surface interactions on mass transport, an adhesive interaction force as shown in Eq. (5.14) was included in the model [29].

$$F_{ads} = -G_{ads}\Psi(x, t) \sum_{k=1}^8 w_k S_{ads}(x + c_k dt, t) c_k \quad (5.14)$$

where, G_{ads} and S_{ads} are the adsorption strength and solid switch, respectively. S_{ads} takes values 0 or 1 depending on the neighbor phase. If the neighbor is solid, then it becomes 1, otherwise 0.

The adsorption strength controls the contact angle between the solid and liquid. The contact angles of PTFE and carbon with water are set to 104° [58] and 63° [59]. G_{ads} is calculated by Eq. (5.15) [5].

$$G_{ads} = G\Psi_l \quad (5.15)$$

where, Ψ_l is computed by Eq. (5.12). Similar to the previous work of Cekmer et al. [57], G_{ads} is computed as -165.29 and -229.35 for PTFE and carbon, respectively.

Finally, the well-known Carman model was used to determine the effective diffusion coefficient.

$$D_{eff} = D_{bulk} \frac{\phi}{\tau} \quad (5.16)$$

A sample simulation of the entire process for MRC-105 is explained in detail here. A 2-D slice was extracted from the 3-D structure shown in Fig. 5.1. The extracted 2-D slice, which has a porosity of 81.46%, can be seen in Fig. 5.3, where the white nodes and black nodes are void and solid, respectively. The bottom boundary is inlet, whereas the upper one is the outlet, and the

sides are reflective. Then, 5% of PTFE was injected on the selected slice. A little portion of the slice is presented in Fig. 5.4. In this figure, the gray nodes are PTFE, and the resulting PTFE content is 5.14%. Cluster labeling process was applied, and no orphan pore was detected. Since the effective porosity is equal to the porosity (81.46%). After that, subdomain extraction was performed. A total of 10 subdomains were extracted from the 2-D slice, and one of them is presented in Fig. 5.5. The effective porosity and the PTFE content are 81.48% and 5.13%, respectively. Then, 11 RAEs were extracted, hence the SRAE set was constructed. The first RAE in the set is presented in Fig. 5.6. The PTFE content of the RAE is 4.84%, and the effective porosity is 81.44%. A single-phase LBM was applied on the RAE, and the velocity distribution is demonstrated in Fig. 5.7. The effective tortuosity was computed 1.04. A multi-phase LBM was applied on RAE, and the density distribution is found as shown in Fig. 5.8(a). The cluster labeling process was applied on the channel to obtain the effective domain for a gas transport after the liquid formation, and the effective porosity was reduced to 70.44% as seen in Fig. 5.8(b). A single-phase LBM was applied on the effective domain to simulate gas transport in a saturated medium with 10% liquid formation. The effective tortuosity was increased to 1.207. The results for 20% liquid formation is presented in Figure 9. Effective tortuosity and porosity were reduced to 1.083 and 64.78%, respectively. A detailed information about the reduction of the tortuosity with liquid formation in 2-D simulations can be found in [55].

The statistical results include the diffusion ratio (D_{eff}/D_{bulk}), and discussed in the following section.

Results and Discussion

In this study, mass diffusion behavior of gases in MRC-105 and SGL-25BA GDL samples was investigated. A confidence-level study initiated this work. According to the confidence-level study, 2-D slices were extracted from the micro-computed tomographies of these two samples. A 5% of PTFE was loaded on these 2-D slices. An SRAE extraction process was performed on 2-D slices to obtain domains for single- and multi-phase LBM. The effects of liquid formation on effective porosity and tortuosity was analyzed. Then, Carman's model was utilized to examine the dimensionless mass diffusion ratio in these two samples. Finally, the critical liquid formation in two GDL samples were determined statistically, and compared.

First of all, the effective porosity distributions against occurrence frequency of each effective porosity were plotted for subdomains and RAEs as shown in Fig. 5.10. Porosities of MRC-105 and SGL-25BA were reported as 81.46% and 84.24%, respectively by Micro Photonics Inc. It is observed that the effective porosity distribution range is wider in both subdomains and RAEs of SGL-25BA, than those of MRC-105. The reason is that the confidence level study resulted more subdomains and RAEs for MRC-105. Although, the results were overlapped with the actual porosities of these samples within an error range of 1×10^{-3} , as stated in the previous section.

The next step was the PTFE loading, and the results are presented in Fig. 5.11. The loaded PTFE was 5% of the total solid surface. Since the confidence-level study was based on the porosity, the relative error between the desired and resulting PTFE loading is larger than that of the effective porosity as seen in Fig. 5.11(a). Nevertheless, the maximum occurrence frequency is very close to 5% for both samples. The other parameter considered is the active PTFE area. Although about 5% of the surface is PTFE, the entire PTFE surface is not in contact

with void region. The PTFE area, which is in contact with fluid, is called the active area, and the results are presented in Fig. 5.11(b). The mostly occurred active area is slightly higher in MRC-105 than that of SGL-25BA. The results lie between 35% and 38%, and overlapped with the results of a previous work of Cekmer et al. [57], in which random low-tortuosity porous channels were generated by double-path-percolation theory.

To investigate the diffusion behavior of gases in partially saturated MRC-105 and SGL-25BA, changes in effective porosity, tortuosity, and diffusion ratio with liquid formation were examined. Fig. 5.12 shows the effects of liquid formation on effective porosity for both samples. The results are in accordance with previous multi-phase path-percolation works [55, 57]. The effective porosity distribution range gets wider, which means the effective porosity becomes less predictable, and shifts to the left, which means it is decreasing with the liquid formation. Clearly, the reason is that the liquid molecules plugged many of the paths for the gas molecules. For a dry medium, the effective porosity is almost the same as the initial porosity of the GDL samples. Fig. 5.13 presents the changes in effective tortuosity with liquid formation in GDL samples. In dry MRC-105 and SGL-25BA samples, the effective tortuosity can take values less than 1.5. When liquid formation occurs in the systems, tortuosity is increased, in other words; the effective tortuosity distribution range shifts to the right. The results for the cases with 10% and 20% liquid formation almost overlapped. To compare with the previous works for low- and high-tortuosity systems, the results of the current study lies between them. It was shown that in high-tortuosity systems, the effective tortuosity was increased with low liquid formation, and when the condensate amount continued to increase, tortuosity started decreasing [55]. In low-tortuosity systems, effective tortuosity decreases with the increased liquid formation [57]. As the effective

porosity decreases and tortuosity decreases with liquid formation, it is expected that the diffusion ratio would also decrease with the increased condensate amount. This result is shown in Fig. 5.14(a) for SGL-25BA, and in Fig. 5.14(b) for MRC-105. Diffusion behavior of a gas becomes less predictable with the liquid formation. The effective diffusion coefficient of a gas in SGL-25BA is slightly higher than that of MRC-105, since the porosity of the former is higher.

Critical liquid formation is defined as the condensate amount in the channel that makes the effective porosity zero. In other words, no gas diffusion occurs beyond the critical liquid formation. The results for both samples are shown in Fig. 5.15. The critical liquid formation mostly takes values between 40% and 88% for both samples.

This study introduces an alternative statistical approach in diffusion studies with the actual micro-computed GDL geometries, which is based on the law of large numbers [42] with a 99% confidence level in two-dimensions. The cluster labeling process of the path-percolation theory is another method, which differs this work from the previous ones. However, it must be noted that the simulations performed here are in two-dimensions. A three-dimensional study would change the results. First of all, the effective porosity may be underestimated here. There would be more void nodes in the missing direction, hence the number of trapped (orphan) pores would be less than that of a two-dimensional simulation. Second, the effective tortuosity will definitely increase, since the shortest path between the inlet and the outlet will be the same, but there will be additional paths for the fluid molecules in the missing direction. The effective diffusion ratio will increase, if the increase in the effective porosity is more than that of the effective tortuosity. Finally, the critical liquid formation results of the current study is underestimated, since the effective porosity is also smaller than that of the actual three-

dimensional geometries. The methodology of this work can be adapted to three-dimensional simulations, and the results can be compared. To extend the current study into three dimensions, a high-performance computing system can be applied in the codes [54, 55, 57]. Parallel programming would also lead much higher confidence levels, since the computing performance is increased significantly. Moreover, better SRAE sets with an increased number of larger RAEs can be constructed for the single- and multi-phase LBM simulations. Furthermore, the methods used here can be applied in any system involved with multi-phase flow in inhomogeneous porous medium, and the statistical outcome is valid for macroscopic PEFC models with mass diffusion.

Conclusions

A statistical analysis was performed on multi-phase mass transport in micro-computed tomographies of MRC-105 and SGL-25BA GDL samples in this study. PTFE loading was also performed computationally, and the hydrophobic contents of the extracted domains were statistically analyzed. A 99% confidence level was applied for two-dimensional simulations. Two-point statistics was applied to extract smaller domains from the tomographies for the single- and multi-phase LB models. A Lattice-Boltzmann model with a D2Q9 lattice with fluid-fluid and surface-fluid interactions. The effects of 10% and 20% liquid formation on gas diffusion in both GDL samples were investigated. Finally, the critical liquid formation, which makes the effective porosity of the domain zero, was examined. The conclusions are listed below.

- The effective porosity decreases with increased liquid formation in the channel, and becomes less predictable.
- The effective tortuosity is increased, when the 10% of the channel was occupied with liquid clusters. When, the condensate amount is further increased, the tortuosity is

slightly decreased in SGL-25BA, and almost overlapped with the case of 10% liquid formation in MRC-105.

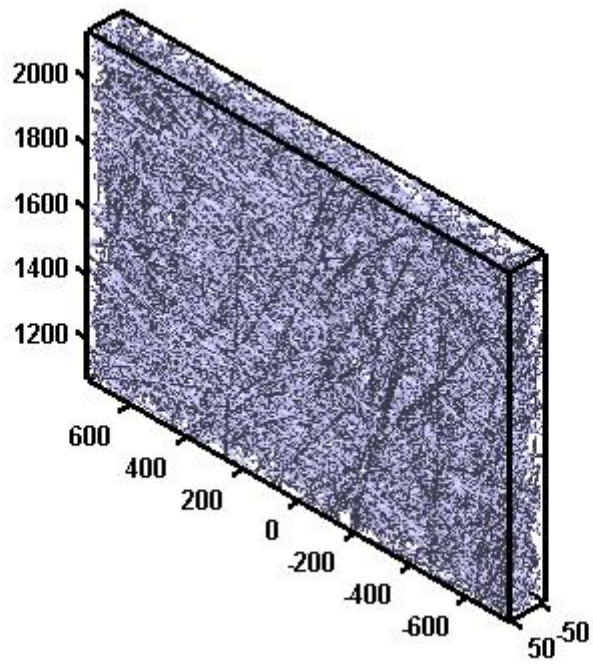
- The diffusion ratio is decreased, and becomes less predictable with the liquid formation. In high-tortuosity low-porosity systems, liquid content decreases the tortuosity.
- In both samples, the critical liquid formation mostly takes values between 40% and 88%.

The methods and the statistical outcome of this study can be applied in any porous medium application involved with single- and multi-phase mass transport with surface-fluid interactions. The dimensionless diffusion ratio distribution ranges can be used in macroscopic PEFC models. More advanced three-dimensional models can be developed by the same approach introduced in this study.

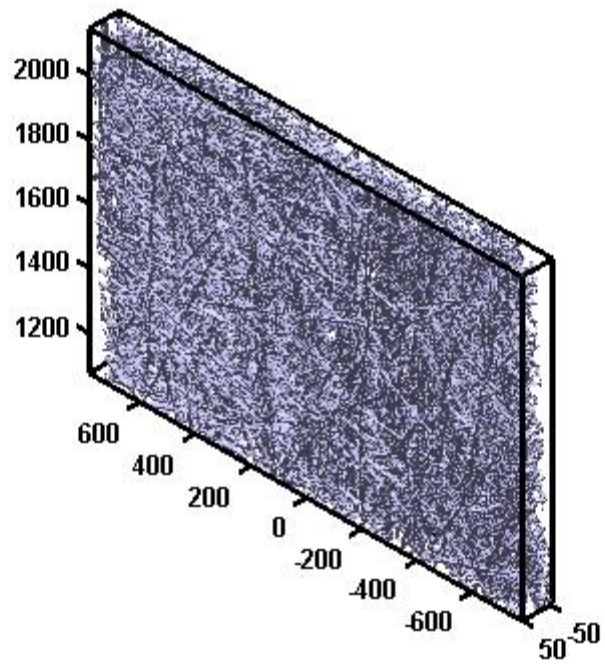
Appendix

Table 5.1. History calculations for MRC-105 and SGL-25BA.

Confidence Level	$\text{erf}\left(\varepsilon \sqrt{\frac{n}{pq}}\right)$	$\varepsilon \sqrt{\frac{n}{pq}}$	GDL	p	n	# of 2D slices	Subdomain size	RAE size	# of subdomains	RAE # in a size
99%	0.495	2.5767	MRC 105	0.8	4,010,900	10	100x100	30x30	10	11
			SGL 25A	0.8					3,525,837	



(a)



(b)

Figure 5.1. Three-dimensional micro-tomography of (a) MRC-105, (b) SGL-25BA.

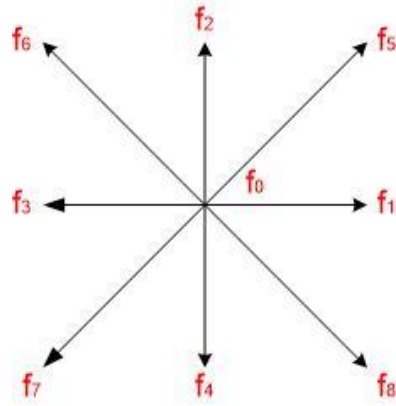


Figure 5.2. A square D_2Q_9 lattice with nine velocity components for LBM.

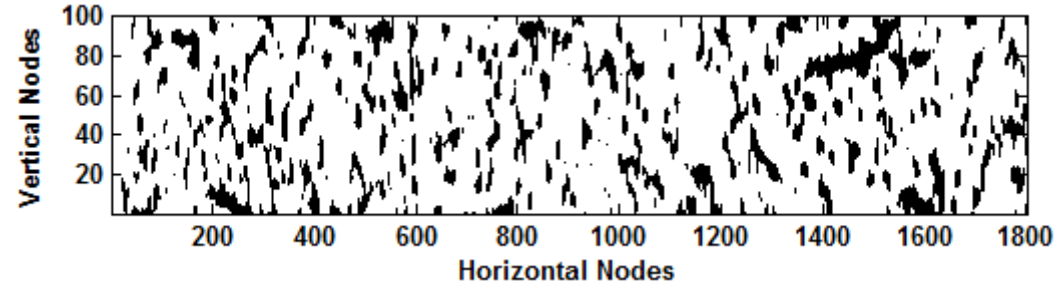


Figure 5.3. A two-dimensional slice extracted from the three-dimensional digitized micro-tomography of MRC-105.

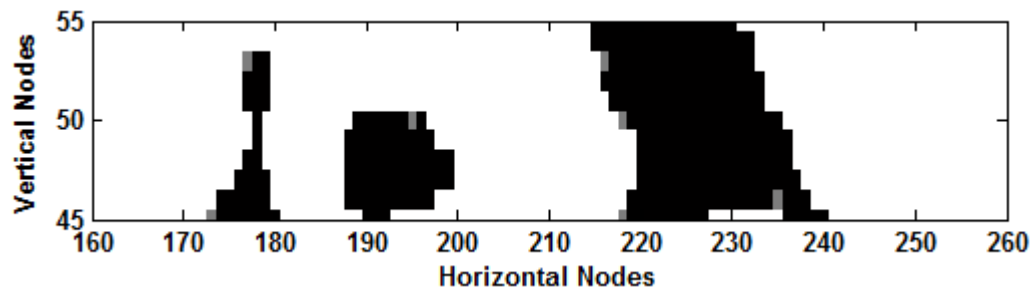


Figure 5.4. A small portion of the selected 2-D slice with 5% PTFE loading.

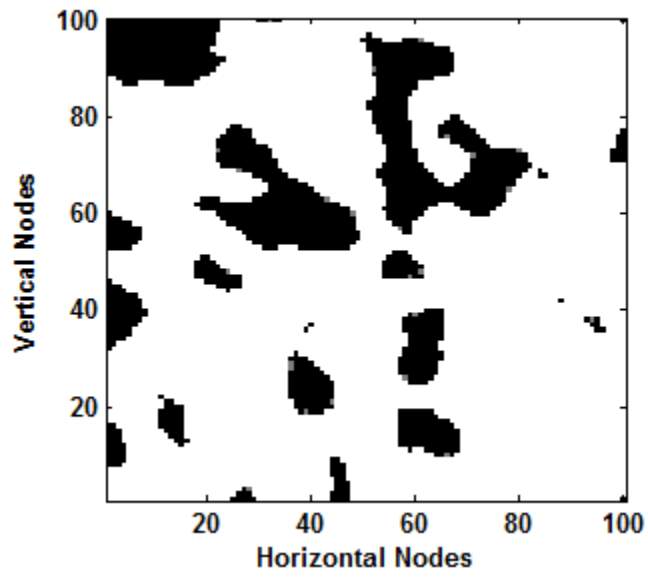


Figure 5.5. A subdomain extracted from the 2-D slice.

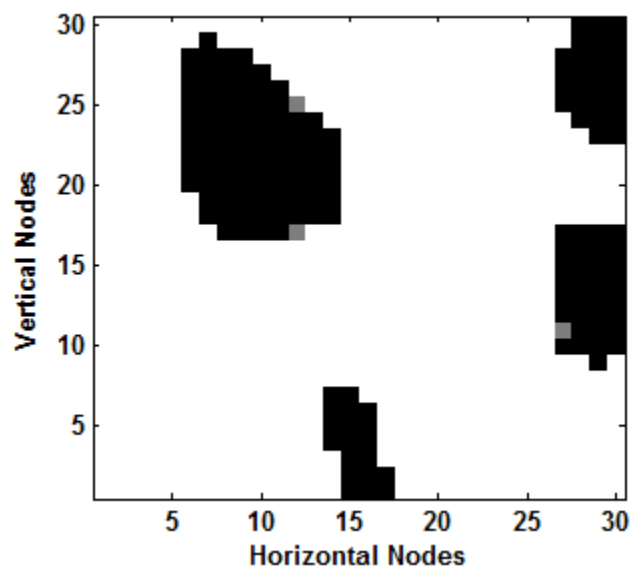


Figure 5.6. RAE # 1 of the constructed SRAE set.

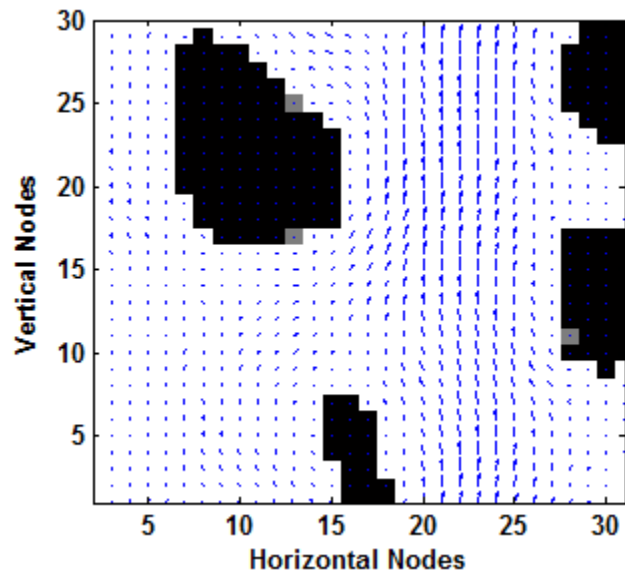


Figure 5.7. Single-phase velocity distribution in RAE # 1.

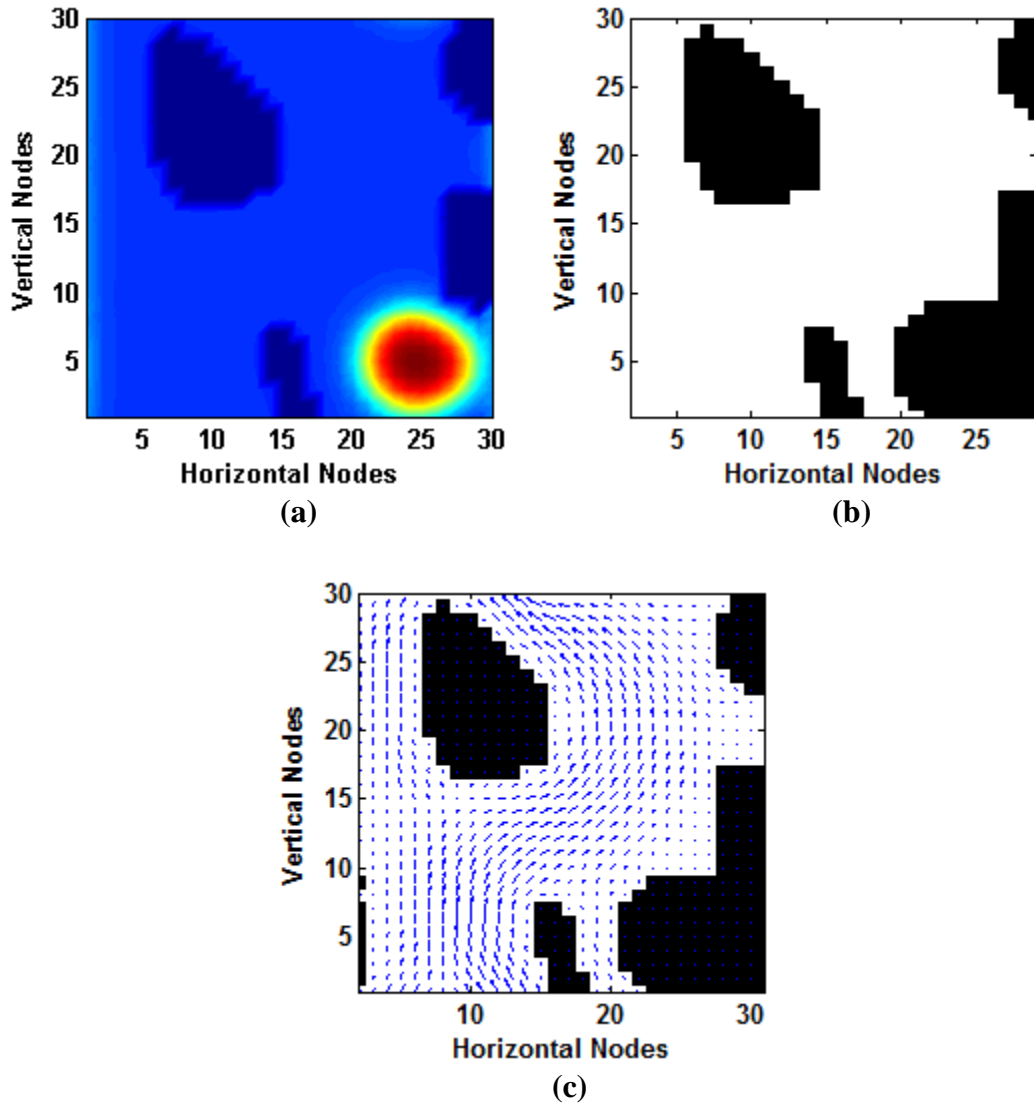


Figure 5.8. 10% liquid formation in RAE #1; (a) density distribution, (b) the effective domain after cluster labeling, (c) velocity distribution of a single-phase gas in the saturated medium.

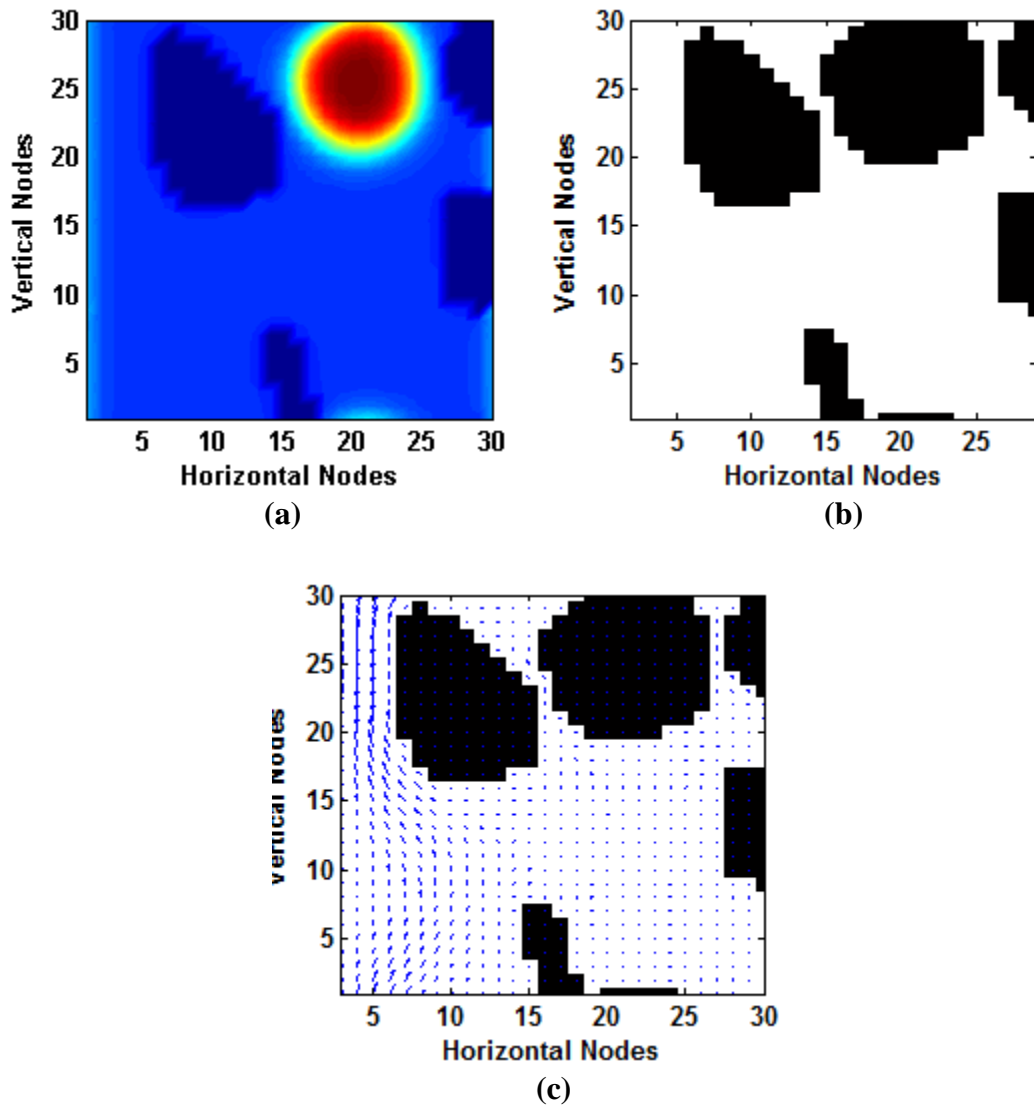


Figure 5.9. 20% liquid formation in RAE #1; (a) density distribution, (b) the effective domain after cluster labeling, (c) velocity distribution of a single-phase gas in the saturated medium.

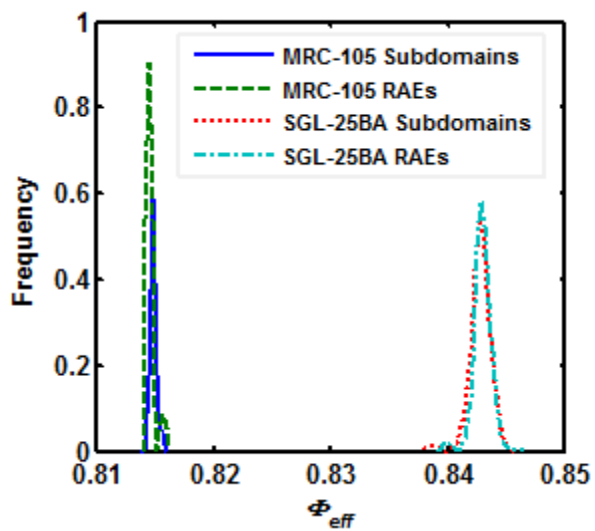


Figure 5.10. Effective porosity distributions of subdomains and RAEs extracted from MRC-105 and SGL-25BA data.

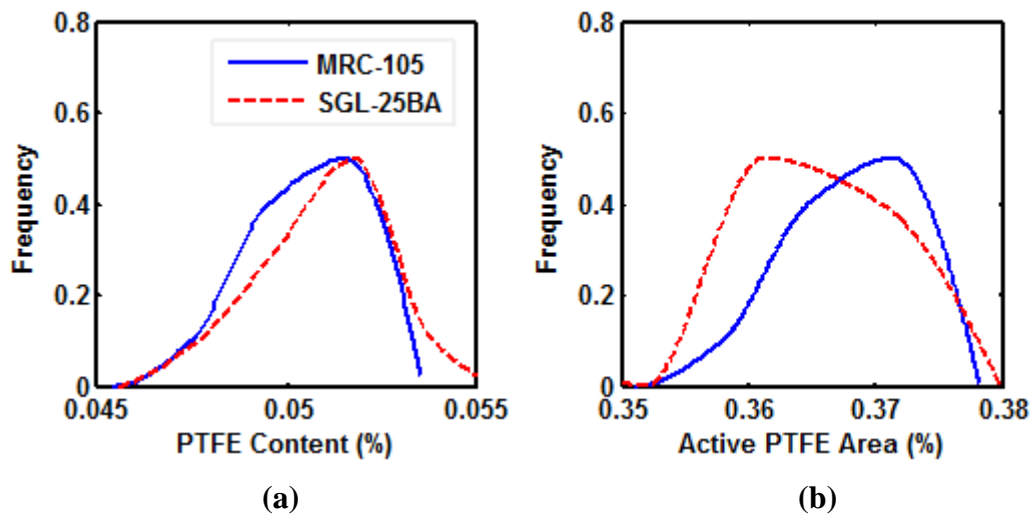


Figure 5.11. PTFE loading (a) PTFE content in solid surface, (b) the ratio of active and total PTFE areas.

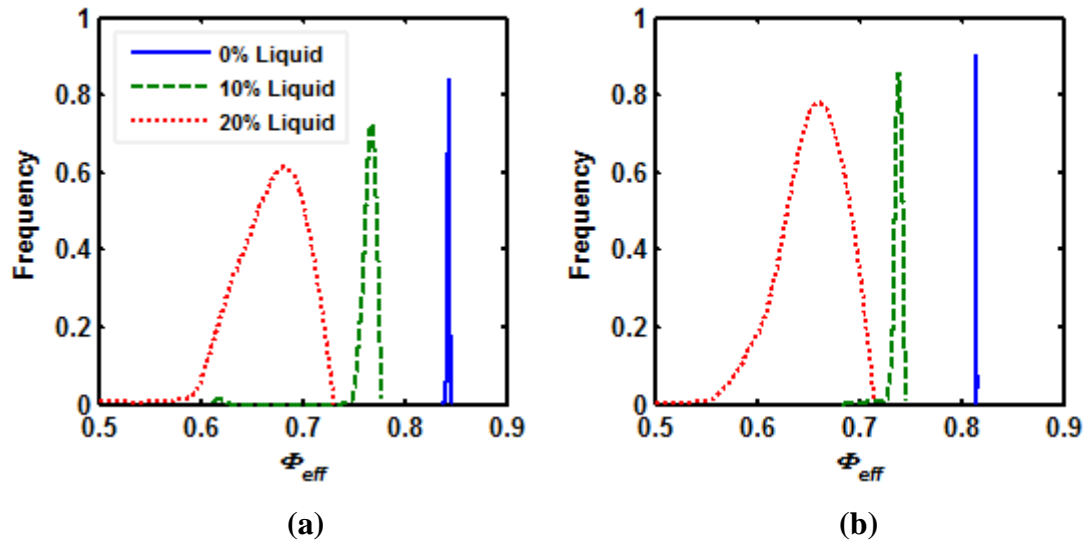


Figure 5.12. Effects of liquid formation on effective porosity for (a) SGL-25BA, (b) MRC-105.

CONCLUSION

In this dissertation, statistical based path-percolation theories were utilized to construct random inhomogeneous porous channels with a wide range of effective porosity. A statistical analysis was also performed on micro-computed tomographies of MRC-105 and SGL-25BA gas diffusion samples. Hydrophobic loading on the surface of the channels was also performed computationally, and the results were statistically analyzed. A 99% confidence level was applied for two-dimensional simulations. Two-point statistics was applied to extract smaller domains from the initially generated domains for single- and multi-phase LB models. Lattice-Boltzmann models were developed with a D2Q9 lattice to obtain the velocity distribution in the channels. Fluid-fluid and surface-fluid interactions were added to the codes to include the effects of 10% and 20% liquid formation and hydrophobic solid addition on surface on gas diffusion in all channels generated with the techniques mentioned above. Finally, the critical liquid formation, which makes the effective porosity of the domain zero, was examined. The general conclusions are listed as:

- Single-path-percolation model was used to simulate high-tortuosity (above 1.07) flow channels.
- Double-path-percolation model was used to simulate low-tortuosity (between 1.0005 and 1.0700) flow channels.
- In both low- and high-tortuosity systems, increased liquid volume increases the tortuosity.
- In high-tortuosity low-porosity systems, added liquid content decreases the tortuosity.

- In MRC-105 and SGL-25BA, the effective tortuosity is increased when the 10% of the channel was occupied with liquid clusters. When, the condensate amount is increased further, the tortuosity is slightly decreased in SGL-25BA, and almost overlapped with the case of 10% liquid formation in MRC-105.
- In all porous channels, liquid formation decreases the effective porosity and effective diffusion coefficient. Both parameters become less predictable with liquid formation.
- Hydrophobic solid particle addition in channels increases the effective tortuosity, and slightly decreases the effective diffusion coefficient in low-tortuosity domains.
- The effects of hydrophobic content on gas diffusion is negligible in high-tortuosity porous channels, since effective tortuosity does not change significantly.
- In MRC-105 and SGL-25BA, the critical liquid formation mostly takes values between 40% and 88%.

The effective porosity may be underestimated here because of the missing third dimension. There would be more void nodes in the missing direction, hence the number of orphan pores would be less than that of a two-dimensional simulation. Moreover, the effective tortuosity will definitely increase, since the shortest path between the inlet and the outlet will be the same, but there will be additional paths for the fluid molecules in the missing direction. Furthermore, a software was developed, and four high performance systems were implemented. Computing performances were examined to determine the optimal application programming interface for this particular work. The best performance of 2.8 GFLOPs was achieved by the pthreads implementation with four processors, and the gained speedup was computed as 3.962. The introduced porous channel simulation techniques in this dissertation can be utilized in any

porous medium application involved with transport phenomena in solid and void paths, and the statistical results of the current work can be applied in any mass diffusion study with low- and high-tortuosity porous channels with surface-fluid interactions. The dimensionless diffusion ratio distribution curves for both SGL samples can be used in macroscopic PEFC models. More advanced three-dimensional mesoscopic models can be developed by the same approach introduced in this work.

LIST OF REFERENCES

- [1] H. Kesten, What is percolation?, Notices of the American Mathematical Society, 53 (2006) 572-573.
- [2] H.M. Jung, W. Choi, S. Um, Path-percolation modeling of the electrical property variations with statistical procedures in spatially-disordered Inhomogeneous media, J Korean Phys Soc, 56 (2010) 591-597.
- [3] L. Boltzmann, Lectures on Gas Theory, University of California Press, Berkeley, 1964.
- [4] S. Succi, The Lattice Boltzmann Equation for Fluid Dynamics and Beyond, Clarendon Press; Oxford University Press, Oxford New York, 2001.
- [5] M.C. Sukop, D.T. Thorne, Lattice Boltzmann Modeling: An Introduction for Geoscientists and Engineers, Springer, Berlin ; New York, 2006.
- [6] A.A. Mohamad, Lattice Boltzmann Method: Fundamentals and Engineering Applications with Computer Codes, Springer-Verlag, London, 2011.
- [7] M.C. Sukop, D.T. Thorne, Lattice Boltzmann Modeling An Introduction for Geoscientists and Engineers, Springer-Verlag, Berlin, Heidelberg, 2006.
- [8] B. Ghanbarian, H. Daigle, A.G. Hunt, R.P. Ewing, M. Sahimi, Gas and solute diffusion in partially saturated porous media: Percolation theory and Effective Medium Approximation compared with lattice Boltzmann simulations, J Geophys Res-Sol Ea, 120 (2015) 182-190.
- [9] A. Nabovati, A.C.M. Sousa, Fluid flow simulation in random porous media at pore level using Lattice Boltzmann Method, New Trends in Fluid Mechanics Research, (2007) 518-521.
- [10] A. Adrover, M. Giona, A predictive model for permeability of correlated porous media, Chemical Engineering Journal, 64 (1996) 7-19.
- [11] P.C. Carman, Flow of Gases Through Porous Media, Academic Press, New York., 1956.
- [12] R.B. Bird, W.E. Stewart, E.N. Lightfoot, Transport phenomena, Rev. 2nd ed., J. Wiley, New York, 2007.
- [13] A. Koponen, M. Kataja, J. Timonen, Tortuous flow in porous media, Phys Rev E, 54 (1996) 406-410.
- [14] A. Koponen, M. Kataja, J. Timonen, Permeability and effective porosity of porous media, Phys Rev E, 56 (1997) 3319-3325.
- [15] M. Matyka, A. Khalili, Z. Koza, Tortuosity-porosity relation in porous media flow, Phys Rev E, 78 (2008) 026306.
- [16] A. Grucelski, J. Pozorski, Lattice Boltzmann simulation of fluid flow in porous media of temperature-affected geometry, J Theor App Mech-Pol, 50 (2012) 193-214.
- [17] M.C. Sukop, H.B. Huang, P.F. Alvarez, E.A. Variano, K.J. Cunningham, Evaluation of permeability and non-Darcy flow in vuggy macroporous limestone aquifer samples with lattice Boltzmann methods, Water Resour Res, 49 (2013) 216-230.
- [18] X.P. Li, Y. Zhang, X.W. Wang, W. Ge, GPU-based numerical simulation of multi-phase flow in porous media using multiple-relaxation-time lattice Boltzmann method, Chem Eng Sci, 102 (2013) 209-219.
- [19] H.B. Huang, J.J. Huang, X.Y. Lu, M.C. Sukop, On simulations of high-density ratio flows using color-gradient multiphase lattice Boltzmann Models, Int J Mod Phys C, 24 (2013) 1350021.
- [20] A. Genty, V. Pot, Numerical simulation of 3D liquid-gas distribution in porous media by a two-phase TRT Lattice Boltzmann method, Transport Porous Med, 96 (2013) 271-294.

- [21] H. El Abrach, H. Dhahri, A. Mhimid, Numerical simulation of drying of a saturated deformable porous media by the Lattice Boltzmann method, *Transport Porous Med*, 99 (2013) 427-452.
- [22] H.B. Huang, Z.T. Li, S.A.S.A. Liu, X.Y. Lu, Shan-and-Chen-type multiphase lattice Boltzmann study of viscous coupling effects for two-phase flow in porous media, *Int J Numer Meth Fl*, 61 (2009) 341-354.
- [23] H.B. Huang, L. Wang, X.Y. Lu, Evaluation of three lattice Boltzmann models for multiphase flows in porous media, *Comput Math Appl*, 61 (2011) 3606-3617.
- [24] M.C. Sukop, H. Huang, C.L. Lin, M.D. Deo, K. Oh, J.D. Miller, Distribution of multiphase fluids in porous media: Comparison between lattice Boltzmann modeling and micro-x-ray tomography, *Phys Rev E*, 77 (2008) 026710.
- [25] J.F. Chau, D. Or, M.C. Sukop, Simulation of gaseous diffusion in partially saturated porous media under variable gravity with lattice Boltzmann methods, *Water Resour Res*, 41 (2005) W08410.
- [26] J.F. Chau, D. Or, M.C. Sukop, Simulation of gaseous diffusion in partially saturated porous media under variable gravity with lattice Boltzmann methods, *Water Resour Res*, 41 (2005).
- [27] X.W. Shan, H.D. Chen, Simulation of nonideal gases and liquid-gas phase-transitions by the Lattice Boltzmann-equation, *Phys Rev E*, 49 (1994) 2941-2948.
- [28] X.Y. He, G.D. Doolen, Thermodynamic foundations of kinetic theory and Lattice Boltzmann models for multiphase flows, *J Stat Phys*, 107 (2002) 309-328.
- [29] N.S. Martys, H.D. Chen, Simulation of multicomponent fluids in complex three-dimensional geometries by the lattice Boltzmann method, *Phys Rev E*, 53 (1996) 743-750.
- [30] N. Zamel, N.G.C. Astrath, X.G. Li, J. Shen, J.Q. Zhou, F.B.G. Astrath, H.J. Wang, Z.S. Liu, Experimental measurements of effective diffusion coefficient of oxygen-nitrogen mixture in PEM fuel cell diffusion media, *Chem Eng Sci*, 65 (2010) 931-937.
- [31] C. Chan, N. Zamel, X.G. Li, J. Shen, Experimental measurement of effective diffusion coefficient of gas diffusion layer/microporous layer in PEM fuel cells, *Electrochimica Acta*, 65 (2012) 13-21.
- [32] J.H. Rohling, J. Shen, C. Wang, J. Zhou, C.E. Gu, Photothermal deflection measurement of effective gas diffusion coefficient of a porous medium, *European Physical Journal-Special Topics*, 153 (2008) 111-113.
- [33] J.M. LaManna, S.G. Kandlikar, Determination of effective water vapor diffusion coefficient in pemfc gas diffusion layers, *Int J Hydrogen Energ*, 36 (2011) 5021-5029.
- [34] R. Rashapov, F. Imami, J.T. Gostick, A method for measuring in-plane effective diffusivity in thin porous media, *Int J Heat Mass Tran*, 85 (2015) 367-374.
- [35] J. Kuva, M. Voutilainen, P. Kekalainen, M. Siitari-Kauppi, J. Timonen, L. Koskinen, Gas Phase Measurements of Porosity, Diffusion Coefficient, and Permeability in Rock Samples from Olkiluoto Bedrock, Finland, *Transport Porous Med*, 107 (2015) 187-204.
- [36] D. Mu, Z.S. Liu, C. Huang, N. Djilali, Determination of the effective diffusion coefficient in porous media including Knudsen effects, *Microfluidics and Nanofluidics*, 4 (2008) 257-260.
- [37] N. Zamel, X.G. Li, J. Shen, Correlation for the effective gas diffusion coefficient in carbon paper diffusion media, *Energy & Fuels*, 23 (2009) 6070-6078.

- [38] M. Yoshida, U. Gosele, M. Morooka, S. Tanaka, Effective diffusion coefficients of self-interstitials and vacancies in interactive diffusion in silicon in oxidizing atmosphere, *Journal of the Electrochemical Society*, 154 (2007) H86-H90.
- [39] J.G. Liu, Y.F. Nie, Fractal scaling of effective diffusion coefficient of solute in porous media, *Journal of Environmental Sciences-China*, 13 (2001) 170-172.
- [40] A. Genty, V. Pot, Numerical Calculation of Effective Diffusion in Unsaturated Porous Media by the TRT Lattice Boltzmann Method, *Transport Porous Med*, 105 (2014) 391-410.
- [41] G. Grimmett, Percolation and disordered systems, *Lect Notes Math*, 1665 (1996) 153-300.
- [42] A. Papoulis, Probability, Random-Variables, and Stochastic-Processes, *Cc/Eng Tech Appl Sci*, (1980) 14-14.
- [43] E.A. Wargo, A.C. Hanna, A. Cecen, S.R. Kalidindi, E.C. Kumbur, Selection of representative volume elements for pore-scale analysis of transport in fuel cell materials, *Journal of Power Sources*, 197 (2012) 168-179.
- [44] E.A. Wargo, A.C. Hanna, A. Cecen, S.R. Kalidindi, E.C. Kumbur, A representative volume element approach for pore-scale modeling of fuel cell materials, *Polymer Electrolyte Fuel Cells* 11, 41 (2011) 131-139.
- [45] D.A.G. Bruggeman, Calculation of various physics constants in heterogenous substances I Dielectricity constants and conductivity of mixed bodies from isotropic substances, *Ann Phys-Berlin*, 24 (1935) 636-664.
- [46] D.W. Chung, M. Ebner, D.R. Ely, V. Wood, R.E. Garcia, Validity of the Bruggeman relation for porous electrodes, *Model Simul Mater Sc*, 21 (2013) 074009.
- [47] O. Cekmer, S. Um, M.M. Mench, Application of path-percolation theory and Lattice-Boltzmann method to investigate structure-property relationships in porous media, *Int J Heat Mass Tran*, 86 (2015) 101-112.
- [48] A. Papoulis, Citation Classic - Probability, Random-Variables, and Stochastic-Processes, *Cc/Eng Tech Appl Sci*, (1980) 14-14.
- [49] J.J. Dongarra, *Sourcebook of Parallel Computing*, Morgan Kaufmann Publishers, San Francisco, CA, 2003.
- [50] B. Chapman, G. Jost, R.v.d. Pas, *Using OpenMP : portable shared memory parallel programming*, MIT Press, Cambridge, Mass., 2008.
- [51] S. Browne, J. Dongarra, N. Garner, G. Ho, P. Mucci, A portable programming interface for performance evaluation on modern processors, *International Journal of High Performance Computing Applications*, 14 (2000) 189-204.
- [52] M.M. Mench, *Fuel Cell Engines*, John Wiley & Sons, Hoboken, N.J., 2008.
- [53] S. Browne, J. Dongarra, N. Garner, G. Ho, P. Mucci, A portable programming interface for performance evaluation on modern processors, *Int J High Perform C*, 14 (2000) 189-204.
- [54] O. Cekmer, S. Um, M.M. Mench, Single- and multi-phase flow analysis in inhomogeneous random porous channels: I. Single-phase, low-tortuosity flow with double path-percolation theory, *Int J Heat Mass Tran*, (2015 (in prep.)).
- [55] O. Cekmer, S. Um, M.M. Mench, A combined path-percolation - Lattice-Boltzmann model applied to multiphase mass transfer in porous media, *Int J Heat Mass Tran*, (2015 (under review)).
- [56] A.A. Mohamad, *Lattice Boltzmann Method*, in, Springer,, Dordrecht, 2011, pp. 1 online resource (185 p.).

- [57] O. Cekmer, S. Um, M.M. Mench, Single- and multi-phase flow analysis in inhomogeneous random porous channels: II. Effects of hydrophobic solid structures on mass transfer with single- and double-path-percolation theories, *Int J Heat Mass Tran*, (2015 (in prep.)).
- [58] K. Grundke, A. Augsburg, On the determination of the surface energetics of porous polymer materials, *Journal of Adhesion Science and Technology*, 14 (2000) 765-775.
- [59] M.E. Tadros, P. Hu, A.W. Adamson, Adsorption and contact angle studies. 1. Water on smooth carbon, linear polyethylene, and stearic acid-coated copper., *Journal of Colloid and Interface Science*, 49 (1974) 184-195.

APPENDIX

The derivation of Lattice-Boltzmann equation is described here. The probability density function, f , must be introduced before analyzing the Lattice-Boltzmann model. The probability of a molecule to be at position \vec{x} at time t with momentum \vec{p} is called the probability density (or probability distribution) function, and symbolized as $f(\vec{x}, \vec{p}, t)$. At time $t+dt$, new positions and momenta of the molecules will be as follows [5]:

$$x + \frac{\vec{p}}{m} dt = x + \frac{m\vec{u}}{m} dt = x + \vec{u}dt = x + \frac{d\vec{x}}{dt} dt = x + d\vec{x} \quad (\text{A.1})$$

$$\vec{p} + \vec{F} dt = \vec{p} + \frac{d\vec{p}}{dt} dt = \vec{p} + d\vec{p} \quad (\text{A.2})$$

where m is the mass of the particle, and \vec{F} is an external force field that is assumed to be much smaller than the intermolecular forces. Hence, at time $t+dt$, the probability distribution function is written as $f(\vec{x} + d\vec{x}, \vec{p} + d\vec{p}, t + dt)$. If there are no collisions, the following streaming equation is obtained:

$$f(\vec{x} + d\vec{x}, \vec{p} + d\vec{p}, t + dt) d\vec{x} d\vec{p} = f(\vec{x}, \vec{p}, t) d\vec{x} d\vec{p} \quad (\text{A.3})$$

However, there are intermolecular collisions that must be considered. Some of the molecules start at the condition of \vec{x}, \vec{p} but at time $t+dt$, they collide with other molecules and cannot reach $\vec{x} + d\vec{x}, \vec{p} + d\vec{p}$, and the number of these molecules is called *loss*, Γ^L . Similarly, some of the molecules start with a condition other than \vec{x}, \vec{p} but after the collisions they reach the condition of $\vec{x} + d\vec{x}, \vec{p} + d\vec{p}$, which is called *gain*, Γ^G . Then, Equation (A.3) becomes:

$$f(\vec{x} + d\vec{x}, \vec{p} + d\vec{p}, t + dt) d\vec{x} d\vec{p} - f(\vec{x}, \vec{p}, t) d\vec{x} d\vec{p} = (\Gamma^G - \Gamma^L) d\vec{x} d\vec{p} dt \quad (\text{A.4})$$

Furthermore, the first term on LHS of Equation (A.4) can be written in the first order Taylor series expansion form as follows:

$$f(\vec{x} + d\vec{x}, \vec{p} + d\vec{p}, t + dt)d\vec{x}d\vec{p} = \left(1 + dt \frac{\partial}{\partial t} + d\vec{x} \cdot \frac{\partial}{\partial \vec{x}} + d\vec{p} \cdot \frac{\partial}{\partial \vec{p}}\right) f(\vec{x}, \vec{p}, t)d\vec{x}d\vec{p} \quad (\text{A.5})$$

Inserting Equation (A.5) into Equation (A.4), dividing both sides of Equation (A.5) by $d\vec{x}d\vec{p}dt$, and performing the further steps as follows, the Boltzmann equation is obtained as shown in Equation (A.6).

$$f d\vec{x}d\vec{p} + dt \frac{\partial f}{\partial t} d\vec{x}d\vec{p} + d\vec{x} \frac{\partial f}{\partial \vec{x}} d\vec{x}d\vec{p} + d\vec{p} \frac{\partial f}{\partial \vec{p}} d\vec{x}d\vec{p} - f d\vec{x}d\vec{p} = (\Gamma^G - \Gamma^L) d\vec{x}d\vec{p}dt$$

$$\frac{\partial f}{\partial t} + \frac{d\vec{x}}{dt} \cdot \frac{\partial f}{\partial \vec{x}} + \frac{d\vec{p}}{dt} \cdot \frac{\partial f}{\partial \vec{p}} = \Gamma^G - \Gamma^L$$

$$\frac{\partial f}{\partial t} + \vec{u} \cdot \frac{\partial f}{\partial \vec{x}} + \vec{F} \cdot \frac{\partial f}{\partial \vec{p}} = \Gamma^G - \Gamma^L \quad (\text{A.6})$$

or

$$\frac{Df(\vec{x}, \vec{p}, t)}{Dt} = \Omega \quad (\text{A.7})$$

where

$$\frac{D}{Dt} = \left(\frac{\partial}{\partial t} + \vec{u} \cdot \frac{\partial}{\partial \vec{x}} + \vec{F} \cdot \frac{\partial}{\partial \vec{p}} \right) \quad (\text{A.8})$$

$$\Omega = \Gamma^G - \Gamma^L \quad (\text{A.9})$$

When, Equation (A.6) is solved, the distribution function will be determined. To obtain the macroscopic variables; density and velocity, the following equations are used:

$$\rho = \int f d\vec{c} \quad (\text{A.10})$$

$$\rho \vec{u} = \int \vec{c} f d\vec{c} \quad (\text{A.11})$$

where ρ , \vec{c} , \vec{u} are fluid density, unit velocity vector, and macroscopic flow velocity vector ($\vec{u} = u_x \vec{i} + u_y \vec{j}$), respectively.

VITA

Ozgur Cekmer was born in Istanbul, Turkey in September 21, 1981. He completed his primary school in Istanbul, and moved to Kadirli, Osmaniye. After completing the high school in this town, he attended the Hacettepe University in Ankara to study Nuclear Engineering. Then, he studied Energy Engineering in Izmir Institute of Technology for his master's degree. After three years, he attended the University of Tennessee as a PhD student in mechanical engineering major and interdisciplinary graduate minor in computational science. Ozgur will get his PhD degree in August 2015.